SENSOR FAULT DETECTION AND ISOLATION USING SYSTEM DYNAMICS IDENTIFICATION TECHNIQUES

by

Li Jiang

A dissertation submitted in partial fulfillment
of the requirements for the degree of
Doctor of Philosophy
(Mechanical Engineering)
in The University of Michigan
2011

Doctoral Committee:

Professor Jun Ni, Co-Chair
Assistant Professor Dragan Djurdjanovic, Co-Chair
Professor A. Galip Ulsoy
Associate Professor Mingyan Liu
Elizabeth A. Latronico

© Li Jiang 2011
All Rights Reserved

ACKNOWLEDGEMENTS

My foremost gratitude goes to my advisor Prof. Jun Ni. Without him, this dissertation would not have been possible. I thank him not only for his insights and valuable feedback that contributed greatly to this dissertation, but also for his understanding, support and guidance through the years. I would also like to thank Prof. Dragan Djurdjanovic, who introduced me into the research center of intelligent maintenance systems and helped to sharpen my research skills with his patience, encouragement and advices.

I would also like to express my gratitude to Dr. Elizabeth Latronico for offering me the internship opportunities to work at Robert Bosch Research and Technology Center as a research assistant. Her expert advices and experiences in automotive fault diagnosis inspired new ideas in my dissertation. I also would like to thank Prof. A. Galip Ulsoy and Prof. Minyan Liu for their valuable feedback that helped to improve the dissertation in many ways.

My graduate studies would not have been the same without the friendship of Jianbo Liu, Jing Zhou, Yi Liao, Shiming Duan and many others. Together we studied and had fun over the years.

Finally, and most importantly, I would like to thank my dearest parents. Their unconditional support, encouragement and unwavering love has been the bedrock upon which my life has been built. It is them who have given the confidence to face challenges and fight through difficulties over the years.

TABLE OF CONTENTS

LIST OF FIGURES

Figure

LIST OF TABLES

Table

CHAPTER I

Introduction

1.1 Motivation and Objectives

The performance of machines and equipment degrades as a result of aging and wear, which decreases performance reliability and increases the potential for failures [Djurdjanovic et al., 2002]. To ensure proper functionality of complex systems, advanced technologies for performance diagnosis and control are incorporated into engineering designs, especially in the case of sophisticated, expensive and safety critical systems, such as manufacturing equipment [Rao, 1996], computer networks [Dasgupta and Gonzalez, 2002; Harmer et al., 2002], automotive [Crossman et al., 2003; Murphey et al., 2003] and aircraft engines [Kobayashi and Simon, 2005], etc. These performance diagnosis and control functionalities necessitate the use of an ever-increasing number of sophisticated sensors and measurement devices to deliver data about the key indicators of the system status and performance.

However, just as any dynamic system, a sensor fails if a failure occurs in any of its components including the sensing device, transducer, signal processor, or data acquisition equipment. An abrupt failure in the sensor can be caused by a power failure or corroded contacts, while an incipient failure such as drift and precision degradation can be caused by deterioration in the sensing element. As defined in [Isermann, 1984],

both an abrupt and an incipient failure can cause non-permitted deviation from the characteristic property in a sensor, which leads to inaccurate measurements from the monitored[1] system. Consequently, a faulty sensor can cause process performance degradation, process shut down, or even fatal accident in a safety critical system. In fact, the problem of instrument fault detection, identification and accommodation has already received extensive attention in both industrial and academic fields [Betta and Pietrosanto, 2000; Crowe, 1996; Qin and Li, 2001]. Nevertheless, the detection of sensor incipient failures that is important for critical information to diagnosis and control systems has received limited attention in literature [Alag et al., 2001].

The detection and isolation of a faulty sensor is not an easy problem. The measurements of a sensor depict characteristics of both the monitored system and the sensor itself. Thus, any abnormal deviation in the measurements of a sensor could be caused by a change either in the monitored system or in the sensor. In addition, as an engineering system becomes more complex, the number of its interconnected subsystems and the associated sensors also increases, in which various failures may occur either independently or simultaneously. Moreover, the imperfect nature of a sensor as well as the process disturbances add noise to its measurements [Alag et al., 2001]. All these aforementioned issues raise the challenge of detecting and isolating a faulty sensor from a failure occurred in the monitored system. Furthermore, a method developed for the detection, isolation, and accommodation of a faulty sensor should be able to run in a real-time environment so that its measurements could be validated within a desirable time duration for the purpose of diagnosis and control. This imposes additional constraints on the development of a feasible solution due to the limited computational power and storage capacity available in a real-time

[1]This could be a monitored or a controlled system. For the sake of simplicity, this system is referred as the monitored system in the reminder of the thesis.

diagnosis and control system.

In order to address the above issues, a method for the detection, isolation and accommodation of a faulty sensor should satisfy the following desirable characteristics:

- able to distinguish where a failure occurred in the sensor or in the monitored system,
- able to validate the measurements of a sensor without the use of redundant sensors and the requirement of a detailed physical model of the monitored system,
- able to detect, isolate, and accommodate a faulty sensor promptly for the purpose of diagnosis and control in a real-time environment,
- applicable to a wide range of sensors, and
- capable of detecting and isolating a faulty sensor even in the case when multiple sensors fail at the same time.

A conventional engineering method for sensor validation is to check and recalibrate the sensor periodically by following a set of predetermined procedures [Pike and Pennycook, 1992]. Although it is effective in dealing with abrupt sensor failures, this method is not able to accomplish continuous assessment of sensor performance and may be insufficient to achieve desirable performance, especially in the case of complex and safety critical dynamic systems. Moreover, with the increasing number of interconnected subsystems and associated sensors, it has become less and less feasible and cost effective to check all sensors periodically. On the other hand, the hardware redundancy approach that has been widely used in many safety-critical systems measures one critical system variable using two or more sensors. The faulty sensor can be detected by checking the consistency among the redundant sensor measurements and then isolated using majority voting schemes [Broen, 1974], with

three or more sensors usually being necessary to identify the faulty sensor. It has been shown that these methods are relatively easy to implement and can grant a high certainty in the detection and isolation of faulty sensors. However, the use of redundant sensors may not always be feasible due to the cost and space constraints. Moreover, it is highly possible that the redundant sensors could also fail and show similar symptoms because they are operated in the same working environment and thus tend to have similar life expectations [Patton et al., 1989].

To avoid the use of redundant sensors, the analytical redundancy approach employs mathematical models to capture the dynamics of the monitored system as well as the sensors themselves. Based on a nominal model established for the fault-free conditions, residuals can then be generated as the difference between the actual sensor readings and the values estimated from the nominal model. The generated residuals can be employed to detect and isolate a faulty sensor by incorporating an appropriate residual evaluation scheme in the well-developed literature on model-based fault detection and isolation methodologies. Nevertheless, such methods need an accurate analytical model of the monitored system as well as the sensor, and thus require *a priori* deep understanding of their underlying physics.

As illustrated in Figure 1.1, this proposed methodology aims to *identify and isolate incipient sensor failures in a dynamic system*, *quantitatively assess these failures*, and *compensate for their effects on the measurements*. Inspired by the fact that the measurements of a sensor depict the dynamic characteristics of the monitored system as well as those of the sensor itself, a methodology has been developed in this thesis to detect and isolate incipient sensor failures by decoupling their dynamics directly based on the measurements. This enables the monitoring of a sensor separately from its associated monitored system without the use of redundant sensors. To reduce

the amount of *a priori* knowledge required, system identification techniques have been employed in the proposed method to identify the analytical relations among the measured variables in the dynamic system.

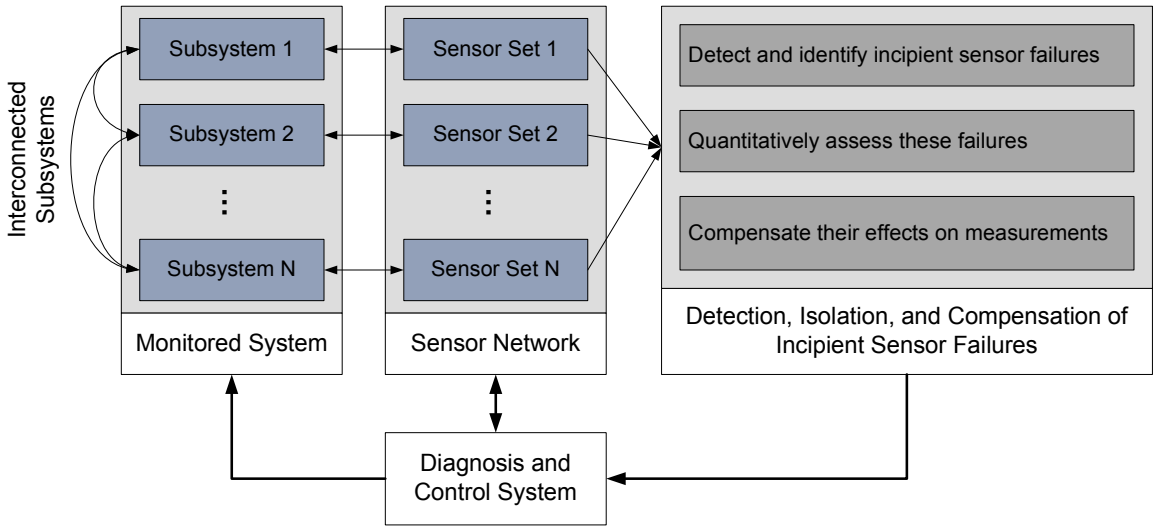

Figure 1.1: Objectives of this research on the detection, isolation, and accommodation of a degraded sensor

1.2 Thesis Outline

The remainder of the thesis is organized as follows.

In Chapter II, the state-of-the-art techniques for fault detection and isolation and their applications in the field of instrumentation and measurement systems are reviewed. In contrast to the hardware redundancy approaches, analytical redundancy approaches incorporate *a priori* system knowledge and extract key information from the measurement system for the detection and isolation of a faulty sensor instead of deploying multiple sensors for the same measured variable. Due to their benefits in system cost and complexity, analytical redundancy approaches have attracted a lot of attention in both academic research and industry applications. In this chapter, the various analytical redundancy approaches are reviewed in the categories of model-

based methods, knowledge-based expert systems, and data-driven methods. The research and application challenges in the reviewed topic are also identified, and associated future research topics are proposed.

In Chapter III, a method is proposed to detect, isolate, and accommodate an incipient sensor failure in a single-input-single-output system under the assumption that the dynamics of the monitored system as well as the associated sensor is linear. In the proposed method, a subspace system identification algorithm is used to track the changes of the time constants and gains of the sensor and the monitored system, simultaneously. Without the use of redundant sensors, this method utilizes the fact that the sensor readings depict dynamic characteristics of the sensors as well as the monitored system. To evaluate its performance, this method has been implemented to detect incipient failures in a throttle position sensor using simulations of an automotive electronic throttle system.

In Chapter IV, an input selection method is proposed to identify the underlying relations embedded in a nonlinear dynamic system, which helps to deal with the increased complexity of detecting and isolating sensor faults in a multiple-input-multiple-output system. The proposed method converts the problem of selecting the most correlated input variables for the target output variable of a nonlinear dynamic system into one of a set of properly linearized models. In order to enable the approximation of the nonlinear system behavior with a set of linear models, a growing self-organizing map is employed to appropriately partition the system operating region into sub-regions via unsupervised clustering. Evaluated based on the minimum description length principle, genetic algorithm is employed in this work to identify the more related input variables and the associated dynamic model structure for efficient computation. The performance of the algorithm was evaluated with two

commonly cited numerically examples in the literature of system identification.

In Chapter V, an approach is then developed to detect and isolate sensor faults and air leaks in a diesel engine air path system, a highly dynamic complex multiple-input-multiple-output system. The proposed approach captures the analytical redundancies among the air mass flow rate through intake air system and the pressures in the boost and intake manifolds. Without the need for a complete model of the target system, fault detectors are constructed in this work using the growing structure multiple model system identification algorithm. Given the addition information on operation regime from the identified model, the proposed approach evaluates both the global and local properties of the generated residuals to detect and isolate the potent sensor and system faults.

In Chapter VI, the contributions of the research accomplished in this thesis are summarized and its possible future work is proposed.

CHAPTER II

State-of-the-Art Methodologies for Sensor Fault Detection, Isolation, and Accommodation of Sensor Failures

2.1 Introduction

In this chapter, the state-of-the-art techniques for fault detection and isolation and their applications in the field of instrument fault detection, isolation and accommodation are reviewed. The importance of sensor validation was first recognized in the safety-critical processes such as nuclear power plants. However, driven by the stricter regulations on safety and environment, topics in the domain of instrument fault detection, isolation and accommodation have received extensive attention in various engineering applications. It has become even more crucial as more sensors are integrated into a system for advanced functionalities.

A conventional engineering method for sensor validation is to check and recalibrate a sensor periodically according to a set of predetermined procedures [Pike and Pennycook, 1992]. Although this method has been widely implemented in industry for detecting abrupt sensor failures, it is not able to accomplish continuous assessment of a sensor, and thus is not effective in detecting its incipient failure. Moreover, due to their ever-increasing number, it has become cost-ineffective and even infeasible to check all sensors periodically. Therefore, significant efforts have been made for the development of more systematic methods, which can be generally categorized

into hardware and analytical redundancy approaches [Ibarguengoytia et al., 2001].

The general idea of the hardware redundancy approaches is to measure one critical variable using two or more sensors, and then detect as well as isolate the faulty sensor by consistency checking and majority voting. These approaches have been widely used in safety-critical systems for their simplicity and robustness. Without the use of additional sensors, the analytical redundancy approaches identify the functional relations between the measured variables via a mathematical model that can be either developed based on the underlying physics or derived directly from the measurements. Residuals between the sensor measurements and the modeled outputs can then be generated for the detection and isolation of the faulty sensor. As illustrated in Figure 2.1, analytical redundancy approaches can be further categorized according to the type of their required *a priori* knowledge as model-based methods, knowledge-based expert systems, and data-driven methods. A similar classification was used to present the state-of-the-art methods for process fault detection and diagnosis in [Venkatasubramanian et al., 2003a,b,c].

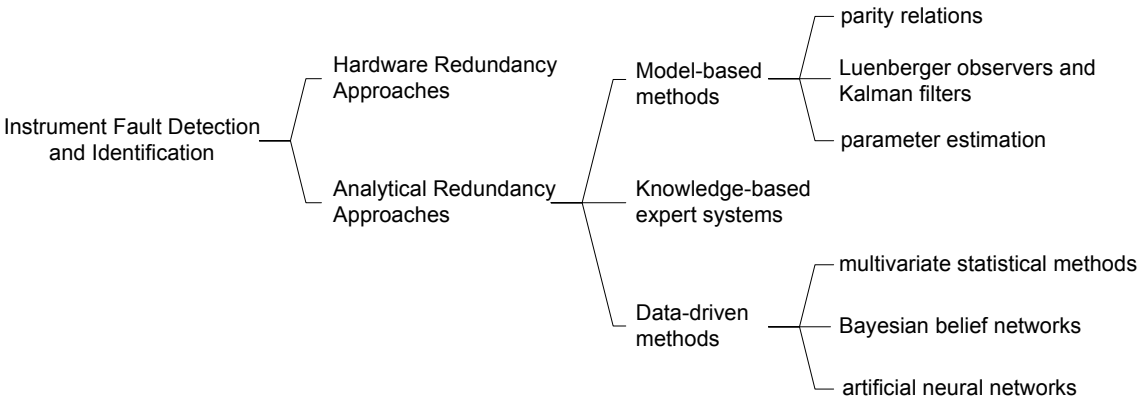

Figure 2.1: Categorization of the state-of-the-art methods for Instrumentation Fault Detection and Identification

Among the various analytical redundancy approaches, a model-based method requires an accurate mathematical model of the target dynamic system that can be

described using parity relations, Luenberger observers and Kalman filters, and parameter estimators. A knowledge-based expert system incorporates the expert domain knowledge that is generally captured with a set of rules according to some knowledge representation formalism. Instead of requiring a deep understanding of the physical system, a process history based method demands the availability of a sufficient amount of data that are representative of the system performance. Due to demands for improved system control and diagnosis, an increased number of sensors have been employed in a complex system such as the automotive engine. As a result, abundant data can be collected for the purpose of system control and diagnosis. This has not only encouraged the development of various data-driven methods including the multivariate statistical methods, Bayesian belief networks, and artificial neural networks, but also enabled their wide industrial applications.

2.2 State-of-the-Art Methodologies for the Detection, Isolation and Accommodation of a Sensor Failure

2.2.1 Hardware redundancy approaches

The hardware redundancy approaches find their first and main applications in nuclear power plant monitoring and other safety-critical processes. It has been shown that these methods can grant a high certainty in the detection and isolation of faulty sensors with relatively easy implementation. However, the use of redundant sensors may not always be feasible due to cost and space constraints. Moreover, it is highly possible that the redundant sensors could fail together with similar symptoms because they are operated in the same working environment and thus tend to have similar usage life expectations [Patton et al., 1989].

The general idea of the hardware redundancy approaches is to measure one critical variable using two or more sensors. The faulty sensor can be detected by checking

the consistency among the redundant sensor measurements, and isolated using a majority voting scheme if more than two redundant sensors are installed. In [Broen, 1974], a class of voter-estimators, derived from least-square estimation, were developed to detect and isolate a faulty sensor among a group of redundant measurements. The proposed method first estimated the measured variable by fusing the group of redundant measurements, and then identified the faulty sensor if its readings were significantly different from the estimated value. Inspired by the same idea, the method in [Desai and Ray, 1984] concurrently checked the relative consistencies among all redundant measurements, and used the most consistent and inconsistent subsets for the estimation of measured variable and the identification of a faulty sensor, respectively. Developed for application to nuclear power plants, the signal validation system proposed in [Holbert and Upadhyaya, 1990] integrated several established fault detection methods with a modular architecture and evaluated the validity of measurements using fuzzy membership functions. In addition, a complex logic algorithm was presented in [Glockler et al., 1989] to check the consistency among multivariate measurements, in which prediction models were used to estimate each variable based on its redundant measurements. In [Dorr et al., 1997], mean-value detectors were employed instead to estimate the variable via a linear combination of its redundant measurements.

In order to overcome the limitations of a static threshold, the concept of fuzzy sets was employed in [Park and Lee, 1993] to develop a rule-based diagnostic logic for a set of redundant sensors so that the dynamic disturbances and noises in the measurements can be taken into account. The fuzzy sets described the mean-value and uncertainty differences among sensor measurements with triangular membership functions. Once a fault occurs, an uncertainty reductive-fusion technique was used to

find the infusible sensor measurements, which enables the detection and identification of a faulty sensor.

The hardware redundant approaches, as discussed above, are able to detect a sensor failure with two redundant sensors, but they generally require three or more redundant sensors to identify the faulty sensor. A method has been developed in [Deckert et al., 1977] to address such an issue by constructing an additional virtual sensor for the target variable based on other non-redundant sensor measurements, in which the quality sequential probability ratio is used as the identification logic.

2.2.2 Analytical redundancy approaches

Analytical redundancy (also known as functional, inherent, or artificial redundancy) is realized through the functional relationships among the measured variables, which constitutes a model for the system. Residuals can then be generated as the differences between the model outputs and the actual measurements, based on which various techniques have been developed for fault detection and isolation. The use of such an analytical model enables the detection and identification of a faulty sensor without the requirement for additional redundant sensors.

As discussed in [Frank, 1990; Venkatasubramanian et al., 2003c], analytical redundancy can generally be classified as direct and temporal. Derived directly from physical laws, direct redundancies can be expressed using algebraic equations, based on which one measured variable can be algebraically determined from its related sensor measurements. Since the computed values should only deviate from the associated sensor measurements during a sensor failure, such direct redundancies can be employed for the detection and isolation of a faulty sensor. In addition, temporal redundancies capture the dynamic relations among the sensor measurements as well as actuator control signals with differential or difference equations.

2.2.2.1 Model-based methods

The model-based method requires an explicit mathematical model of the target system for the generation of residuals between the modeled outputs and sensor measurements. Since different faults in the system can cause different patterns in the residuals, various fault detection and isolation methods have been developed based on residual evaluation. With a deep understanding of the target system, such an analytical model can be developed directly using the first principles of physics. Although the development of a first-principle model can be time-consuming and generally requires a great amount of *a priori* knowledge about the target system, it provides more information for system diagnosis and control algorithm design because each model parameter has a one-to-one relationship with its corresponding physical parameter [Frank, 1990; Venkatasubramanian et al., 2003c]. As a result, a great number of model-based methods have been developed in the literature and implemented in various applications. As presented in [Nyberg and Stutte, 2004], a first-principle model is developed for an automotive diesel engine, based on which different faults such as a deteriorated sensor and a leakage in the air system can be detected and isolated using a series of structured hypothesis tests. In order to handle the modeling errors as well as the measurement noise, the structured hypothesis test developed in [Nyberg, 1999] employs an adaptive threshold.

Figure 2.2 illustrates the general architecture of a model-based fault detection and isolation method. A target dynamic system generally consists of a monitored system that can be further decomposed into a number of subsystems, a properly designed controller, and a set of actuators and sensors. Based on the sensor measurements y_s, the controller outputs a set of control commands u_a to the actuators that operate the monitored system. Such a dynamic system can be subjected to various component

failures that may occur in an actuator, any subsystem in the monitored system, an sensor, or the controller. In Figure 2.2, f_a refers to an actuator failure, f_p denotes a failure in the monitored system, f_s describes a sensor failure, and f_c represents a controller failure. In addition to the component failures, the monitored system and the sensors are also subjected to unexpected external disturbances d and measurement noise n, respectively. Derived from the control commands u_a and the sensor measurements y_s, an analytical model, termed as *modeled system* in Figure 2.2, can then be identified to capture the current system behavior. Along with this modeled system, models that present the nominal or faulty system behavior may also be identified and used as reference models for the purpose of system diagnosis. After the completion of system modeling, various features can be extracted based on the estimated states, identified system parameters, and the residuals generated between the sensor measurements and the outputs estimated either from the nominal or faulty system model. With the availability of appropriate diagnostic features, various techniques have been developed to detect and isolate the faults. In the remainder of this section, various fault detection and isolation approaches including residual evaluation, parameter estimation, and the use of parity relations, Luenberger observers and Kalman filters are briefly reviewed. For a more comprehensive survey of the model-based methods, one may refer to the papers [Frank, 1990; Isermann, 1984, 1997, 2005; Venkatasubramanian et al., 2003c] as well as the books [Gertler, 1998; Patton et al., 1989].

parity relations First developed in [Chow and Willsky, 1984; Lou et al., 1986; Potter and Suman, 1977], the parity relation approaches aim to re-arrange and transform an input-output or a state-space model of the monitored system into a set of parity

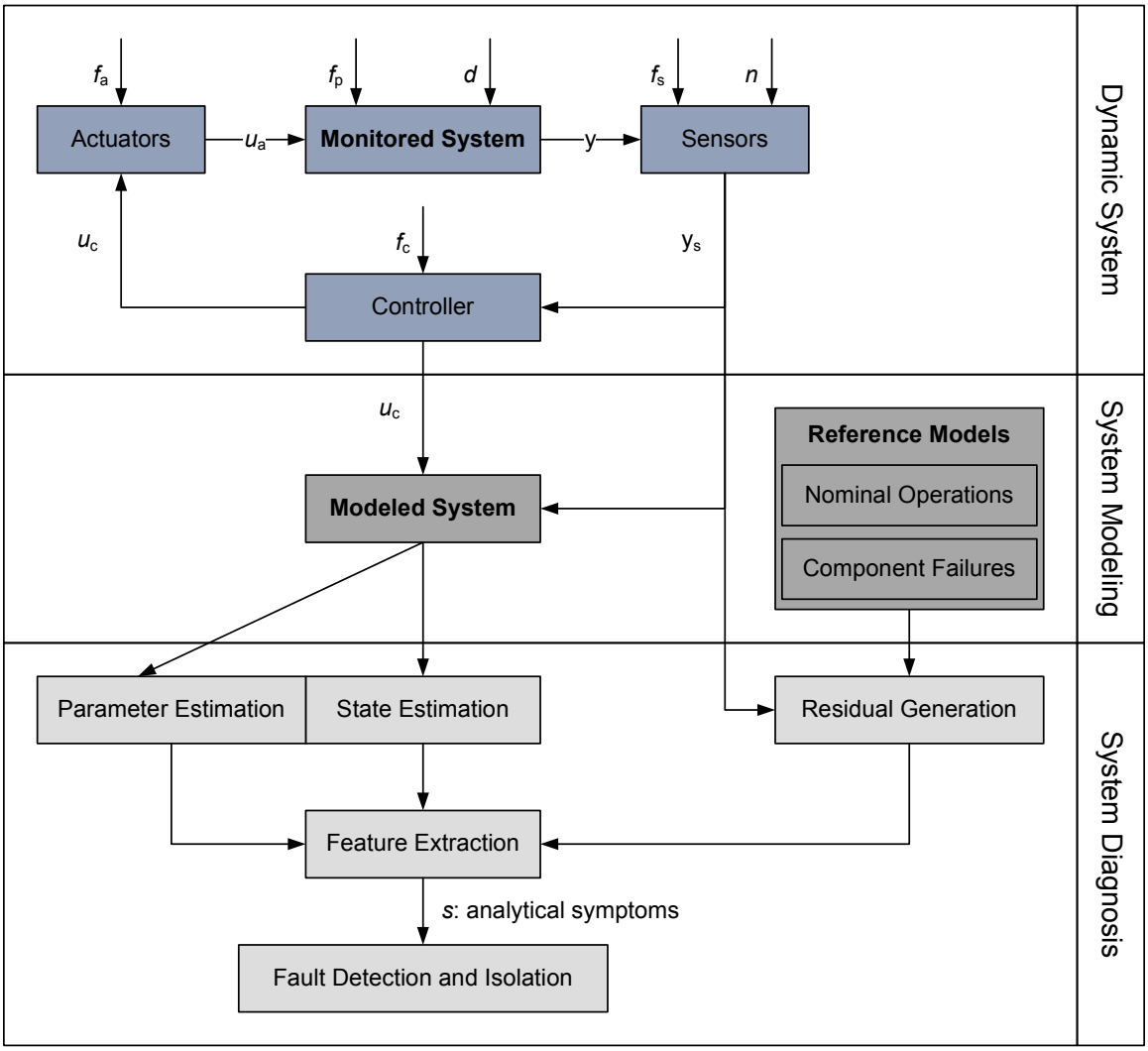

Figure 2.2: General architecture of a model-based fault detection and isolation method [Isermann, 1984]

relations to achieve the best performance in fault detection and isolation. The general idea of these approaches is to check the parity (consistency) between modeled system with the sensor measurements and control commands. The residuals generated by the parity equations are ideally zero under nominal steady-state system operations, but are generally non-zero in a real system due to the presence of external disturbances, measurement noise, and model inaccuracies. In addition to the proposal of dynamic parity equations in [Willsky, 1976], further development and

application of the parity relation approaches can be found in [Gertler et al., 1995, 1990, 1999; Gertler and Monajemy, 1995; Gertler and Singer, 1990].

The parity relation approaches have also been applied to detect and isolate the faulty sensor among redundant sensors. However, as stated in [Betta and Pietrosanto, 2000], the use of the parity relation approaches in such applications is limited because they require

- an accurate analytical model of the monitored system as well as the associated actuators,
- sufficient analytical redundancy among the measured variables,
- reliable and accurate sensor measurements, and
- powerful computational capability for real-time applications.

In order to avoid the requirement for an accurate model of the monitored system, the parity relation approach developed in [Qin et al., 1998] identified an input-output model for the target system using a recursive least-square system identification method based on the sensor measurements and control commands. An errors-in-variables subspace identification algorithm was then proposed for developing a proper analytical system model in [Qin and Li, 2001] to handle noisy sensor measurements. Applied for the detection of a faulty sensor, a dynamic structured residual approach was developed in [Qin and Li, 2004] to maximize the sensitivity of the generated residuals to different failures. As first proposed in [Qin and Li, 2001], the optimality of the primary residual vector and the structured residual vectors that are generated using an extended observability matrix and a lower triangular block Toeplitz matrix of the system was proved in [Li and Shah, 2002]. After the determination of the maximum number of multiple sensors that are most likely to fail simultaneously, a

unified scheme for the isolation of single and multiple faulty sensors based on a set of structured residual vectors is also proposed in [Li and Shah, 2002].

Due to the implicit equivalence between the principal component analysis and the parity relation approach, methods have been developed to combine their advantages and applied for instrument fault detection and isolation. In addition, methods have also been developed to describe the parity relations among the measured variables with a properly trained artificial neural network. Furthermore, the knowledge-based expert system was employed in [Betta et al., 1995; Kim et al., 1992] to detect and isolate the faulty sensor in the cases of incomplete or noisy sensor measurements. These methods will be further discussed in the following sections of multivariate statistical methods, neural networks, and knowledge-based expert system, respectively.

Luenberger observers and Kalman filters The general idea of the observer-based methods is to model the system outputs from measured variables using a single or a bank of estimators, among which the Luenberger observers and the Kalman filters have been most widely applied. Then, residuals between the modeled and measured system outputs can be generated and evaluated for the fault isolation and detection using various methods such as the sequential probability test, the generalized likelihood ratio approach, and the fixed/adaptive threshold logic. A review and comparison of the methods developed based on the Luenberger observers and the Kalman filters was presented in [van Schrick, 1994].

The dedicated observer scheme [Clark, 1978a; Clark et al., 1975], as illustrated in Figure 2.3(a), uses one Luenberger observer for each system output to detect incipient sensor failures. Since each observer is only used to reconstruct one system output, such a method does not require the full observability for each measured

variable. Furthermore, with a bank of estimators, this scheme provides a flexible, selective and robust solution and enables the detection and isolation of multiple and even simultaneous sensor failures. However, the construction of one observer for each system output has become impossible as the complexity of the target system increases. Therefore, a simplified approach based on the dedicated observer scheme was proposed in [Clark, 1978b], in which a single observer was used to reconstruct all the system outputs using the set of measured variables that are most sensitive to potential sensor failures. Such a simplified configuration is able to detect and isolate multiple sensor failures as long as the faulty sensor measurements are not used as the inputs to the observer. Inspired by the same concept, another instrument fault detection method was then proposed in [Frank and Keller, 1980], in which a pair of sensitivity discriminating Luenberger observers were constructed for each system output. Within each pair of observers in Figure 2.3(b), one was designed to be insensitive to system parameter variations, while the other was designed to be sensitive to sensor failures. The use of such a pair of sensitivity discriminating observers improves the reliability and robustness of the proposed instrument fault detection method by eliminating the influence of system parameter variations. Considered as an alternative form of the dedicated observer scheme, the generalized observer scheme was presented in [Frank, 1987], in which one observer was constructed for each system output based on all the measured variables except the one it is associated with.

As outlined in [Patton and Chen, 1997], various methods have also been developed in the literature to further improve the robustness of the observer-based methods for the detection and isolation of sensor failures. In order to reduce the number of required observers, an approach for the design of structured residuals for fault detection and isolation was proposed in [Alcorta Garcia and Frank, 1999]. In addition,

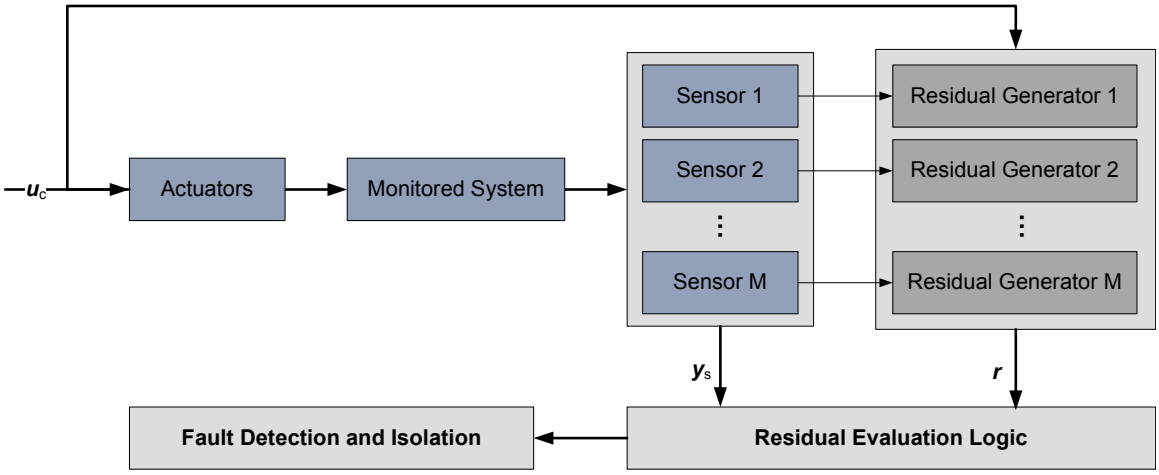

(a) Dedicated observer scheme [Clark et al., 1975]

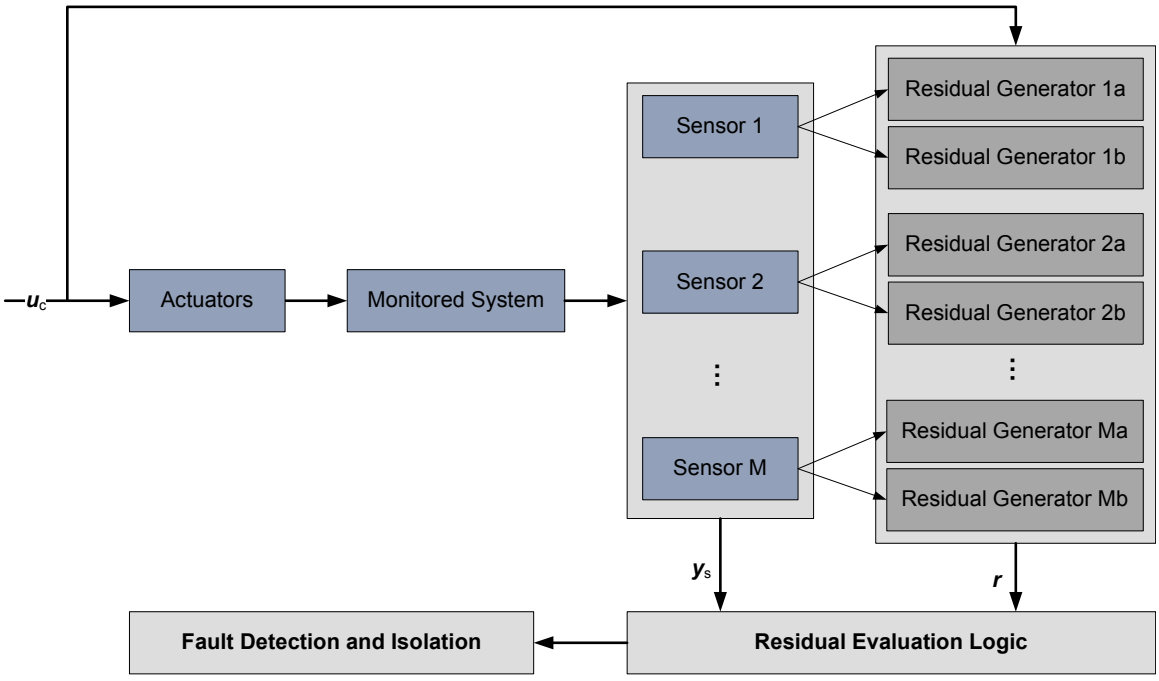

(b) Sensitivity discriminating observer scheme [Frank and Keller, 1980]

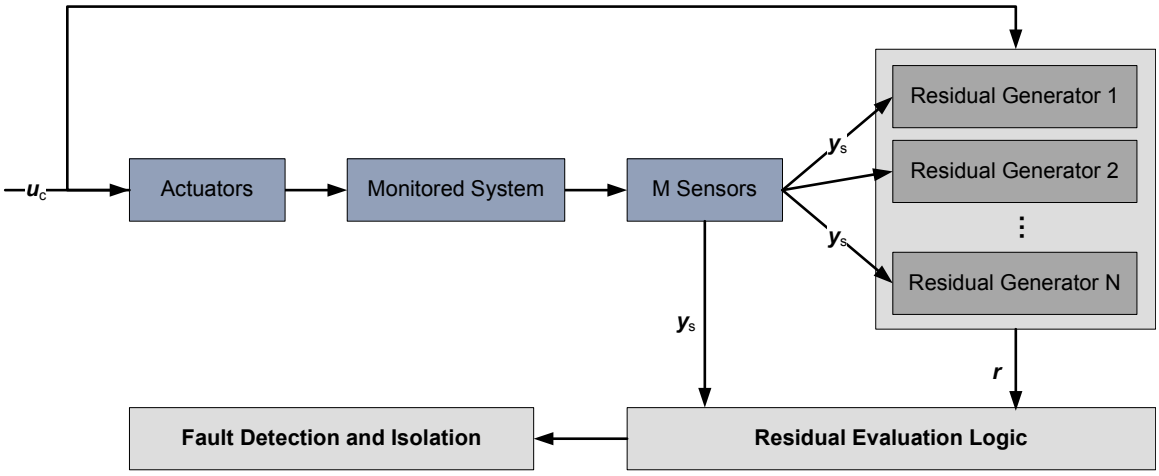

(c) Generalized observer scheme [Frank, 1987]

Figure 2.3: Various configuration schemes for the observer-based methods

the genetic algorithm was employed in [Chen et al., 1994] to optimize the design for an observer-based residual generator according to the performance index that is defined based on the frequency distributions of various failures, measurement noise, and modeling uncertainties. These observer-based methods were applied for detecting and isolating sensor failures in a turbo jet engine [Johansson and Norlander, 2003], and the navigation system in an aerospace vehicle [Halder et al., 2004].

The Kalman filters have been widely applied to stochastic systems where the state variables are considered as random variables with known parameters for their statistical distributions. Based on a nominal system model, a well-designed Kalman filter is proved to be the optimal state estimator in terms of estimation error if the system variables are subjected to Gaussian distribution. Due to their simplicity and optimality, the Kalman filters have been widely used in various applications [Hsiao and Tomizuka, 2005; Scheding et al., 1998; Spina, 2000; Simani et al., 2000; Turkcan and Ciftcioglu, 1991]. In [Simani et al., 2000], the standard system identification techniques were employed to derive the state estimators, dynamic observers and Kalman filters from the input-output data in the form of an autoregressive model with exogenous inputs, and an error-in-variables model. In order to apply to a discrete system, the generalized observer scheme was extended in [Lunze and Schroder, 2004] to detect and isolate a failure with the Kalman filters in a discrete-event system. Furthermore, the extended Kalman filters were employed to detect and isolate sensor failures in nonlinear dynamic systems [Mehra and Peschon, 1971; Watanabe and Himmelblau, 1982; Watanabe et al., 1994].

The Luenberger observers and the Kalman filters have been applied to detect and isolate a single or multiple sensor failure(s) in linear and nonlinear systems. In addition, observer-based approaches have been also developed to address the issue of

external disturbances, measurement noise and modeling errors. However, similar to the parity relation approaches, the observer-based methods still require a significant amount of *a priori* knowledge about the target system.

parameter estimation Inspired by the fact that a fault in the system can be observed through changes in the associated parameters in the model, parameter estimation techniques have been developed to detect and isolate a fault by tracking the changes in its characteristic parameters. Since the characteristic parameters are generally not measurable directly, a parametric model in the form of (2.1) is required.

$$y(t) = f\left(u(t), \Theta\right) \tag{2.1}$$

where $u \in \mathbb{R}^q$ and $y \in \mathbb{R}^p$ denote the system inputs and outputs, and $\Theta \in \mathbb{R}^m$ is the vector of model parameters that is a function of the characteristic physical parameters $\phi \in \mathbb{R}^n$. As described in [Isermann, 1984], the changes in the physical parameters ϕ can thus be captured via the estimated model parameters $\hat{\Theta}$, which enables the detection and isolation of a fault. For instance, the sensor response characteristics were captured in [Upadhyaya and Kerlin, 1978] using the noise analysis technique and employed for detecting and isolating a sensor failure.

2.2.2.2 Knowledge-based expert systems

While a model-based method requires a quantitative mathematical model, an expert system employs a qualitative model that is derived from the accumulated experiences and engineering domain knowledge for the target system. With its first application in the medical domain, the knowledge-based expert systems are generally established based on both *passive* and *active* knowledge. The *passive* knowledge is composed of known facts and past data, while the *active* knowledge consists of production rules in the *if-then* format.

As illustrated in Figure 2.4, a knowledge-based expert system is generally composed of a user interface, a knowledge base, an inference engine and an interpretation element. The knowledge base stores the historical data as well as the accumulated rules, facts and expert experiences, based on which the useful analytical or heuristic information is derived via the inference engine. Through the user interface, an expert can not only provide the domain knowledge as inputs but also supervise the fault identification and isolation process.

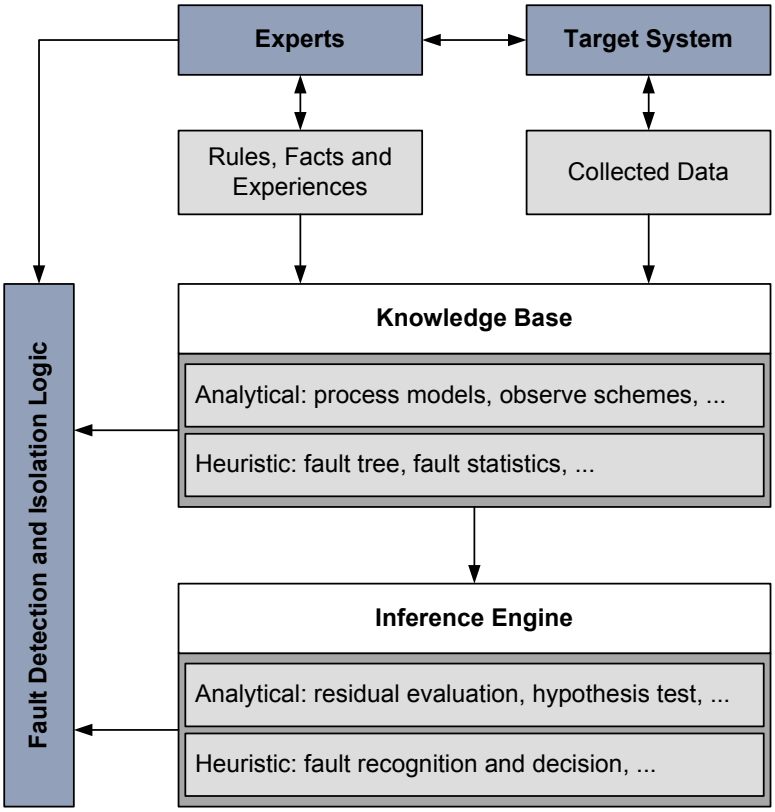

Figure 2.4: General architecture of a knowledge-based expert system for fault detection and isolation

In [Chandrasekaran and Punch, 1988], an approach based on hierarchical classification was developed for the purpose of sensor validation by adding the associated information into the knowledge group. Another method that can systematically identify the redundancies in a sensor network according to their causal relations was

proposed in [Lee, 1994] for sensor validation. The liquid-oxygen expert system in [Scarl et al., 1987] predicted the state of the target system using model-based knowledge of both function and structure. Although such an expert system can detect a faulty sensor or any other faulty component in the same way using the model-based reasoning approach, it only provides a solution for sensor validation in specific application domains. In addition to the accumulated domain knowledge, the method proposed in [Kim et al., 1992] utilized the analytical information directly extracted from the sensor measurements to identify a faulty sensor in a heuristic manner. In [Betta et al., 1995], a knowledge-based analytical redundancy approach was proposed to integrate both qualitative models and empirical knowledge into an expert system. In order to apply such an expert system to a measurement station consisting a large number of sensors with high uncertainty, the algorithm developed in [Betta et al., 1997] added another layer for the statistical pre-processing of the measurements according to the optimized residual thresholds derived from the rules in the expert system.

Despite its capability in dealing with qualitative knowledge, the performance of the expert system depends significantly on its design ranging from the different ways of embedding the existing knowledge to the selection of fault thresholds. Furthermore, an expert system requires great efforts during the initial development phase, and has limited capability in handling dynamic systems.

2.2.2.3 Data-driven methods

Different from model and knowledge based methods that both require a deep understanding of the target system, data-driven methods, also known as process history based methods, only require the availability of sufficient data. Various methods have been developed to establish the knowledge database for the underlying system by

extracting characteristic features directly from its past performance data. In the remainder of this section, multivariate statistical methods, Bayesian belief networks, and neural networks, especially their application in the field of sensor validation, will be introduced.

multivariate statistical methods Without an explicit input-output model, multivariate statistical methods, such as Principal Component Analysis (PCA) and Partial Least Squares (PLS), have been widely applied in the process industry. Due to the capability of dimension reduction, multivariate statistical methods have been used for performance monitoring in a system with a high-dimension but correlated or even low signal-to-noise ratio measurements. In [Kresta et al., 1991], a multivariate monitoring procedure analogous to the univariate Shewart Chart was proposed, in which methods are employed to compress available measurements into a low-dimension space while retaining most of the information.

First introduced in [Hotelling, 1933] and later generalized in [Pearson, 1901], the PCA method is able to compress a large amount of correlated data into a much lower-dimension data set. However, due to its limitation as a linear transformation, the use of the PCA method for a nonlinear process leads to the loss of important information [Xu et al., 1992]. In order to overcome such a drawback, a Generalized PCA (GPCA) was proposed in [Gnanadesikan, 1997] by introducing an augmented data set to include necessary nonlinear terms. The kernel PCA method developed in [Scholkopf et al., 1998] extracted the principal components from an augmented input space that were expanded by a nonlinear mapping. In addition, a nonlinear factor analysis method in [Etezadi-Amoli and McDonald, 1983] was developed to approximate an n-dimension data set with $k < n$ latent factors with a nonlinear com-

mon factor model with k-dimension polynomial regression function using the linear least square method. Moreover, a Nonlinear PCA (NPCA) method was presented in [Kramer, 1991] using a five-layer neural network. With a similar network structure, the NPCA method proposed in [Dong and McAvoy, 1996] employed the principal curves algorithm [Hastie and Stuetzle, 1989] to extract nonlinear principal components from the available data and trains the network using the compressed data set. Furthermore, the Multi-way PCA (MPCA) method in [Chen and McAvoy, 1998] introduced a real-time monitoring approach and further extends the conventional PCA method to dynamic systems.

Due to its capability in dimension reduction, the multivariate statistical methods have been widely used for process modeling and fault detection in various applications. In general, a principal component or latent variable plane is first established under normal operations, and then an index is calculated to evaluate the process performance. One of the commonly used index is Squared Prediction Error (SPE) that calculates the perpendicular distance between a new observation and the established principal component plane. Based on the calculated SPE, a proper threshold can be established for fault detection. In order to add the capability of fault isolation, the contribution chart [MacGregor et al., 1994; Tong and Crowe, 1995] and the multi-block method [Chen and McAvoy, 1998; MacGregor et al., 1994] were proposed. The contribution chart determines the contribution from each process variable to the prediction errors, while the multi-block method groups the process variables into several blocks with each corresponding to a specific section of the monitored process. Both methods were demonstrated their capabilities to identify the variables that causes the deviation of the process performance from its normal conditions. As stated in [Gertler and McAvoy, 1997], a strong duality exists between PCA and parity rela-

tions. By virtue of this duality, a partial PCA method was proposed to integrate the fault isolation capability of the structured parity relations into the PCA method. In [Gertler et al., 1999], a direct algebraic method was developed to derive the structured PCA residuals as well as to decouple disturbances. In addition, the existence conditions of such residuals were also stated. Furthermore, the partial PCA method was extended in [Huang et al., 2000] to nonlinear problems using the GPCA and the NPCA methods. However, these methods all require an explicit analytical model of the monitored process for the integration with parity relations.

The use of multivariate statistical methods has also received significant attention for sensor fault detection and identification. In [Dunia et al., 1996], the use of PCA for sensor fault identification by reconstructing each variable with a PCA model in an iterative substitution and optimization manner was presented. In addition, a sensor validity index and its on-line implementation were also proposed for differentiating various types of sensor faults. The method proposed in [Dunia et al., 1996] was also applied for air emission monitoring in [Qin et al., 1997]. The self-validating inferential sensor approach presented in [Qin et al., 1997] further explored the effects of the number of principal components and employs different criteria for its selection in the sensor validation and prediction procedures. The use of PCA for sensor validation was also recently applied in [Kerschen et al., 2005] for the monitoring of structure health.

The method proposed in [Qin and Li, 2001], as an extension to the work in [Gertler and McAvoy, 1997], enabled the detection and isolation of two faulty sensors by generating a set of structured residuals, each decoupled from one subset of faults but most sensitive to others. Moreover, the multi-block method was employed in [Wang and Xiao, 2004] for sensor validation in an air-handling unit, in which a contribution

chart along with a few simple expert rules was used for fault isolation. In [Kaistha and Upadhyaya, 2001], the direction of each fault scenarios is first obtained using the Singular Value Decomposition (SVD) on the state and control function prediction errors, and fault isolation was then accomplished from projection on the derived fault directions. In [Benitez-Perez et al., 2005], a Self-Organizing Map (SOM) was first trained for the normal and various faulty process behaviors based on the principal components of the available measurements. Fault isolation was then accomplished by calculating the similarity between the observations with the trained SOM.

For nonlinear processes, an approach was developed in [Huang et al., 2000] to detect sensor and actuator faults by integrating the capability of GPCA and NPCA with the advantages of partial PCA. In [Cho et al., 2004], a sensor fault identification method was proposed using kernel PCA based on two new statistics that were defined as the contribution of each variable to the monitoring statistics of Hotelting's T^2 and SPE. The auto-associative neural network, also considered as a nonlinear extension of PCA, was used to detect, identify, and reconstruct faulty sensors in distillation columns [Kramer, 1991], nuclear plants [Hines et al., 1998], and engine systems [Guo and Musgrave, 1995; Mesbahi, 2001; Uluyol et al., 2001]. In these applications, an auto-associative neural network was first constructed to estimate the measured variables using the current sensor measurements, and then a sensor whose measurements deviate significantly from the estimated values was identified as faulty. However, since measurements from the faulty sensor remained as the inputs to the neural network, the inaccurate estimated values of the measured variables may lead to wrong identification of the faulty sensor. Thus, only the measurements that are most consistent with the PCA model are used in [Wise and Ricker, 1991] as the inputs to the neural network.

Noise analysis in the frequency domain has also been used for the detection of sensor faults. Such methods extract the low-pass filtering characteristics exhibited by most process plants and closed-loop systems, which allows the noise power at higher frequency bands to be used for fault detection [Ying and Joseph, 2000]. After the power spectra of the sensor measurements at different frequency bands are calculated, they are then compared with the pattern established under normal operations for the identification of a faulty sensor. Noise analysis is able to isolate the effects of measurement noise and process disturbances from those caused by the fault within the sensor itself. In [Luo et al., 1998], an approach for sensor validation that integrated the non-parametric empirical modeling and statistical analysis was proposed. Represented in wavelets, the sensor signal was decomposed into different frequency bands, among which specific features were calculated and used for the diagnosis of faulty operation. This work was then extended in [Luo et al., 1999] to dynamic processes by taking into account a window of the sensor data and then applying PCA decomposition to the matrix formed by them. The approach proposed in [Ying and Joseph, 2000] used PCA to reduce the space of secondary variables derived from the power spectrum.

The use of PLS methods for sensor fault detection was originated in [Wise et al., 1989]. It was shown that the PLS monitoring scheme was more sensitive to sensor failures than the PCA method. To address the issue of multiple sensor faults, an algorithm based on a hypothesis testing procedure, in which the ratio of the variances of PLS regression residuals to their means was employed as the index for sensor validation, was proposed in [Negiz and Cinar, 1992]. However, this method is only applicable when there is no significant correlation among the residuals of each variable. An alternative approach, proposed in [Negiz and Cinar, 1997], used a

state-space modeling paradigm based on canonical variable analysis to incorporate the dynamic process information so that the generated residuals were independent.

Bayesian networks A Bayesian network, also known as a Bayesian belief network, is a directed acyclic graph that represents a set of random variables and their probabilistic dependencies. Each node in the network represents a prepositional variable that has a finite set of mutually exclusive states, while each directed arc between two nodes denotes their causal relationship. Each child node is associated with a conditional probability given the state of its parent node, and each root node is associated with *a priori* probability. The probability distribution in a Bayesian network updates following probabilistic inference procedures when new observations, referred as evidence, are available. An example of the Bayesian network is illustrated in Figure 2.5. The Bayesian network, $G = (V, E)$, is composed of the nodes $X = (X_v)_{v \in V}$, $V = (1, 2, 3, 4, 5)$ representing the set of random variables, and the directed links $E = \{(X_1, X_3),\ (X_1, X_4),\ (X_2, X_4),\ (X_4, X_5)\}$ describing the causal relationships among the variables. Given the *a priori* probabilities associated with the root variables X_1, X_2, and the conditional probabilities associated with each directed link as defined in E, the probability of any joint distribution can be calculated using the chain rule as

$$P(X_1 = x_1, \ldots, X_n = x_n) = \prod_{v=1}^{n} P(X_v = x_v | X_{v+1} = x_{v+1}, \ldots, X_n = x_n) \qquad (2.2)$$

As stated in [Neapolitan, 1990; Pearl, 1998], the Bayesian network is the most complete and consistent framework for processing uncertain knowledge, thus providing a better approach than the traditional knowledge-based inferential mechanism. First applied in steady-state operations, Bayesian networks were employed for the detection and identification of emerging sensor faults [Rojas-Guzman and Kramer,

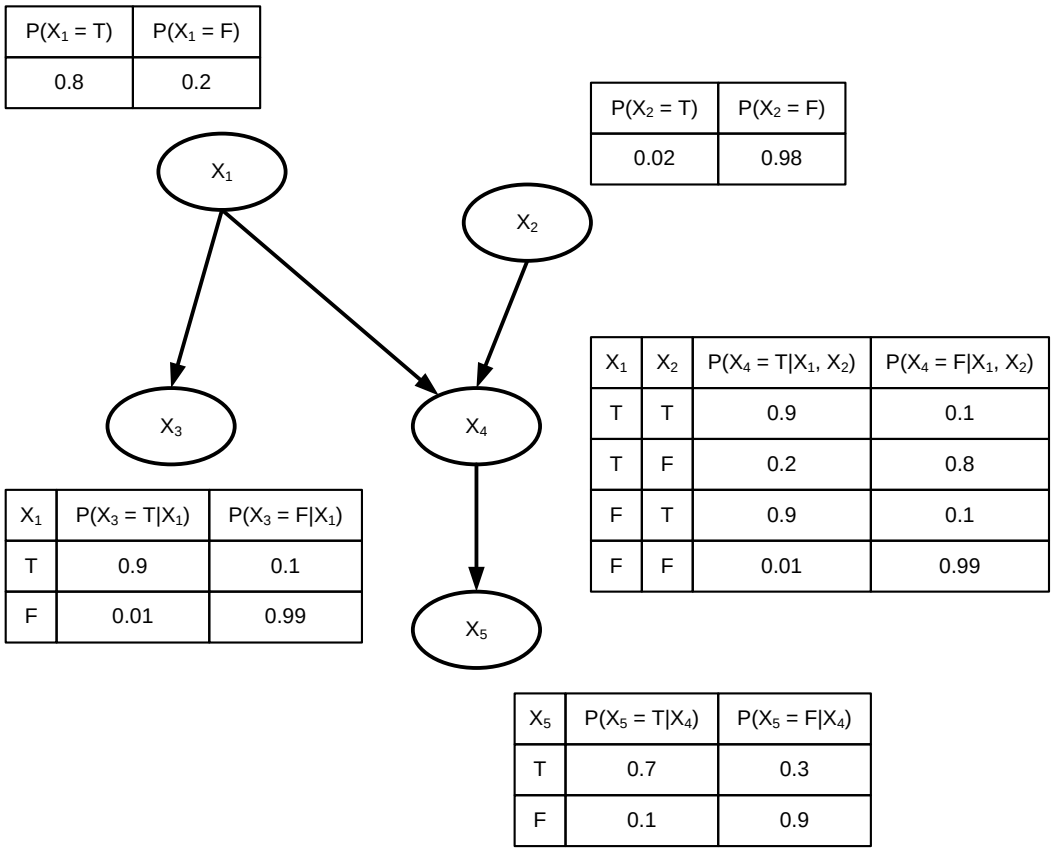

Figure 2.5: Bayesian network example

1993; Ibarguengoytia et al., 2001, 2006; Mehranbod et al., 2003; Mengshoel et al., 2008; Krishnamoorthy, 2010].

The work in [Nicholson and Brady, 1994] was the first attempt to apply dynamic Bayesian networks for the detection and identification of sensor faults, in which sensor observations of discrete events were taken as evidences to the network. Due to the importance of sensor validation during process transitions, methods proposed in [Nicholson and Brady, 1994; Aradhye, 2002; Mehranbod et al., 2005] used dynamic Bayesian networks that were capable of capturing the probabilistic distribution in a changing process. Given the sensor measurements under normal operations, a model that represents the probabilistic relations among measured variables can be established using the Bayesian network learning algorithm. The developed model can

then be used to estimate the expected values of the measured variables via probabilistic propagation. As a result, a sensor whose measurements depict significant inconsistency with the estimated values is detected as faulty.

Due to the propagation of a sensor fault in the network, the estimated values of one sensor may be different from its measurements because they are calculated using the readings of another faulty sensor, which is defined as an apparent fault in [Ibarguengoytia et al., 2001]. In order to distinguish between a real sensor fault and an apparent one, a constraint management method based on the Markov blanket theory was proposed. As an extension to the work in [Ibarguengoytia et al., 2001], the methodology proposed in [Ibarguengoytia et al., 2006] used two Bayesian networks, one identifying a list of sensors with potential faults and the other one isolating the real and apparent sensor faults. In addition, entropy-based selection scheme was developed to determine the sequence of sensors for validation so that sensors with more reliable information are validated first. However, since the network constructed can not handle temporal elements explicitly, separate networks may need to be established for different phases of the process and problems in modeling a time-dependent system may arise.

As illustrated in Figure 2.6, various single-sensor models, used as the building blocks for the development of a Bayesian network for the monitored process, have been proposed in literature. Each associated with discrete states, the four nodes in Model I [Rojas-Guzman and Kramer, 1993] are linked in the following algebraic equation.

$$R_a = X_a + B_a + N_a \tag{2.3}$$

where X_a and R_a denote the real and measured values of the variable a, while B_a and N_a denote the bias and noise associated with the measured value X_a. When a

bias or noise fault occurs in the sensor, the state probabilities at its nodes B_a and N_a deviate significantly from their nominal values.

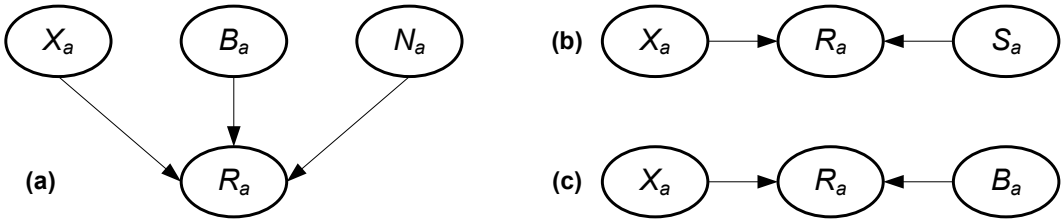

Figure 2.6: Single-sensor Bayesian network models proposed in literature: (a) Model I [Rojas-Guzman and Kramer, 1993], (b) Model II [Aradhye, 2002], and (c) Model III [Mehranbod et al., 2003]

In Model II, a new node S_a is created to denote the status of a sensor. As stated in [Aradhye, 2002], node S_a was associated with four discrete states: normal, biased, noisy, completed failed. Without a mathematical model, functions are selected for the three faulty states to update the probability distribution at node S_a based on their effects. Thus, by tracking the probability at node S_a, sensor validation can be accomplished. However, the one-to-one mapping between causes and effects makes Model II impractical [Mehranbod et al., 2003, 2005]. In Model III, the three nodes are related as

$$R_a = X_a + B_a \tag{2.4}$$

In the form of Model III, the single-sensor models in [Mehranbod et al., 2003] are connected at node X_a based on their cause-effect relations for modeling a steady process monitored with multiple sensors. The detection of a sensor fault is accomplished by tracking the state probability at node B_a, while the isolation of a bias, drift, and noise fault in the sensor is achieved by analyzing the patterns in their changes over time. In addition, the issue of selecting appropriate design parameters in the Bayesian network for the application of sensor validation was also addressed in [Mehranbod et al., 2003]. This work was further extended to transient operations

in [Mehranbod et al., 2005] by introducing adaptable nodes into Model III.

artificial neural networks Given sufficient historical process data, an Artificial Neural Network (ANN) is able to learn the relations among the measured variables. In the past few decades, neural networks have been employed in system modeling as well as fault detection and isolation in various applications. The application of back-propagation neural networks for online sensor validation in fault-tolerant flight control systems was investigated in [Napolitano et al., 1998; Campa et al., 2002]. Known for the learning speed, the probabilistic neural networks were also applied to the detection and isolation of sensor faults in [Mathioudakis and Romessis, 2004; Romesis and Mathioudakis, 2003], even in the presence of system failures. In addition, the cerebellar model articulation controller, one type of neural network based on a model of the mammalian cerebellum, was employed in [Yang et al., 1996] to detect and compensate for failures in capacitance and thermal sensors, thus improving its modeling accuracy of machine tools. Moreover, the neural network proposed in [Yen and Feng, 2000] was developed for the online estimation of critical variables based on the *divide and conquer* strategy and the winner-take-all rule. A growing fuzzy clustering algorithm was employed to divide a complicated problem into a set of simple sub-problems and then an expert was assigned to each sub-problem locally. By integrating information in the frequency domain, the residuals between the measurements and the values that were estimated from the winner-take-all-expert network were used to generate indicators of sensor faults. This method was further extended in [Bernieri et al., 1995] to detect and isolate multiple faults in an automatic measurement systems for the induction motor by developing an algorithm to determine proper thresholds for the output winners. Furthermore, a method was developed

in [Betta et al., 1995, 1996, 1998] to integrate the advantages of neural networks and knowledge based expert systems. The architecture of the neural networks were determined based on the knowledge-based redundancies, while their architecture parameters were optimized using the genetic algorithm. This method demonstrated desirable accuracy and selectivity in fault detection and isolation during steady operations, but it is not applicable to systems under transient conditions due to its insufficient modeling capability. In order to improve its diagnostic performance in dynamic systems, a hybrid solution that integrated neural networks and redundancy rules was presented in [Capriglione et al., 2002].

Methods that involve multiple neural networks have also been proposed in the literature for the detection and isolation of instrument faults. In [Guo and Nurre, 1991], a method using two neural networks was developed, in which one was used to identify the faulty sensor with inconsistent measurements and the other one was used to recover their values. Another method in [Brownell, 1992] developed four neural networks to accomplish (1) signal validation and identification of redundant relations among measured variables, (2) estimation of measured variables based on the identified redundancies, (3) detection and isolation of sensor faults, and (4) estimation of unobserved control parameters. Neural network techniques were also implemented in [Perla et al., 2004] following the generalized observer scheme [Frank, 1987] to validate sensor measurements in a dynamic system with time delays. Furthermore, a systematic methodology that combined the advantages of artificial intelligence and statistical analysis was developed in [Alag et al., 2001] to address the issues of sensor validation in the presence of multiple faulty sensors or system malfunctions. Based on direct measurements from the sensors, the proposed method was developed to accomplish four tasks including redundancy creation, state prediction, sensor mea-

surement validation and fusion, and fault detection via residual change detection.

2.3 Research Challenges

Despite these existing research efforts, the detection, isolation, and compensation of the instrument faults in a dynamic system remains a challenging problem. In the application of the automotive engine, for instance, the demands for higher fuel efficiency and reduced emissions has driven the development of advanced powertrain technologies such as the turbocharger and the dual-cam variable valve-train. The introduction of additional components into the conventional engine enables the exploitation of advanced combustion strategies, which also raises the need for additional sensing elements such as the ethanol sensor in flex-fuel vehicles for the development of dedicated controls. In the mean time, the use of additional sensors also introduces system complexity, and thus raises challenges in diagnosis.

Due to the cost constraints in most applications, the use of a hardware redundancy approach is limited. Moreover, despite accumulated system knowledge, the additional components and sensing elements introduce uncertainties into the system. Thus, significant efforts are required to augment the existing model-based diagnostic system or knowledge-based expert system. With advances in measurement and simulation technologies, the data-driven approach has demonstrated promising potentials in various domains including modeling, optimization, controls, and diagnosis. However, due to the lack of a thorough understanding of the target system, such an approach could encounter challenges in the identification and compensation of faults. Furthermore, the requirements of real-time system monitoring, such as the On-Board Diagnosis (OBD) requirements in automotive applications, raises additional challenges due to the constraints of online memory and computation ca-

pabilities. Therefore, approaches that could integrate the existing first-principle knowledge into the data-driven approaches are necessary to deal with the detection, isolation, and compensation of instrument faults in a dynamic system with increasing complexity.

The goal of the proposed research is to explore methods that can accomplish quantitative assessment of sensor performance in a sensor network and compensation of the effects of its degradation on system control and diagnosis. Without the use of duplicate sensing hardware, the method aims to utilize the embedded analytical redundancies for the detection and isolation of faulty sensors, even in the presence of failures in the monitored system. With a quantitative assessment of the performance of each sensor within the network, the measurements of a faulty sensor can be reconstructed and its effects on the controller as well as other measured variables can be compensated, thus improving the reliability of the target system.

In order to accomplish an independent and quantitative assessment of the performance within a sensor network and its monitored system, research is needed to overcome the following challenges:

- Identify the underlying analytical redundancies in the target system using sensor measurements and control signals observed during regular operations rather than using special inputs
- Isolate the intertwined dynamics of the sensor(s) and the monitored system,
- Eliminate the influences of a fault in one sensor on other sensors
- Isolate of the effects of a fault in the sensor network and one in the monitored system on the collected measurements.

CHAPTER III

Sensor Fault Detection and Isolation in Linear Systems

3.1 Introduction

In this chapter, a subspace model identification based approach is proposed to identify and track the various dynamic components in a linear system. As the sensor measurements depict compound behaviors, the model identified using the control signals and sensor readings should capture the dynamics of the monitored system and the sensor itself. Inspired by the fact that the dynamics of the sensor is much faster than that of the monitored system, this approach is employed to detect, isolate, and compensate for the incipient sensor failures without the need for any redundant sensor or special input signals. In this work, the time constant and the DC gain are identified as the key performance indicators because they characterize the dynamic and steady-state response of a system. The proposed approach extracts and tracks the dominant time constant and gain of the monitored system and the sensor, thus enabling quantitative assessment of the incipient failure.

The reminder of this chapter is organized as follows. In Section 3.2, an approach that can identify the slow and fast dynamics in a linear system and track the associated DC gains is presented to detect and isolate the performance degradation in the monitored plant and that in the sensor. Once the source of the degradation is

identified, the proposed approach compensates the incipient failure in the sensor. In order to evaluate the performance of the proposed approach, a simulation model is developed in Section 3.3 for the automotive electronic throttle system with an angular sensor. The proposed approach has been shown to be effective in detecting and isolating the degradation of the throttle position sensor from that of the electronic throttle system.

3.2 Methods

3.2.1 Problem Statement

The problem of sensor performance assessment considered in this chapter is based on the system structure shown in Figure 3.1, where sensor readings contain the dynamics of the monitored system and the sensor itself, as well as the influence of process disturbances, w_p(t), and measurement noise, w_n(t). Sensor performance will be assessed using the observed control signal $u_c(t)$ and measured output signal $y_m(t)$ without the use of redundant sensors. The method for detection, isolation, and compensation of sensor degradation is developed based on the following assumptions.

(i). There is no nonlinearity involved in the compound system that is composed of a monitored system and a sensor monitoring the system output.

(ii). The dynamics of the sensor is much faster than that of the monitored system. This assumption is not very restrictive because the dynamics of the sensor should be at least 5-10 times faster than that of the monitored system so that the dynamics of the monitored system can be captured.

(iii). The process disturbances $\mathbf{w}_p$(t) and measurement noise $\mathbf{w}_n$(t) are wide-sense stationary processes.

It should also be noted that the process disturbances $\mathbf{w}_p(t)$ and the measurement noise $\mathbf{w}_n(t)$ are assumed to enter the target system at different locations. The process disturbances $\mathbf{w}_p(t)$ enters the system between the monitored plant and the sensor, while the measurement noise $\mathbf{w}_n(t)$ enters after the sensor. This assumption is critical for the isolation of the gain factors in the monitored plant and sensor, which is described in more details in the remainder of this section.

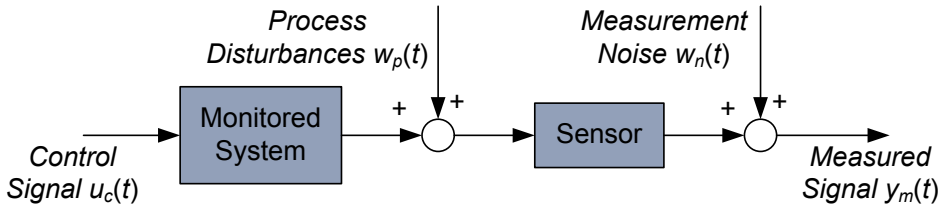

Figure 3.1: Structure of the compound system

Since the compound system in Figure 3.1 is linear and causal, the measured signals y_m can be described in terms of the available input signals u_c and the unknown process disturbances w_p and measurement noise w_n in the following relation.

$$Y_m(s) = G_p(s)G_s(s)U_c(s) + G_s(s)W_p(s) + W_n(s) \tag{3.1}$$

where $G_p(s)$ and $G_s(s)$ describe the dynamics of the monitored system and the sensor, respectively. In this thesis, $G_p(s)$ and $G_s(s)$ are represented in the following pole-zero-gain form

$$\begin{aligned} G_p(s) &= k_p \frac{N_p(s)}{D_p(s)} \\ &= k_p \frac{(s+z_1^p)(s+z_2^p)\dots(s+z_{n_p}^p)}{(s+p_1^p)(s+p_2^p)\dots(s+p_{m_p}^p)}, \quad n_p < m_p \\ G_s(s) &= k_s \frac{N_s(s)}{D_s(s)} \\ &= k_s \frac{(s+z_1^s)(s+z_2^s)\dots(s+z_{n_s}^s)}{(s+p_1^s)(s+p_2^s)\dots(s+p_{m_s}^s)}, \quad n_s < m_s \end{aligned} \tag{3.2}$$

where k_p, N_p, and D_p are the gain, numerator, and denominator of G_p, while k_s, N_s, and D_s are those of G_s. In order to describe the dynamics of a high-order

linear time-invariant (LTI) system, each pole of the system transfer function will be associated with a time constant which is defined as the inverse of the distance between the location of the corresponding pole and the imaginary axis in the complex plane. In the remainder of this chapter, we use τ_p and τ_s to denote the time constants associated with the poles of G_p and G_s, respectively.

The time constants and gains of the sensor indicate its response speed and magnification capability with respect to the measured variable. Degraded sensor measurements can be caused by changes in its associated time constant or gain factor. Similarly, according to (3.2), the performance of a monitored system can also be described in terms of its gain and time constants. Thus, to identify the degrading sensor and distinguish its degradation from that in the monitored system, the gains and time constants of the sensor and the monitored system should be identified and tracked simultaneously.

3.2.2 Subspace Identification Algorithms

During the last two decades, subspace identification algorithms have attracted significant interest in control community because they can deal with multiple-input multiple-output (MIMO) system identification in a straightforward way [Van Overschee and De Moor, 1996; Verhaegen and Dewilde, 1992; Viberg, 1995]. Unlike classical approaches, such as the prediction error methods (PEM), subspace model identification (SMI) approaches obtain the Kalman filter states of a dynamic system directly from the input-output data using numerical linear algebra methods such as QR factorization and singular value decomposition (SVD). In this way, SMI methods avoid those iterative and nonlinear optimization procedures used in classical identification approaches, which not only makes them faster in computation but also intrinsically robust from a numerical point of view. Moreover, in SMI methods, the

order of the model is the only user-specified parameter, which can be determined by the inspection of the dominant singular values of a matrix that is calculated during the identification.

In the subspace identification context, the mathematical model of the unknown system is assumed to be given by an n^{th} order causal linear time-invariant (LTI) state-space model:

$$\begin{aligned} x(t+1) &= Ax(t) + Bu(t) + w(t) \\ y(t) &= Cx(t) + Du(t) + v(t) \end{aligned} \tag{3.3}$$

subjected to zero-mean, white noise processes $w \in \mathbb{R}^n$ and $v \in \mathbb{R}^l$, with covariance matrix

$$\mathbb{E}\left[\begin{pmatrix} w(i) \\ v(i) \end{pmatrix}\begin{pmatrix} w^T(j) & v^T(j) \end{pmatrix}\right] = \begin{pmatrix} Q & S \\ S^T & R \end{pmatrix}\delta_{ij} \tag{3.4}$$

where sufficient measurements of the input $u \in \mathbb{R}^m$ and the output $y \in \mathbb{R}^l$ are given. Derived from the linear system (3.3), the input-output algebraic equation that leads to the main theorem in SMI methods can be expressed as:

$$\mathbf{Y} = \Gamma_r \mathbf{X} + H_r \mathbf{U} + \Sigma_r \mathbf{W} + \mathbf{V} \tag{3.5}$$

where $\mathbf{Y} \in \mathbb{R}^{rl \times N}$ is the output data matrix which can be constructed by the Hankel matrix using $(N + r - 1)$ past and current data as

$$\mathbf{Y} = \begin{bmatrix} Y_r(t), & Y_r(t+1), & \ldots, & Y_r(t+N-1) \end{bmatrix}$$

where

$$Y_r(j) = \begin{bmatrix} y^T(j), & y^T(j+1), & \ldots, & y^T(j+r-1) \end{bmatrix}^T$$

$\mathbf{X} \in \mathbb{R}^{n \times N}$ is the matrix constructed by the system states $x \in \mathbb{R}^n$, while $\mathbf{U} \in \mathbb{R}^{rm \times N}$, $\mathbf{W} \in \mathbb{R}^{rn \times N}$ and $\mathbf{V} \in \mathbb{R}^{rl \times N}$ are constructed similarly to $\mathbf{Y}$, by arranging properly N

(column) vectors of the input u, system noise w, and observation noise v, respectively. Matrix $\Gamma_r \in \mathbb{R}^{rl\times n}$ is the extended observability matrix, and $H_r \in \mathbb{R}^{rl\times rm}$, $\Sigma_r \in \mathbb{R}^{rl\times rn}$ are lower block triangular matrices consisting of system matrices (for detail structures, see e.g. [Ljung, 1999; Verhaegen and Dewilde, 1992]).

The key problem dealt with by the subspace identification algorithms is the consistent estimation of the column space of the extended observability matrix Γ_r from the input-output data, where Γ_r is defined as

$$\Gamma_r = \begin{bmatrix} C^T & (CA)^T & \cdots & (CA^{r-1})^T \end{bmatrix}^T \tag{3.6}$$

Indeed, if the column space of Γ_r is known, then matrices A and C can be determined (up to a similarity transformation) in a straightforward way by exploiting the shift invariance of the column space of Γ_r. If $\widehat{A}$ and $\widehat{C}$ are known, B, D and x_0 can be estimated by solving the linear regression problem:

$$\arg\min_{B,D,x_0} \frac{1}{N}\sum_{t=1}^{N} \|y(t) - \widehat{C}(qI-\widehat{A})^{-1}Bu(t) - Du(t) - \widehat{C}(qI-\widehat{A})^{-1}x_0\delta(t)\|^2$$

where q is the time-shift operator, and I is the identity matrix.

As proved in [Ljung, 1999], under the assumptions that the input u is persistent and uncorrelated with the process noise w and measurement noise v,

$$\mathcal{O}_r = \frac{1}{N}\mathbf{Y}\Pi_{\mathbf{U}}^{\perp}\Phi^T \tag{3.7}$$

converges to the true Γ_r (up to a similarity transformation) as the number of measurements N goes to infinity. $\Pi_{\mathbf{U}}^{\perp}$ in $\mathcal{O}_r$ performs projection, orthogonal to the matrix $\mathbf{U}$, thus removing the $\mathbf{U}$-term in $\mathbf{Y}$. To further remove the noise term in $\mathbf{Y}$, $\Phi \in \mathbb{R}^{s\times N}$ is constructed by arranging N vectors of $\phi_s \in \mathbb{R}^s$ in various forms, among which a typical choice would be $\phi_s(t) = \begin{bmatrix} y^T(t-1) & \ldots & y^T(t-s_1) & u^T(t-1) & \ldots & u^T(t-s_2) \end{bmatrix}^T$.

Rather than being performed directly on $\mathcal{O}_r$, the singular value decomposition is then applied as

$$W_1 \mathcal{O}_r W_2 = \begin{pmatrix} U_1 & U_2 \end{pmatrix} \begin{pmatrix} S_1 & 0 \\ 0 & 0 \end{pmatrix} \begin{pmatrix} V_1^T \\ V_2^T \end{pmatrix} = U_1 S_1 V_1^T \tag{3.8}$$

for more flexibility, where $W_1 \in \mathbb{R}^{rl \times rl}$ and $W_2 \in \mathbb{R}^{(ls_1 + ms_2) \times \alpha}$ are the weighting matrices. Existing algorithms such as MOESP, N4SID, and CVA employ different choices of W_1 and W_2. Discussions on these effects can be found in [Bauer et al., 2001; Bauer and Ljung, 2002].

Directly from (3.8), the N4SID algorithm developed in [Van Overschee and De Moor, 1994] is employed in this chapter to determine the order of the system as the number of non-zero singular values in S_1, while the extended observability matrix is estimated as $\Gamma_r = U_1 (S_1)^{1/2}$. However, when the signal-to-noise ratio (SNR) in the measurements is small, N4SID algorithms would not be able to provide an accurate estimation of the system order because the separation between the signal and noise singular values in S_1 tends to vanish [Bittanti et al., 1997, 2000]. To achieve high accuracy in pole identification, wavelet denoising [Donoho, 1995; Donoho and Johnstone, 1994; Donoho et al., 1995] techniques could be employed to pre-process the noisy measurements.

If we define $\widehat{\mathbf{Y}}$ as the k-step ahead predictors, then it follows from (3.5) that $\widehat{\mathbf{Y}} = \Gamma_r \widehat{\mathbf{X}}$, where $\widehat{\mathbf{X}}$ is made up from the predicted Kalman-filter states $\widehat{x}(t|t-1)$ which is the best estimate of $x(t)$ based on past input-output data. Thus, the state sequence $\widehat{\mathbf{X}}$ can be obtained as $\widehat{\mathbf{X}} = \Gamma_r^{\dagger} \widehat{\mathbf{Y}}$, where the symbol † indicates the operation of pseudo-inverse [Strang, 1998]. With the states $\widehat{x}(t)$ given, we can estimate the

process and measurement noise as

$$\begin{aligned} w(t) &= \widehat{x}(t+1) - \widehat{A}\widehat{x}(t) - \widehat{B}u(t) \\ v(t) &= y(t) - \widehat{C}\widehat{x}(t) - \widehat{D}u(t) \end{aligned} \tag{3.9}$$

and matrices S, R, and Q in (3.4) can be estimated in a straightforward fashion. Given $\widehat{A}$, $\widehat{C}$, $\widehat{S}$, $\widehat{R}$, and $\widehat{Q}$, the Kalman gain K could then be computed from the Riccati equation.

3.2.3 Detection and Isolation of an Incipient Sensor Failure

Using the N4SID algorithm, the compound system in Figure 3.1 with model structure (3.3) is identified as

$$\begin{aligned} \widehat{x}(t+1) &= \widehat{A}\widehat{x}(t) + \widehat{B}u_c(t) + \widehat{K}e(t) \\ y_m(t) &= \widehat{C}\widehat{x}(t) + \widehat{D}u_c(t) + e(t) \end{aligned} \tag{3.10}$$

where the residuals e are white noise with zero-mean, if the model is properly fitted[1] [Ljung, 1999]. This state-space model can be transformed into a transfer matrix as

$$Y_m(q) = \left[\widehat{C}(qI - \widehat{A})^{-1}B + \widehat{D}\right] U_c(q) + \widehat{C}(qI - \widehat{A})^{-1}\widehat{K}E(q) + E(q) \tag{3.11}$$

By comparing (3.1) and (3.2) with (3.11), it follows that $\widehat{C}(qI - \widehat{A})^{-1}\widehat{B}$ and $\widehat{C}(qI - \widehat{A})^{-1}\widehat{K}$ identify $G_p(s)G_s(s)$ and $G_s(s)$ in the discrete domain, respectively. Tracking of the poles of $\widehat{C}(qI - \widehat{A})^{-1}\widehat{B}$ readily yields the time constants of the monitored system and sensor. Due to the presence of gradual degradation, the system in (3.10) slowly varies with time. Originally developed for time-invariant systems, the N4SID algorithm can be applied for time-varying systems if the input-output algebraic relations in (3.5) change slowly [Verhaegen and Deprettere, 1991; Ohsumi and Kawano,

[1] In the reminder of this chapter, we assume the model is properly fitted

2002]. Assuming a gradual degradation in (3.1), the use of a fixed-length moving window in this work enables the N4SID algorithm to track the change of system dynamics. The selection of a small moving window enables fast detection of a change in the target system, but makes the parameter estimation more sensitive to system noise and introduces higher computational requirements.

Within each of these windows, a state-space model in the form of (3.10) is estimated. The matrices of a model identified in the i^{th} window are denoted as $\widehat{A}^i$, $\widehat{B}^i$, $\widehat{C}^i$, $\widehat{D}^i$, and $\widehat{K}^i$. In this way, the dynamics of the system can be continuously monitored with all its associated time constants identified. Then, based on the assumption that the sensor should have much faster dynamics than the monitored system, the time constants associated with the monitored system are expected to be much larger than those of the sensor. Therefore, the changes in the dynamics of the monitored system and those of the sensor can be isolated. Moreover, from $\widehat{C}(qI - \widehat{A})^{-1}\widehat{B}$, the term $k_p k_s$ can be estimated in the product form. With $\widehat{C}(qI - \widehat{A})^{-1}\widehat{K}$ expressed in the form of $\widehat{k}_k \frac{N_k(q)}{D_k(q)}$, it follows from (3.1) and (3.2) that in the i^{th} window

$$\widehat{k}_k^i \cdot \mathbf{std}(e^i) = k_s^i \cdot \mathbf{std}(w_p^i) \tag{3.12}$$

where $\mathbf{std}(\cdot)$ denotes the standard deviation of a probability distribution. Then, k_s can be continuously estimated as

$$k_s^i = \widehat{k}_k^i \frac{\mathbf{std}(e^i)}{\mathbf{std}(w_p^i)} \tag{3.13}$$

Although the statistical properties of the process disturbance are unknown, the changes of the sensor gain can be detected and isolated using the wide-sense stationarity of w_p through normalization of the sensor gain k_s^i. The normalized sensor gain $(k_s^i)^n$ in the ith window, can be estimated as

$$(k_s^i)^n = \frac{k_s^i}{k_s^0} = \frac{\widehat{k}_k^i}{\widehat{k}_k^0} \cdot \frac{\mathbf{std}(e^i)}{\mathbf{std}(e^0)} \cdot \frac{\mathbf{std}(w_p^0)}{\mathbf{std}(w_p^i)} = \frac{\widehat{k}_k^i}{\widehat{k}_k^0} \cdot \frac{\mathbf{std}(e^i)}{\mathbf{std}(e^0)} \tag{3.14}$$

where the 0^{th} window is considered as the reference[2] window for normalization. Subsequently, the normalized gain of the monitored system $(k_p^i)^n$ can be obtained in a straightforward way. The identification and isolation of gain changes in the sensor and monitored plant are summarized in Figure 3.2.

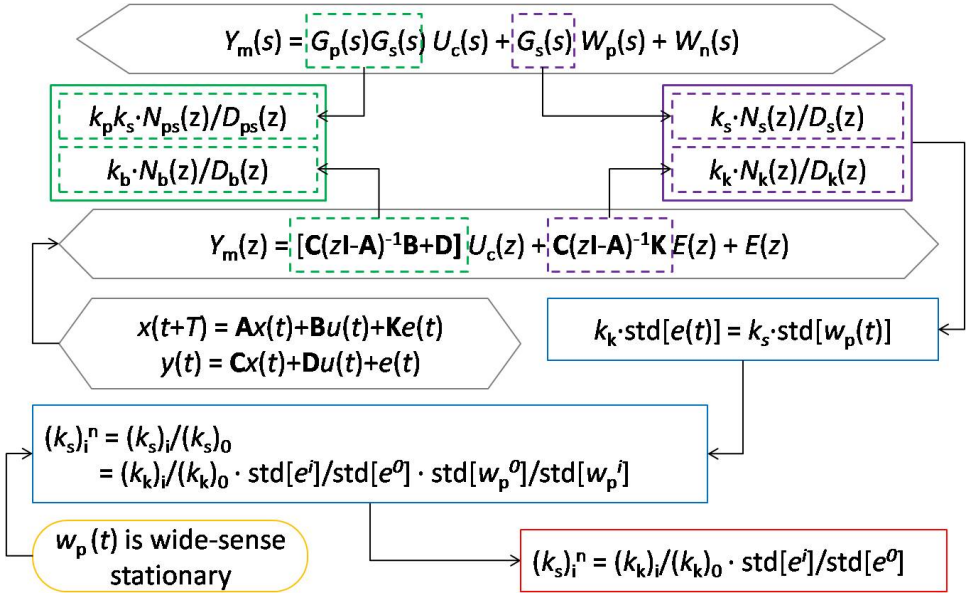

Figure 3.2: Summary of equations to identify gain changes in sensors and monitored plant

Based on this method summarized in Figure 3.3, a sensor with a changed response and/or deteriorated magnification capability can be detected and isolated.

3.2.4 Compensation for an Incipient Sensor Failure

The identified models for the monitored system and the sensor can be utilized to temporarily reconstruct the measurements of the degrading sensor before the sensor is replaced or repaired. This could improve accuracy of the collected information despite the presence of sensor degradation. Once significant changes in any key performance indicator of the sensor are detected, its readings should be corrected correspondingly to compensate for the adverse effect of the degrading parameter, before the sensor readings are used for system performance diagnosis and control.

[2]The reference window should be a window we know the sensor is behaving normally.

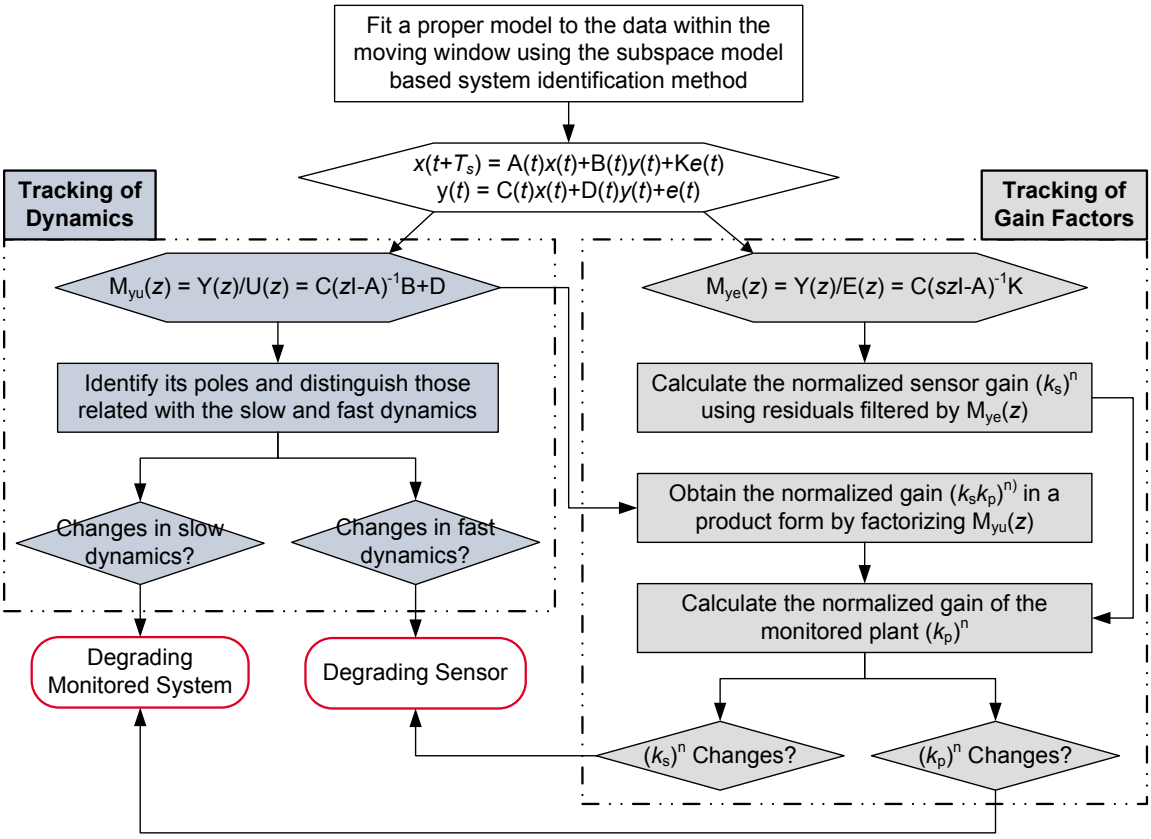

Figure 3.3: Flow chart of the procedures to detect and isolate an incipient sensor failure

As shown in Figure 3.4, if the gain of the sensor decreases, its readings should be inversely magnified with its normalized gain $(k_s^i)^n$ within each time window so that the adverse effects caused by the magnification capability deterioration can be compensated. On the other hand, if the dynamics of the sensor changes, its readings should be reconstructed with a properly constructed filter $\frac{d_s(q)}{d_s^{nom}(q)}$, where $d_s(q)$ and $d_s^{nom}(q)$ denote the degraded and nominal dynamics in the sensor, respectively.

The level of normalized gain or time constant changes at which sensor degradation is considered significant enough, can be selected either in an *ad hoc* way or through more systematic threshold decision schemes, such as those used in Statistical Process Control (SPC) [Norton, 2005; Weaver and Richardson, 2006].

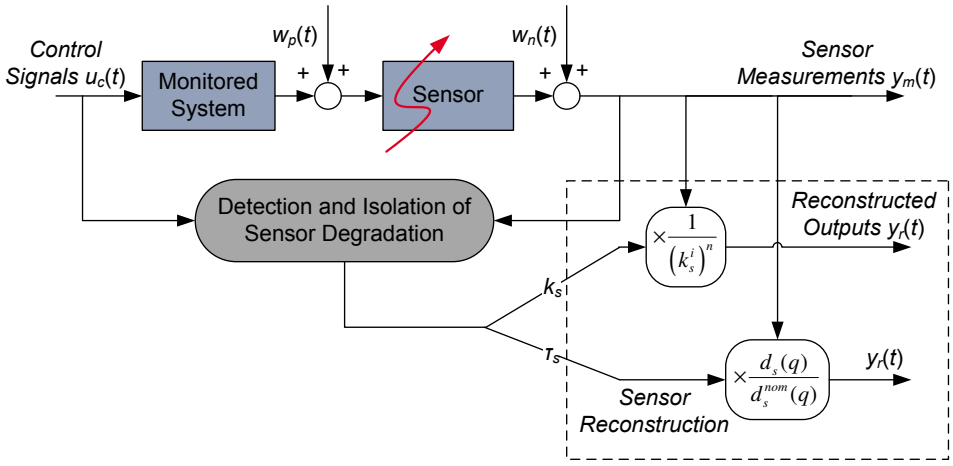

Figure 3.4: Reconstruction scheme for an incipient sensor failure

3.3 Case Study

3.3.1 Electronic Throttle Model

In modern vehicles, an electronic throttle realizes the link between the driver gas pedal and throttle plate with a DC servomotor, which enables the engine control unit to set optimal throttle position reference values for various engine operation modes. In this way, an electronic throttle not only improves drivability, fuel economy, and emissions, but also provides the implementation of engine-based vehicle dynamics control system including traction control [Huber et al., 1991]. The electronic throttle consists of a servo-motor throttle body, a Throttle Position Sensor (TPS), and a position control strategy.

To provide a basis for the development of health monitoring strategies, the dynamic system model, illustrated in Figure 3.5, is presented in [Conatser et al., 2004] to describe the behavior of an electronic throttle body. Based on this model and after neglecting the small torque caused by the airflow through the throttle plate, a linear process model with its nomenclature listed in Table 3.1 is developed in the

state-space model form

$$\begin{bmatrix} \dot{x}_1 \\ \dot{x}_2 \\ \dot{x}_3 \end{bmatrix} = \begin{bmatrix} 0 & 1 & 0 \\ -\frac{K_{sp}}{J} & -\frac{K_f}{J} & -\frac{NK_t}{J} \\ 0 & -\frac{NK_b}{L_a} & -\frac{R_a}{L_a} \end{bmatrix} \begin{bmatrix} x_1 \\ x_2 \\ x_3 \end{bmatrix} + \begin{bmatrix} 0 \\ 0 \\ \frac{1}{L_a} \end{bmatrix} u_c, \tag{3.15}$$

and

$$y = x_1 \tag{3.16}$$

with the system state and input vectors defined as $x = \begin{bmatrix} \theta & \dot{\theta} & i_a \end{bmatrix}^T$, $u_c = e_a$, and $\theta = \theta_t + \theta_0$, and parameters $J = N^2 J_m + J_g$ and $K_f = N^2 b_m + b_t$.

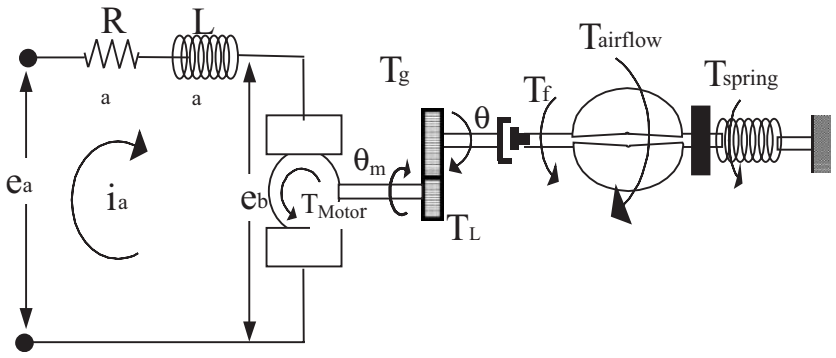

Figure 3.5: Mechatronic system diagram for throttle-by-wire system [Conatser et al., 2004]

Table 3.1: Nomenclature for the electronic throttle system

Symbol	Description	Symbol	Description
b_m	motor damping constant	b_t	throttle damping constant
e_a	motor voltage	i_a	armature current
J_g	throttle moment of inertia	J_m	motor inertia
J	equivalent moment of inertia	K_b	back emf constant
K_{sp}	throttle spring constant	K_t	motor torque constant
L_a	armature inductance	N	gear ratio
R_a	armature resistance	T_a	torque due to airflow
T_g	torque transmitted from gears	T_L	load torque
T_m	torque applied by motor	T_{sp}	torque due to return spring
θ	throttle plate angular position	θ_0	pre-tension angle of spring
θ_m	armature angular position	θ_{ang}	measured throttle angle position
τ_{TPS}	time constant of a TPS	k_{TPS}	voltage constant of a TPS

Taken as the feedback signal, the position of the throttle plate is then measured by TPS. Inside the TPS is a variable resistor with its wiper arm connected to the

throttle plate. As the wiper arm moves along the resistor, its output voltage changes accordingly, thus indicating the position of the throttle plate. Due to existence of magnetic permeability in materials, inductance is also present in the resistor. Thus, the dynamics of the TPS can be modeled as a first-order system with a small time constant.

In (3.15), linear models are utilized for the transmission friction and dual return spring, which significantly simplifies the process model. For the development of a control strategy including compensation of dynamic friction and dual return spring nonlinearities at the limp-home position, a more complex model has been developed in [Scattolini et al., 1997].

3.3.2 Detection and Isolation of an Incipient Sensor Failure

A Matlab/Simulink[3] simulation with the set of parameters used in Conatser et al. [2004] has been created and run for $t = 50.0s$ using a time-step of $\Delta t = 1.0 \times 10^{-4}s$. A set of failures, as listed in Table 3.2, are introduced to explore the detection and isolation capability of the method developed above. These failures are introduced by gradually increasing ($\nearrow$) or decreasing ($\searrow$) the corresponding model parameters, starting at time moment $t = 25.0s$ in the simulation. Fault 1 and Fault 2 are incipient TPS failure caused by an increase of time constant, τ_{TPS}, and a decrease of gain, k_{TPS}, while Fault 3 and Fault 4 are Electronic Throttle (ET) system failure caused by an increase of motor torque constant, K_t, and back emf constant, K_b.

Table 3.2: Faults, parameter changes, and fault decision table

			Parameter values					
No.	Parameter	Magnitude (%)	$\widehat{\tau}_{TPS}$	$\widehat{k}^{(n)}_{TPS}$	$\widehat{k}^{(n)}_{ET}$	$\widehat{a}_1$	$\widehat{a}_2$	$\widehat{a}_3$
1	τ_{TPS}	50 ($\nearrow$)	$\nearrow$	–	–	–	–	–
2	k_{TPS}	40 ($\searrow$)	–	$\searrow$	–	–	–	–
3	K_t	40 ($\searrow$)	–	–	$\searrow$	–	$\searrow$	–
4	K_b	40 ($\searrow$)	–	–	–	–	$\searrow$	–

[3]Registered trademarks of The MathWorks, Natick, MA, 2002.

In this work, thresholds are established in a straightforward fashion as the 3σ limits using standard SPC techniques [Norton, 2005]. Under nominal conditions, the estimated time constants and normalized gains associated with the TPS and ET system are illustrated in Figure 3.6. The time constants, τ_{TPS} and $\tau_{ET} = [\ \tau_{ET,1},\ \ \tau_{ET,2},\ \ \tau_{ET,3}\ ]^T$, identified in Figure 3.6(a) have different magnitudes of 10^{-4},10^{-3},10^{-2}, and 10^{0}. Based on the prior knowledge that TPS has first-order dynamics and its response should be at least 2-5 times faster than that of the ET system, it can be concluded that the time constant of magnitude 10^{-4} is that of the TPS. Due to the small sampling time, the estimation errors of the time constants are magnified when the system poles identified in the discrete domain are transformed into the continuous domain. Nevertheless, despite the occasional outliers, the estimated time constants and gains in Figure 3.6 stay within the thresholds while the system is fault-free.

The effects of Fault 1 and Fault 2 are shown in Figure 3.7 and Figure 3.8, respectively. It can be seen that only parameters $\widehat{\tau}_{TPS}$ and $\widehat{k}_{TPS}$ exceed their thresholds showing the expected degradation pattern in Figure 3.7 and Figure 3.8, respectively. Figure 3.9 and Figure 3.10 show the results from the simulation when Fault 3 and Fault 4 occur in the ET system, respectively. Under both faults, some of the estimated time constants of the ET system exceed the thresholds, while both the time constant and gain of the TPS stay within the thresholds. Furthermore, Fault 3 and Fault 4 can be differentiated since $(\widehat{k}_{ET})^n$ exceed the threshold under Fault 3, but stays within the thresholds under Fault 4.

In fact, the compound system can also be expressed in the form of a transfer

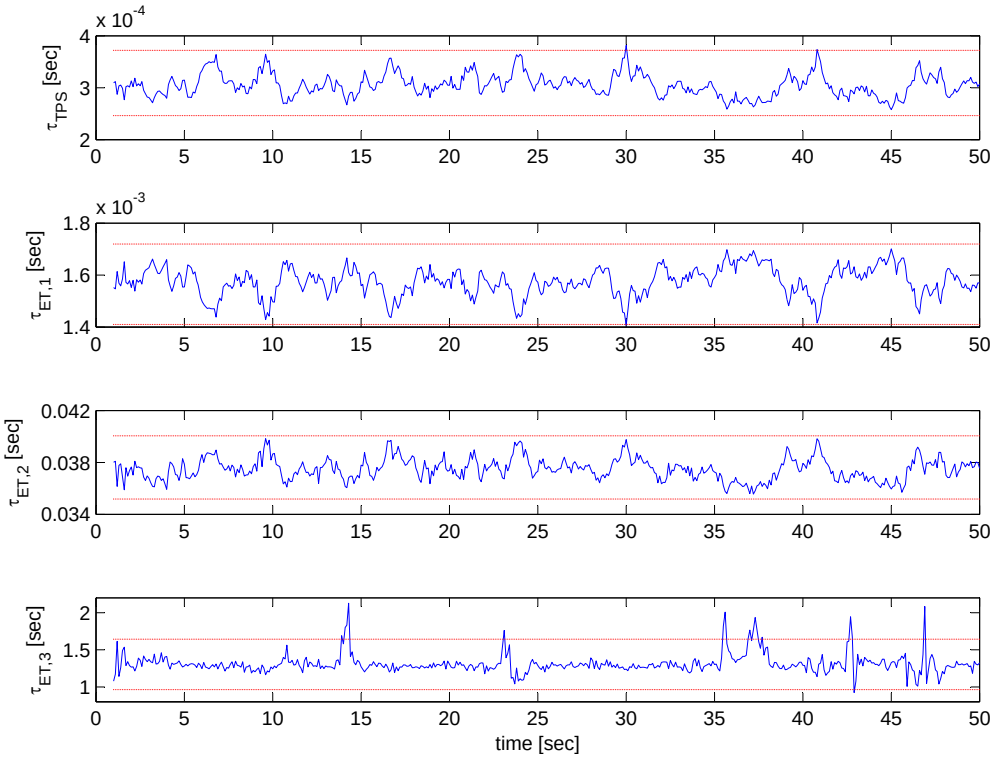

(a) Time constants

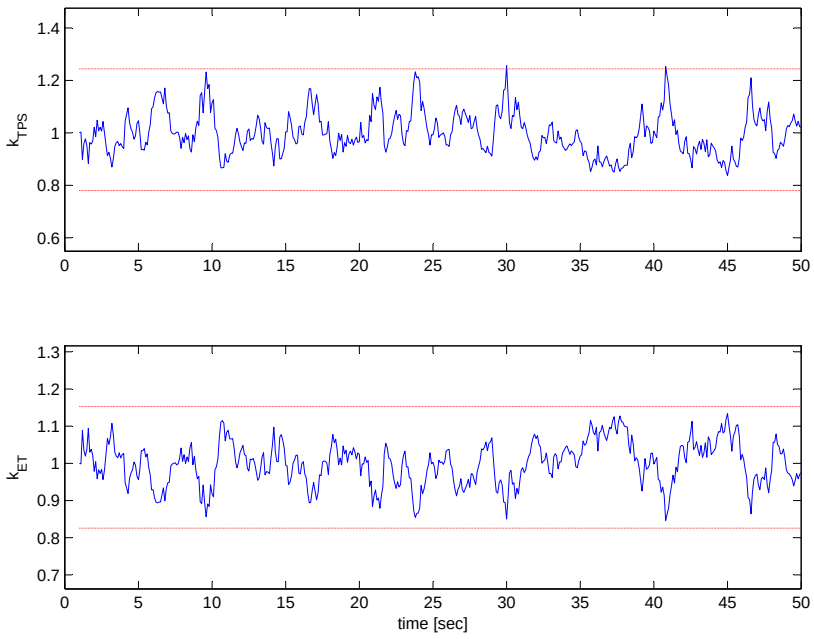

(b) Normalized gain

Figure 3.6: The time constants and normalized gains identified under nominal operations

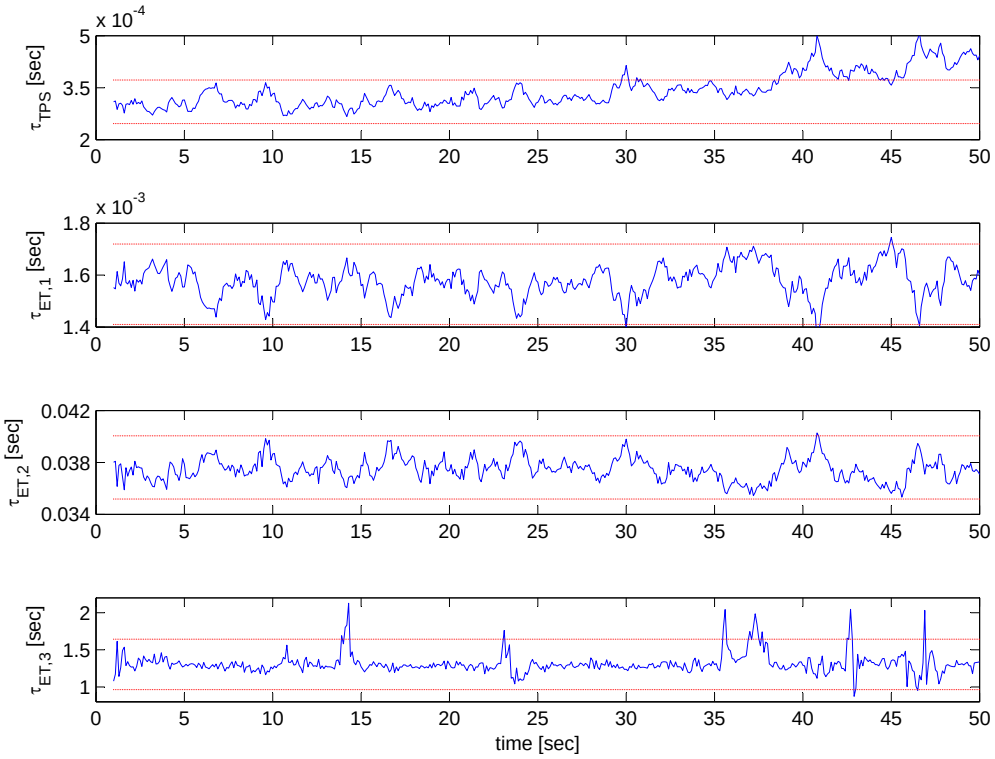

(a) Time constants

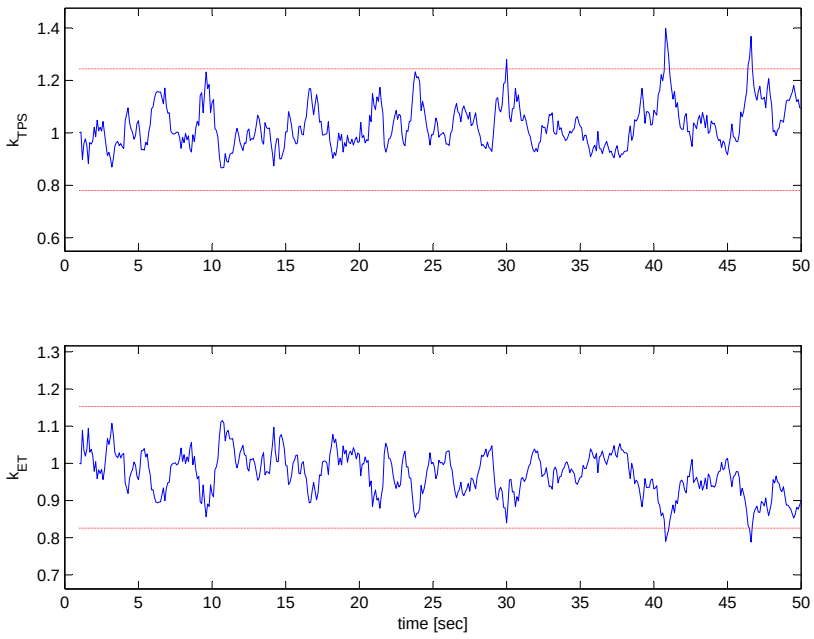

(b) Normalized gain

Figure 3.7: The time constants and normalized gains identified under Fault 1

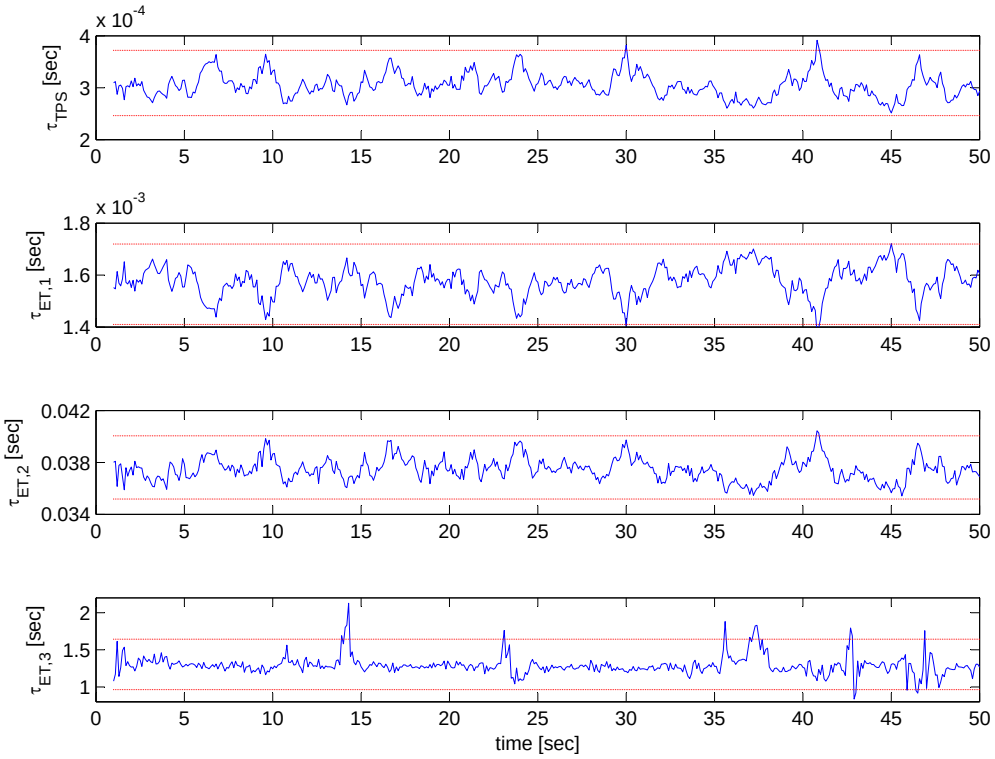

(a) Time constants

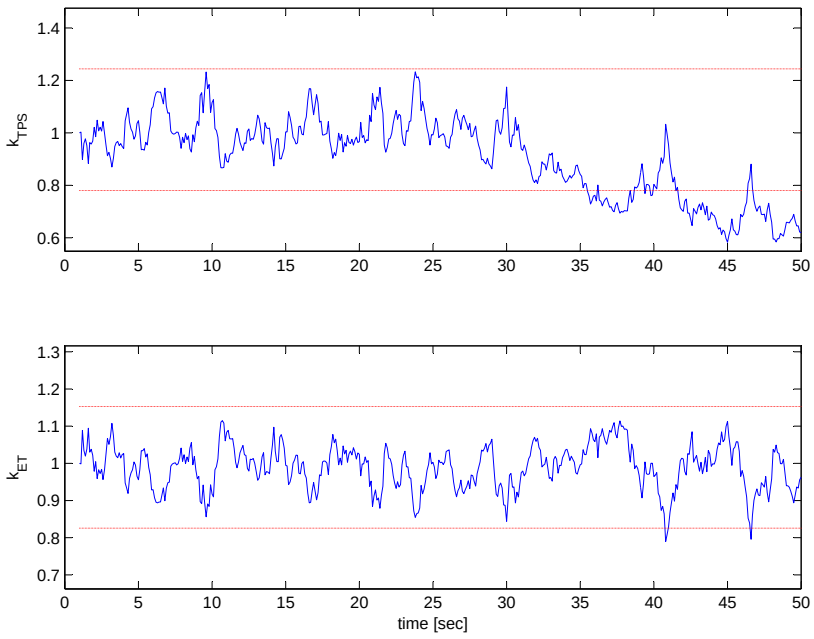

(b) Normalized gain

Figure 3.8: The time constants and normalized gains identified under Fault 2

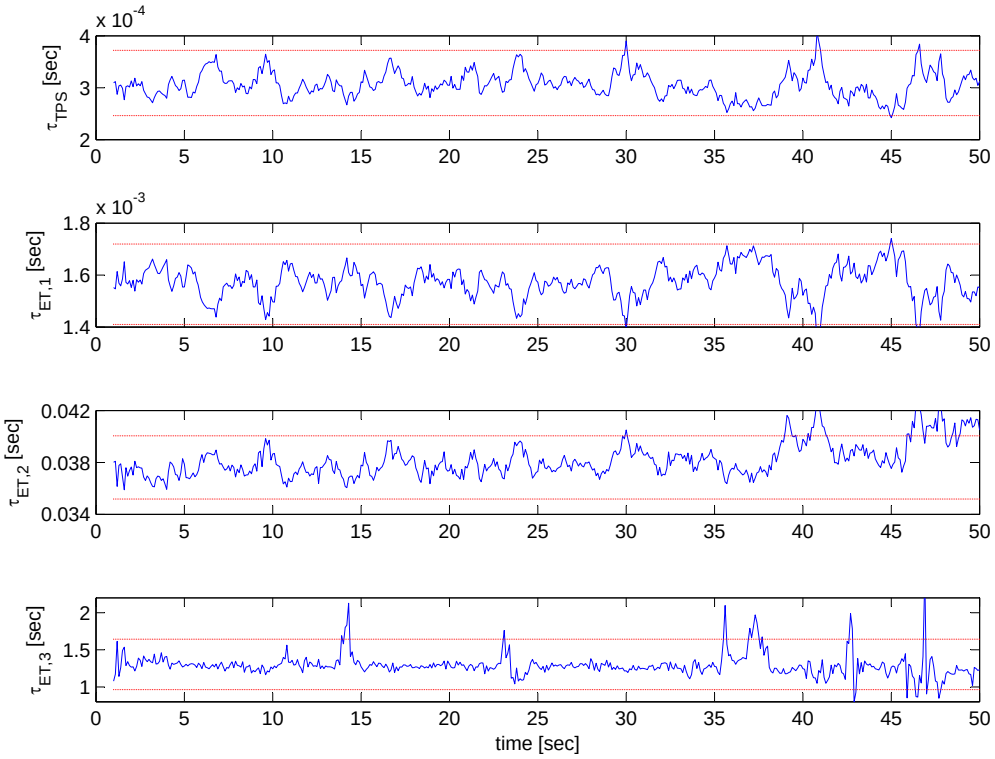

(a) Time constants

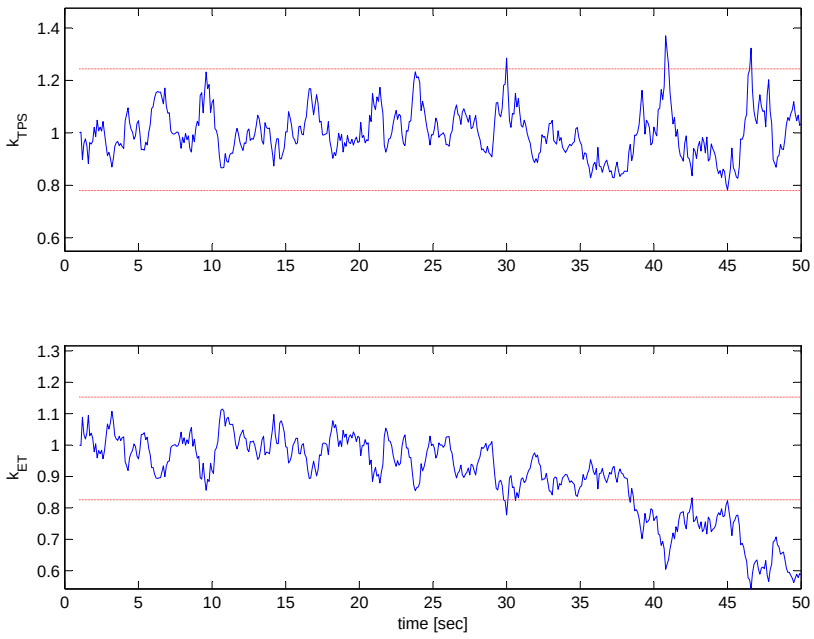

(b) Normalized gain

Figure 3.9: The time constants and normalized gains identified under Fault 3

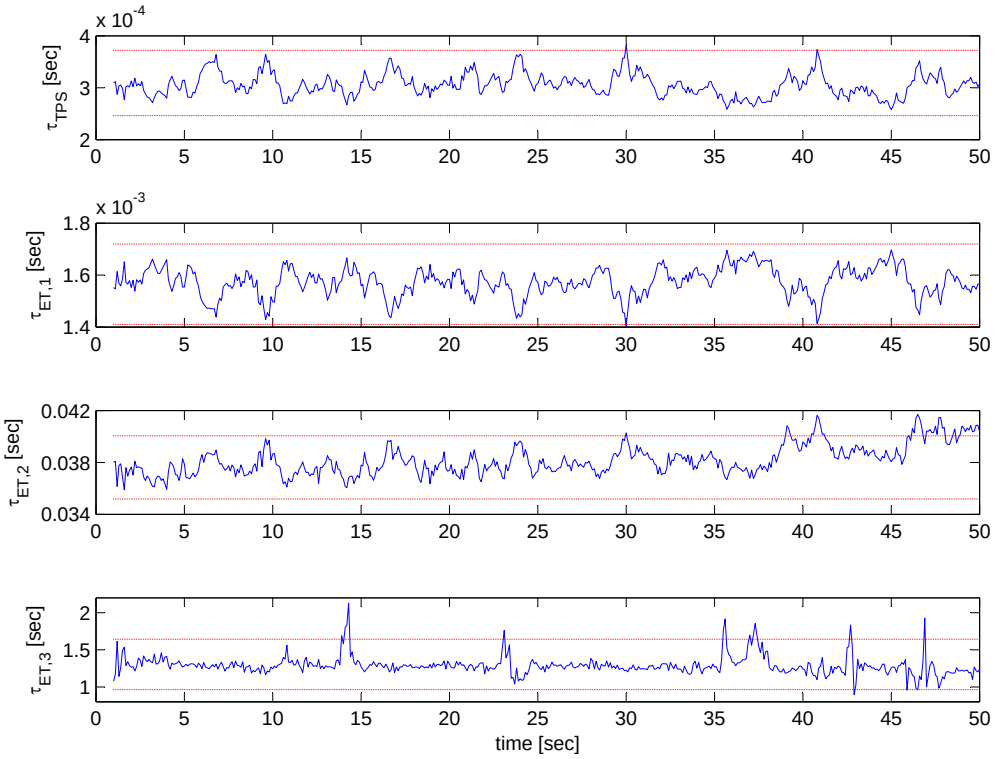

(a) Time constants

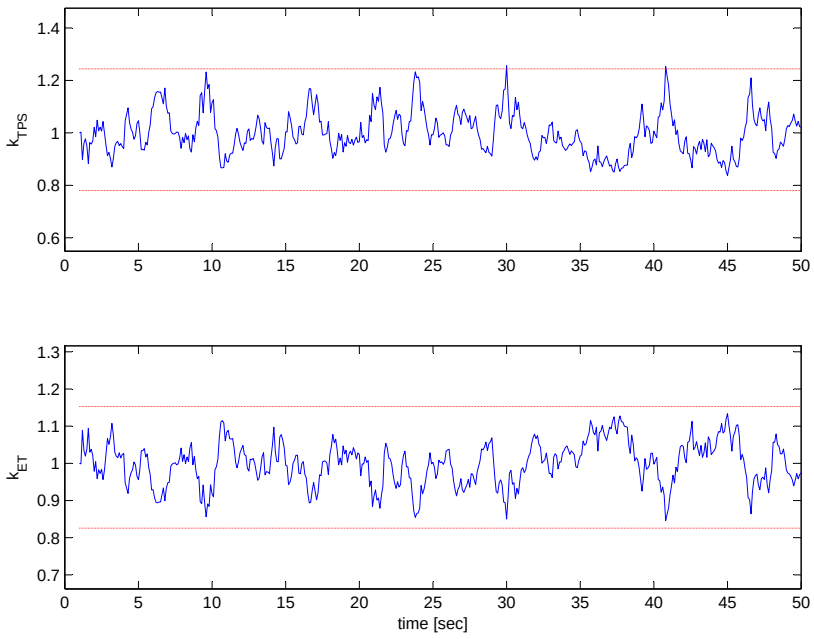

(b) Normalized gain

Figure 3.10: The time constants and normalized gains identified under Fault 4

function as

$$\begin{aligned} \frac{\theta_{ang}(s)}{W_p(s)} &= \frac{\frac{k_{TPS}}{\tau_{TPS}}}{s+\frac{1}{\tau_{TPS}}} \\ \frac{\theta_{ang}(s)}{U_c(s)} &= \frac{\theta_{ang}(s)}{W_p(s)} \cdot \frac{k_{ET}}{s^3+a_{ET,1}s^2+a_{ET,2}s+a_{ET,3}} \end{aligned} \tag{3.17}$$

where

$$\begin{aligned} a_{ET,1} &= \frac{(JR_a+K_fL_a)}{JL_a} \\ a_{ET,2} &= \frac{K_fR_a+N^2K_bK_t+K_{sp}L_a}{JL_a} \\ a_{ET,3} &= \frac{K_{sp}R_a}{JL_a} \end{aligned}$$

with the estimated model coefficients of the ET system, that is parameters $\widehat{a}_{ET,1}$, $\widehat{a}_{ET,2}$, and $\widehat{a}_{ET,3}$ illustrated in Figure 3.11(a) and Figure 3.11(b). As indicated in (3.17), since K_t is involved both in the gain k_{ET} and in the coefficient $a_{ET,2}$, the decrease of K_t causes the decrease of $(\widehat{k}_{ET})^n$ in Figure 3.9(b) and the decrease of $\widehat{a}_{ET,2}$ in Figure 3.11(a). On the other hand, K_b is only involved in the coefficient $a_{ET,2}$, thus causing a decrease in $\widehat{a}_{ET,2}$ in Figure 3.11(b). Thus, with some prior knowledge on the model structure of an ET system, one may be able to trace the degradation down to specific physical parameters, which can further help to isolate faults in the motor and those in the throttle body.

3.3.3 Compensation for an Incipient Sensor Failure

After significant degradation of the sensor has been detected using the method described above, its adverse effects in the readings can be compensated in the way illustrated in Figure 3.12. If the gain of TPS changes, the measurements can be reconstructed by multiplying its readings with $\frac{1}{(\widehat{k}_{TPS})^n}$. On the other hand, if the dynamics in this first-order system deteriorates, the changing dynamics can be compensated by filtering its readings with a filter $\frac{\widehat{\tau}_{TPS}\cdot s+1}{\widehat{\tau}^{nom}_{TPS}\cdot s+1}$ where $\widehat{\tau}^{nom}_{TPS}$ denotes the mean

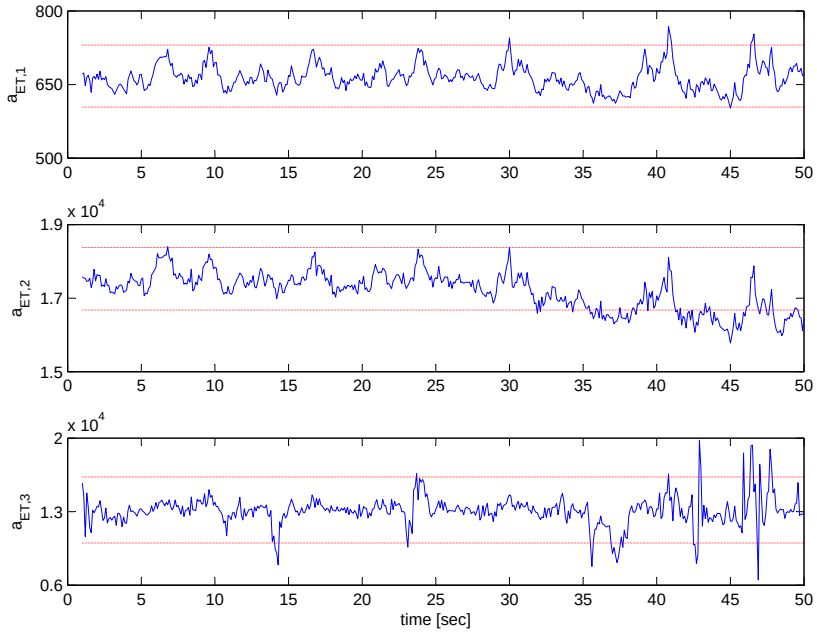

(a) Fault 3

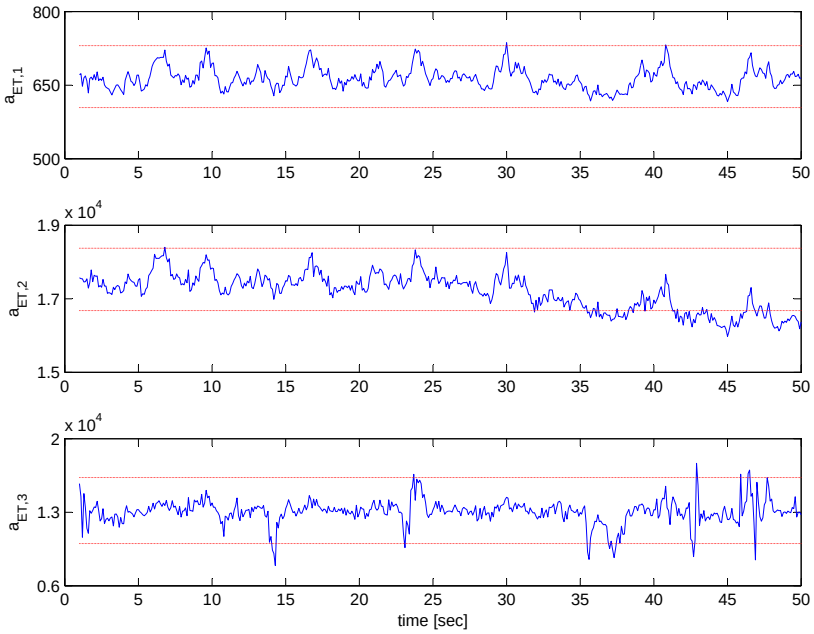

(b) Fault 4

Figure 3.11: The model coefficients identified under Fault 3 and Fault 4

value of the sensor time constants identified under normal operation. In this way, the deteriorated dynamics in the sensor is in fact replaced with the nominal one. Once $\widehat{\tau}_{TPS}$ or $(\widehat{k}_{TPS})^n$ identified in Figure 3.7(a) and Figure 3.8(b) exceed their control limits, the sensor readings are considered no longer reliable and the reconstructed measurements are taken instead as the feedback signals. As shown in Figure 3.12, such reconstruction scheme is able to reduce the errors in the readings of a degraded sensor, thus achieving improved accuracy despite the presence of degradation. In the figure, the measurement errors of a degrading sensor with and without reconstruction capability are denoted as e^d and e^r, respectively. In fact, only the errors illustrated in the red dotted line are obtained when reconstruction is implemented.

3.4 Summary

The method introduced in this chapter is able to identify the dynamics of the compound system consisting of a sensor and a monitored system, as well as separate the dynamics of the sensor from that of the monitored system. As a result, the method is capable of detecting and quantifying sensor performance degradation in the compound system without the use of redundant sensing equipment, where either the plant or the sensor monitoring that plant could undergo degradation in their dynamic properties. In addition, the method accomplishes identification of sensor and plant dynamics using inputs observed during normal system operations, rather than using special inputs. Consequently, such method is capable of assessing sensor health as the system operates, rather than off-line. Furthermore, this method is able to improve the accuracy of collected information despite the presence of sensor degradation by directly compensating for the adverse effects of the degradation in its readings.

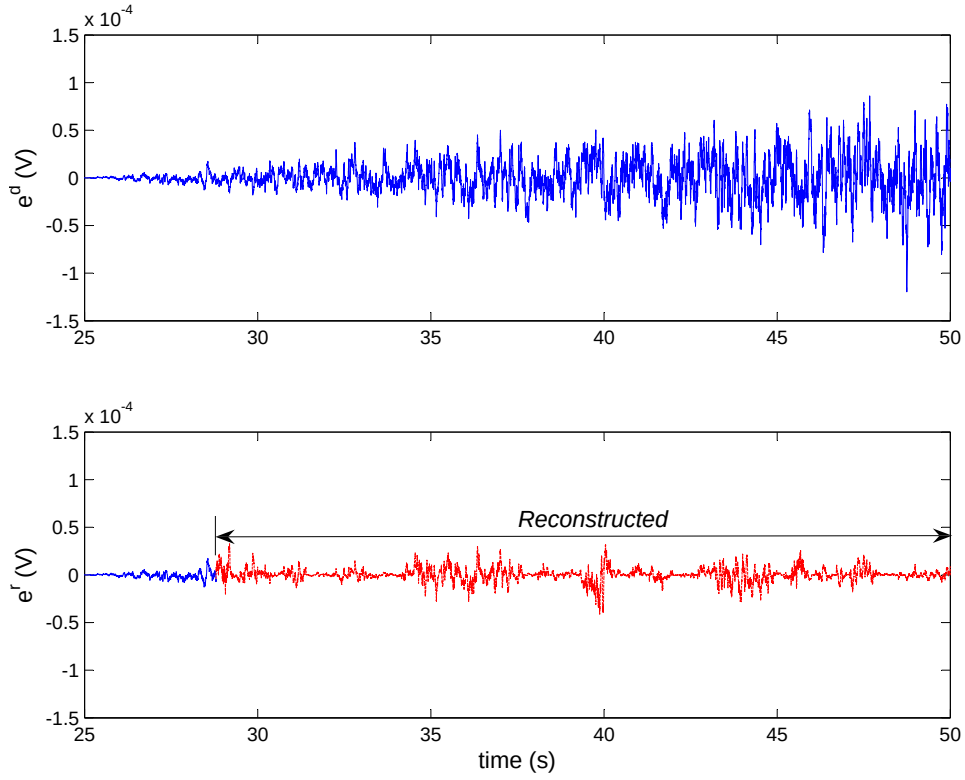

(a) Fault 1 (an incipient failure caused by deteriorated sensor response)

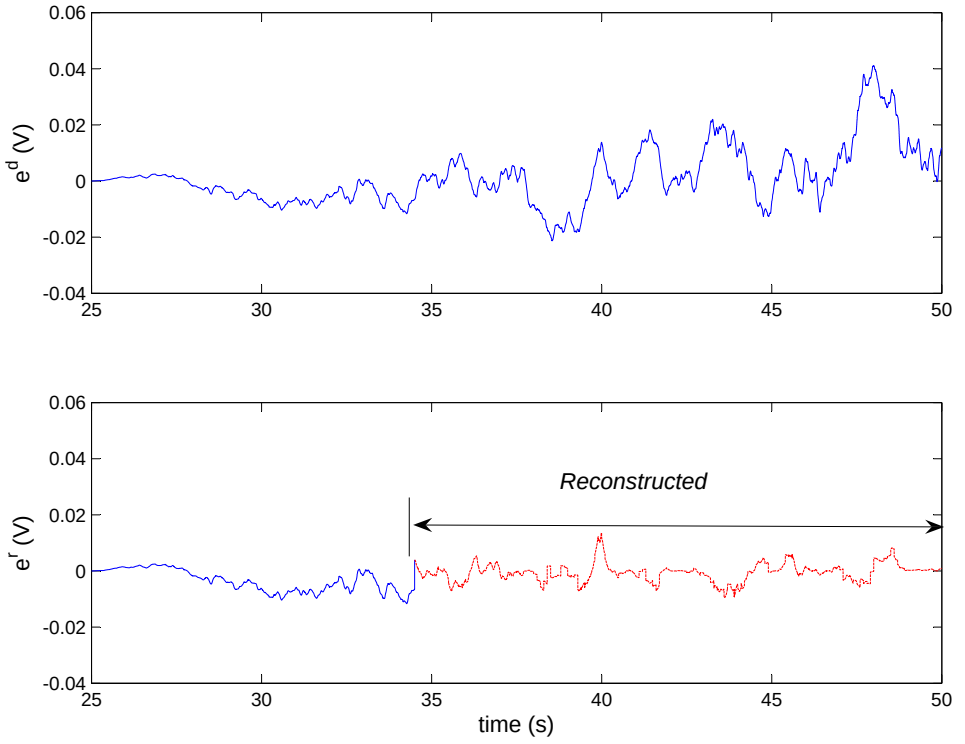

(b) Fault 2 (an incipient sensor failure caused by deteriorated magnification capability)

Figure 3.12: Measurement error of a degrading sensor with and without reconstruction

In terms of possible future work, sensor validation in nonlinear systems represents a natural extension of the work developed for linear systems in this chapter. Furthermore, considerations of sensor dynamics identification and separation from those of the monitored system, in the presence of multiple connected systems that are monitored by many sensors is another possible future challenge.

CHAPTER IV

Input Selection for Nonlinear Dynamic System Modeling

4.1 Introduction

As more advanced functionalities are incorporated into single engineering application for superior performance, an ever-increasing number of interconnected electro-mechanical components are equipped, which results in a dramatic increase in the complexity after nonlinearities are introduced. Since the conventional first-principle modeling techniques require a thorough understanding of the target physical system, they have become insufficient and even impossible to handle such complex and highly nonlinear dynamic systems. Consequently, data-driven modeling techniques have been employed during the past few decades in various applications. Despite the differences in their underlying development concepts and mathematical theories, the performance of these algorithms depends significantly on the selection of input variables.

In order to properly select the input variables for a nonlinear dynamic system, several approaches based on Principal Component Analysis (PCA) [Li et al., 2006; Zhang, 2007] and mutual information [Battiti, 1994; Zheng and Billings, 1996] have been developed and applied for pattern recognition and classification using artificial neural networks. However, these classical, linear multi-variate statistical tools have

been shown to be unreliable and insufficient for the input selection problem when there exists high correlation among the candidate input variables and their relation with the system outputs is highly nonlinear [Neter et al., 1996]. Moreover, the use of PCA also hampers the link back to the physical variables of the system.

Another straightforward method to solve such a problem is to compare all possible combinations of the candidate input variables using a predefined evaluation criterion. Inspired by this idea, several methods such as hypothesis testing [Cubedo and Oller, 2002], forward selection, and backward elimination [Mao, 2004; Whitley et al., 2000] have been developed to reduce its computational load and applied for input selection in linear system modeling. Although they can be used to detect the model structure of nonlinear polynomial models [Gaweda et al., 2001; Lin et al., 1996; Sugeno and Yasukawa, 1993], which have or can be converted into linear-in-the-parameters structures, these algorithms are in fact performing term[1] selection rather than variable selection for the nonlinear relations [Mao and Billings, 1999].

This chapter presents an alternative solution to the problem of selecting the appropriate input variables[2]. for nonlinear dynamic models by converting it into one of a set of linear models. The proposed method integrates a linearization sub-region division procedure using the Growing Self-Organizing Network (GSON) together with the all-possible-regression linear subset selection method. Compared with the conventional input selection, genetic algorithm is employed to solve the combinatorial optimization problem introduced by the all possible regression algorithm. In addition, a performance evaluation criterion is also proposed for the multiple model

[1] A term is defined here to be a composition of the input variables via nonlinear operations. For example, for a nonlinear function $y = a_1x_1^2 + a_2cos(x_2) + a_3x_1x_2$, x_1 and x_2 are considered as the input variables, while x_1^2, $cos(x_2)$, and x_1x_2 are the corresponding terms.

[2] In the reminder of this thesis, the input variables of a nonlinear dynamic system in fact include the regressors of both system inputs $\mathbf{u}$ and outputs $\mathbf{y}$. For example, in a two-input single-output nonlinear dynamic model $y(t+1) = \cos(y(t)) + u_1(t)e^{u_2(t-1)}$, $\mathcal{S} = \{\ y(t),\quad u_1(t),\quad u_2(t-1)\ \}$ lists all the input variables to $y(t+1)$.

system based on the minimum description length principle [Rissanen, 1978; De Ridder et al., 2005]. Without requiring a great amount of prior knowledge of the target system, this method can be applied for a wide range of nonlinear model forms such as the nonlinear polynomial model and neural networks. As demonstrated with the numerical simulation examples as well as a real-world system identification problem with the diesel engine airflow system, this method can be used to automate the modeling process and achieve models with desirable modeling accuracy as well as generalization capability.

The remainder of the chapter is organized as follows. In Section 4.2, the method for the selection of input variables in a nonlinear dynamic model is proposed. The input selection problem is first stated and then the linearization sub-region partition algorithm as well as the use of genetic algorithm is presented. In Section 4.3, the effectiveness of this method is demonstrated via two numerical simulation examples and the air path system of a diesel engine.

4.2 Method

4.2.1 Problem Statement

Consider a nonlinear dynamic system with p outputs and q inputs described by

$$y_i(t) = f_i(\mathbf{s}) + e_i(t), \;\; i = 1, \ldots, p \tag{4.1}$$

where $\mathbf{s}_i = [s_{i,1}, \ldots, s_{i,d_i}]^T$ is a d_i-dimension vector including the candidate input variables, y_i and e_i denote the scalar output and white noise respectively. Based on the assumption that the target system is causal, the candidate input variable $\mathbf{s}_i$ can be either the regressor of the output $y_i(t - n_{y_i})$, $\forall y_i \in [y_1, \ldots, y_p]^T$, $n_{y_i} > 0$ or that of the system input $u_j(t - n_{u_j})$, $\forall u_j \in [u_1, \ldots, u_q]^T$, $n_{u_j} > 0$. In this work, the system outputs are defined as the key performance variable of the target system,

while the system inputs are the available signals collected from the controller and the sensors.

To develop the novel input selection method, consider a nonlinear dynamic model (4.1) with the following assumptions

A1 The input variables $\mathbf{s}_i = [s_{i,1},\ \ldots,\ s_{i,d_i}]^T$ are bounded in a d_i-dimensional compact domain denoted by $\mathcal{S}$

$$\mathbf{s}_i = [s_{i,1},\ \ldots,\ s_{i,d_i}]^T \in \mathcal{S},\ i = 1, \ldots, p$$

A2 The system outputs $\mathbf{y} = [y_1,\ \ldots,\ y_p]^T$ are bounded.

A3 The nonlinear dynamic model $\mathbf{f} = [f_1,\ \ldots,\ f_p]^T$ is composed of smooth functions.

Given an operating point $\mathbf{s}^0 = [s_1^0,\ \ldots,\ s_d^0]^T$ in the interior of the domain $\mathcal{S}$, assumption **A3** ensures there exists the Taylor expansion of $\mathbf{f}(\cdot)$ at point $\mathbf{s}^0$ as

$$\mathbf{f}(\mathbf{s}) = \mathbf{f}(\mathbf{s}^0) + \frac{\partial \mathbf{f}}{\partial \mathbf{s}}(\mathbf{s}^0)(\mathbf{s} - \mathbf{s}^0) + \frac{1}{2!}(\mathbf{s} - \mathbf{s}^0)^T \frac{\partial^2 \mathbf{f}}{\partial^2 \mathbf{s}}(\mathbf{s}^0)(\mathbf{s} - \mathbf{s}^0) + \ldots \tag{4.2}$$

Then, within a small region $\{\mathbf{s} : \|\mathbf{s} - \mathbf{s}^0\| < \varepsilon\}$ around $\mathbf{s}^0$, the nonlinear dynamic system $\mathbf{f}(\mathbf{s})$ can be approximated with the first few terms of the Taylor series in (4.2) with arbitrary accuracy as $\varepsilon \to 0$, which enables the linearization of $\mathbf{f}(\mathbf{s})$ at $\mathbf{s}^0$ in the form

$$\hat{\mathbf{f}}_L = \mathbf{b}_L + \mathbf{a}_L^T \mathbf{s} + \xi \tag{4.3}$$

where $\mathbf{b}_L = \mathbf{f}(\mathbf{s}^0) - \frac{\partial \mathbf{f}}{\partial \mathbf{s}}(\mathbf{s}^0)\mathbf{s}^0$, $\mathbf{a}_L^T = \frac{\partial \mathbf{f}}{\partial \mathbf{s}}(\mathbf{s}^0)$, and $\mathbf{e}_L$ is the modeling error due to the linearization.

After comparing the nonlinear dynamic system (4.1) and the linearized model (4.3), it is not difficult to conclude that if any input variable $\forall s_{i,l} \in [s_{i,1},\ \ldots,\ s_{i,d_i}]^T$

is relevant to the output y_i in the original nonlinear function $f_i, i = 1, \ldots, p$, it will also make a significant contribution to the output in the linearized model [Mao and Billings, 1999]. Furthermore, since the coefficients of the linearized model in (4.3) are operating region dependent [Billings and Voon, 1987], the significance of input variables is also operating region dependent. Therefore, the method proposed in this chapter incorporates a linearization sub-region division algorithm to convert the input selection problem of a nonlinear dynamic model into one of a set of linear models.

4.2.2 Linearization Sub-Region Partition

The divide-and-conquer modeling paradigm solves a complicated problem by breaking it down into multiple sub-problems that are simpler to solve, and the global model is obtained by combining these local solutions using a proper interpolation function. Due to its capability of providing simple and efficient solutions to difficult problems, this concept has been employed in the design of algorithms for various engineering applications. In the field of system identification, the divide-and-conquer concept has driven the development of effective modeling techniques, such as Takagi-Sugeno fuzzy modeling [Babuska, 1998], piecewise linear modeling [Billings and Voon, 1987], and the growing structure multiple model algorithm [Liu et al., 2009a]. Instead of identifying a complex dynamic nonlinear system in a direct manner, these methods first partition its operating region into multiple sub-regions within each of which a simpler model is fitted, and then combine these local models for the approximation of the global system behavior.

While too fine a partition may result in surplus sub-regions and cause the problem of over-fitting, too coarse a partition may lead to poor approximation of the system behavior using a linearized model in the sub-region with high nonlinearity. A simple

and intuitive approach for sub-region division is to equally divide each candidate input variable into proper value ranges so that desirable modeling accuracy in all operating sub-regions can be guaranteed. This approach has been successfully applied for the piecewise linear identification of nonlinear systems [Mao and Billings, 1999]. Since the nonlinearity of a system is not necessarily evenly distributed over its operating region, a clustering approach was used in [Billings and Voon, 1987] to merge some of the evenly divided sub-regions based on a similarity based measure. The Takagi-Sugeno fuzzy model [Babuska, 1998], on the other hand, partitions the operating region according to a number of implications based on pre-determined premise variables. Each premise variable is then divided into different value ranges so that a region with higher nonlinearity can be accordingly partitioned into more sub-regions. However, it requires a lot of *a priori* knowledge of the physical system for these methods to determine either a proper set of premise variables and implications or appropriate value ranges.

Self-organizing networks (SON) [Kohonen, 1995], one of the vector quantization techniques known for its capability of unsupervised learning, have been proposed in [Barreto and Araujo, 2004; Principe et al., 1998] to partition the operating region into sub-regions through Voronoi tessellation:

$$V_m = \{\mathbf{s} : \|\mathbf{s} - \xi_m\| \leq \|\mathbf{s} - \xi_n\|, \ \forall n = 1, \ldots, m-1, m+1, \ldots, M\} \tag{4.4}$$

where ξ_m, $m = 1, \ldots, M$ are the weight vectors of the SON. Given the number of regions M, locations and shapes of those regions defined by ξ_m need to be adjusted according to the input-output mapping. Since the input selection problem is generally solved in an off-line manner, the batch SON training algorithm is employed for

updating the weight vector ξ_m at iteration step k using the following equation.

$$\xi_m(k+1) = \xi_m(k) + \zeta_m(k)h(k, dis(m,c))\left[\bar{\mathbf{s}}_m - \xi_m(k)\right] \tag{4.5}$$

where $\bar{\mathbf{s}}_m(k)$ is the mean of the data vectors in the m^{th} region. $\zeta_m(k)$, the normalized modeling errors at iteration step k, introduces a penalty to achieve a balance between the effects of visiting frequency and modeling errors in a local region m Liu et al. [2009a]. $\zeta_m(k)$ is calculated as

$$\zeta_m(k) = \frac{\bar{e}_m(k)}{max_i \bar{e}_i(k)} \tag{4.6}$$

$\bar{e}_m$ is the mean of the modeling error of $\|e_m(k)\|$ with $e_m(k) = y(k) - \hat{y}_m(k)$. $h(\cdot,\cdot)$ is the neighborhood function [Kohonen, 1995] with a common choice in the following form

$$h(k, dis(m,c)) = \exp\left(\frac{-dis(m,c)^2}{2\sigma^2(k)}\right), \ \ m = 1, \ \ldots, \ M \tag{4.7}$$

Here, $\sigma(k)$ denotes the width of the neighborhood function employed in the growing self-organizing network, and $c(k)$ is the Best Matching Unit (BMU) of the training vector $\mathbf{s}$ at iteration step k, which is obtained as

$$c = \arg\min_m \|\mathbf{s} - \xi_m(k)\|, \ \forall m \leq M \tag{4.8}$$

Then, a partition of the operating region of the system can be defined by assigning BMUs to the observation vectors $\mathbf{s}$. $\sigma^2(k)$ is generally a non-increasing function over iterations that defines the width of the effective range of the neighborhood function.

However, the number of Voronoi regions M (i.e., nodes in the self-organizing networks) and the network structure (i.e., connections among the nodes in the self-organizing networks) still need to be selected in advance. In order to avoid the distortion caused by the fixed structure and size in the conventional self-organizing networks, the GSON such as growing neural gas [Fritzke, 1995], growing cell structure

[Fritzke, 1994] and growing self-organizing map [Alahakoon et al., 2000], have been recently developed. By incorporating specific growth and deletion mechanisms, the GSON can automatically determine the number of nodes as well as its structure, thus resulting in a more accurate description of inherent data structures. The growth and deletion mechanism enables the network to start growing from a small number of nodes and stop once a stopping criterion is satisfied such as the maximum number of nodes and the maximum tolerable quantization error.

In order to reduce the amount of required *a priori* knowledge about the target physical system, the GSON is employed in the proposed method, as shown in Figure 4.1, to partition the input-output mapping space into small sub-regions by including both inputs and desirable outputs into the vector $\mathbf{s}$ [Ge et al., 2000]. The proposed method is schematically illustrated in Figure 4.1. Table 4.1 lists the associated parameters are employed in this approach.

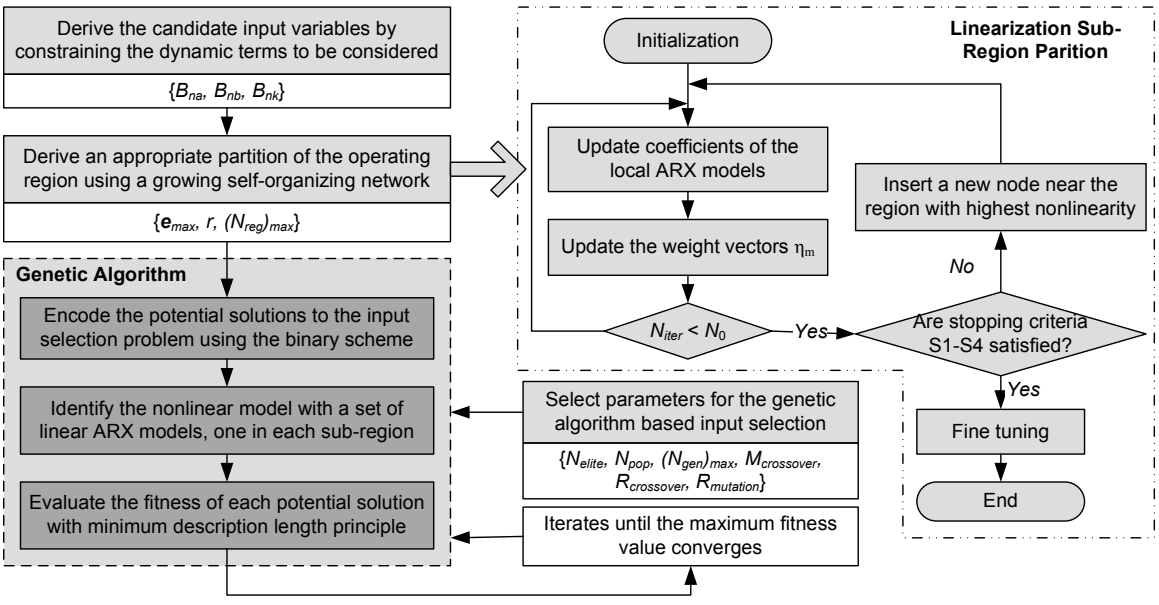

Figure 4.1: Flow chart of the genetic algorithm based input selection methodology

Within each sub-region, the efficient least square algorithms are used to estimate

Table 4.1: List of parameters used in the method proposed in Figure 4.1

Parameter	Description
$B_{n_a}, B_{n_b}, B_{n_k}$	number of bits to encode n_a, n_b, n_k
$\mathbf{e}_{\max}$	maximum allowed error evaluated based on the root mean square error
r	minimum ratio of the number of samples in each sub-region to that of free parameters in the model
N_{elite}	number of top ranked solutions of the current generation to be preserved into the next one
N_{pop}	number of solutions evaluated in each generation
$(N_{gen})_{\max}$	maximum number of generations
$(N_{reg})_{\max}$	maximum number of linearization sub-regions
M_c	crossover methods: one, two, multiple point crossover
R_c	crossover rate
R_m	mutation rate

the parameters of an Auto-Regressive model with eXogenous inputs (ARX) in the following form.

$$A(z)\mathbf{y}(t) = B(z)\mathbf{u}(t - n_k) + \mathbf{e}(t) \tag{4.9}$$

where $n_k \in \mathbb{R}^{p\times q}$ defines the transport delays between the output and candidate input variables, while $A(z)$ and $B(z)$ are polynomials in terms of the backshift operator z^{-1} that can be expressed in the form of

$$\begin{aligned} A(z) &= a_1 z^{-1} + a_2 z^{-2} + \ldots + a_{n_a} z^{-n_a} \\ B(z) &= b_1 + b_2 z^{-1} + \ldots + b_{n_b} z^{-n_b+1} \end{aligned} \tag{4.10}$$

Here, $n_a \in \mathbb{R}^{p\times p}$ denotes the auto-regressive order of model in (4.9)), while $n_b \in \mathbb{R}^{p\times q}$ is the order of its exogenous part. For the purpose of system identification, $\|\mathbf{e}(t)\|$ is employed in the GSON as a measure for modeling accuracy. In order to achieve a proper partition of the operating region, the following stopping criteria are imposed in the GSON.

S1 The maximum allowed output error $\mathbf{e}_{\max}$ in the estimated multiple model system to ensure the modeling accuracy

S2 The maximum number of nodes $(N_{reg})_{\max}$ in the GSON to constrain complexity

S3 The number of samples in each sub-region with the constraint of $N_m > rn_\theta,\ m = 1, \ldots, M$ where n_θ is the number of free parameters in the model

S4 The condition imposed on the least-squares estimator $\hat{\theta}_m = (S_m^T S_m)^{-1} S_m^T Y_m$ in each sub-region V_m as

$$\frac{\text{cond}(S_m^T S_m)}{1/\epsilon} < 1 \times 10^8$$

where function cond$(\cdot)$ computes the condition number of a matrix; θ_m denotes the coefficients of the local ARX model, while S_m and Y_m are matrices constructed using the samples of input variables and outputs in sub-region V_m respectively. $\epsilon = 2.2204 \times 10^{-16}$ is defined as the floating-point relative accuracy in MATLAB®[3]

While stopping criterion **S1** avoids the problem of poor estimation performance caused by insufficient number of sub-regions, stopping criteria **S2** - **S4** help to solve the problem of surplus partitions, which results in some sub-regions ending up with too few training samples.

Given a partition of the operating region along with the corresponding local ARX models, the overall dynamics of the nonlinear dynamic system described by (4.1) can then be approximated by combining the local models from different sub-regions via the following interpolation function.

$$\begin{aligned} \hat{\mathbf{y}}(t+1) &= \sum_{m=1}^{M} \nu_m(\mathbf{s}(t)) \hat{\mathbf{F}}_m(\mathbf{s}(t)) \\ \nu_m(\mathbf{s}(t)) &= \frac{\rho_m(\mathbf{s}(t))}{\sum_{i=1}^{M} \rho_i(\mathbf{s}(t))},\ m = 1, \ldots, M \end{aligned} \tag{4.11}$$

where $\hat{\mathbf{y}}$ denotes the estimated outputs and $\hat{\mathbf{F}}_m,\ m = 1, \ldots, M$ are the local models identified using least square algorithms, while $\rho_m(\mathbf{s}),\ m = 1, \ldots, M$ are the validation functions describing the validity of the local function in terms of $\mathbf{s}$. In this

[3]Registered trademarks of The MathWorks, Natick, MA 2002.

chapter, an interpolation function

$$\rho_m(\mathbf{s}(t)) = \begin{cases} 1, & \mathbf{s}(t) \in V_m \\ 0, & o.w. \end{cases} \tag{4.12}$$

is employed so that a local model $\mathbf{F}_m$ is only valid when the vector $\mathbf{s}$ is located in sub-region V_m (For more details, please refer to [Liu et al., 2009a] and references therein).

4.2.3 Input Selection

Once a proper partition of the operating region is obtained, the input selection for the nonlinear dynamic model can be converted into one for a set of linear ARX models, which enables the use of algorithms for forward selection, backward elimination, stepwise selection, all possible regression, etc. Due to its superior performance as demonstrated in [Gunst, 1980], the all possible regression algorithm is used, which in fact solves the input selection problem using a combinatorial optimization strategy. Since the all possible regression algorithm selects the target model from a set of models that are constructed with different combinations of the candidate inputs, it also introduces a significant computation load. For example, a model with k candidate input variables in $\mathcal{S}$ actually requires the all possible regression algorithm to evaluate $2^k - 1$ models. Therefore, genetic algorithm [Goldberg, 1989] is employed in the present study to solve this combinatorial optimization problem. Inspired by evolutionary biology, genetic algorithm has been widely used as a search technique to find the exact or approximate solution(s) to an optimization problem. Known for its robustness, genetic algorithm is able to perform an effective search as long as its solution domain is represented in a proper genetic form and the fitness functions is well defined.

Gene Encoding The input variables $s_l,\ l = 1,\ \ldots,\ d$ to be selected for the nonlinear dynamic system in (4.1) can be represented via the model structure parameters n_a, n_b, and n_k as defined in (4.10). The set of candidate input variables $\mathcal{S}$ is derived as

$$\mathcal{S} \ = \ \left\{ \ \mathbf{y}(t-1), \ \ \ldots, \ \ \mathbf{y}(t-n_a), \ \ \mathbf{u}(t), \ \ \ldots, \ \ \mathbf{u}(t-n_d-n_b+1) \ \right\}$$
$$\text{with } \mathbf{y} = \left[\ y_1, \ \ \ldots, \ \ y_p \ \right]^T \text{ and } \mathbf{u} = \left[\ u_1, \ \ \ldots, \ \ u_q \ \right]^T$$

Due to its simplicity, the binary coding scheme is employed here to encode parameters n_a, n_b and n_k into p binary strings in G in the form of

$$G = \left\{ \ g_1, \ \ \ldots, \ \ g_p \ \right\} \tag{4.13}$$

where $g_i,\ i = 1,\ \ldots,\ p$ encodes all the information that belongs to output variable y_i as

$$g_i = \left\{ \ \left(g_{y_1}^{n_a}\right)^i, \ \ \ldots, \ \ \left(g_{y_p}^{n_a}\right)^i, \ \ \left(g_{u_1}^{n_b}\right)^i, \ \ \ldots, \ \ \left(g_{u_q}^{n_b}\right)^i, \ \ \left(g_{u_1}^{n_k}\right)^i, \ \ \ldots, \ \ \left(g_{u_q}^{n_k}\right)^i \ \right\}$$

Here, $\left(g_{y_{i'}}^{n_a}\right)^i,\ \forall y_{i'} \in [y_1,\ \ldots,\ y_p]^T$ encodes the auto-regressive order n_a of output $y_{i'}$ on output y_i, while $\left(g_{u_j}^{n_b}\right)^i$ and $\left(g_{u_j}^{n_k}\right)^i,\ j = 1, \ldots, q$ encodes the exogenous order n_b and its corresponding transport delay between output y_i and input u_j, respectively. Furthermore, a gene is considered as illegal if $\left(g_{u_j}^{n_k}\right)^i$ is nonzero while $\left(g_{u_j}^{n_b}\right)^i,\ \forall u_j \in [u_1,\ \ldots,\ u_q]^T$ is zero. With some *a priori* knowledge of the system dynamics, parameters B_{n_a}, B_{n_b}, and B_{n_k} are employed to constrain the number of potential input variables to be considered by specifying the number of bits to encode the maximum values of n_a, n_b and n_k in binary strings, respectively.

Fitness Function With an interpolation function in (4.11), the multiple model algorithm introduced above in fact minimizes the objective function $\mathbf{J} = \left[\ J_1, \ \ \ldots, \ \ J_p \ \right]^T$

as

$$\begin{aligned} J_i &= \sum_{t=0}^{N} \left(y_i(t) - \hat{y}_i(t)\right)^2 \\ &= \sum_{m=1}^{M} \sum_{\mathbf{s}(t)\in V_m} \left(y_i(t) - \hat{y}_i(t)\right)^2, \;\; i = 1, \ldots, p \end{aligned} \tag{4.14}$$

With a proper partition of M sub-regions, as more candidate input variables $\mathbf{s}_i$ are included in the model, the value of the objective function $J_i, \;\; i = 1, \ldots, p$ decreases, thus resulting in a more accurate model. However, the generalization capability of the model also decreases because as more free parameters are added, the identified model tends to get over-fitted to the training data [Ljung, 1999; Pintelon and Schoukens, 2001].

To achieve a balance between modeling accuracy and model complexity, statistical information theory has been widely applied to various system identification problems. Compared with Akaike information criterion (AIC) [Akaike, 1974], the minimum description length (MDL) criterion [Rissanen, 1978] has shown its capability of providing more accurate estimation of the model order, especially in the case of short data. Therefore, a modified MDL criterion [De Ridder et al., 2005] has been incorporated in this method as the fitness function.

$$\begin{aligned} f^i_{MDL} &= \sum_{m=1}^{M} \left(\frac{1}{N_m} \sum_{\mathbf{s}(t)\in V_m} \left(y_i(t) - \hat{y}_i(t)\right)^2 + \frac{\ln(N_m)(n_\theta + 1)}{N_m - n_\theta - 2} \right), \\ & \quad i = 1, \ldots, p \end{aligned} \tag{4.15}$$

where N_m is the number of samples located in sub-region V_m, and n_θ is the number of candidate input variables s_i that are selected (i.e., the number of free parameters) in the model.

4.3 Validation and Evaluation

4.3.1 Numerical Examples

Example 1 A two-input and two-output nonlinear system

$$\begin{aligned} y_1(t) &= 0.8y_1(t-1) - 0.1y_2(t-1) + u_1(t-2) + 0.4u_1^2(t-2) \\ &\quad -1.2u_1(t-1)u_2(t-2) + e_1(t) \\ y_2(t) &= 0.5y_2(t-1) + 0.5y_2(t-2)u_2^2(t-1) + u_2(t-2) \\ &\quad +u_1^2(t-1) + e_2(t) \end{aligned} \tag{4.16}$$

where inputs u_1 and u_2 are independent random variables uniformly distributed in the range of $(0, 0.5)$ and $(0, 1)$, respectively; noises e_1 and e_2 are normally distributed random variables with zero mean and variance 0.01 and 0.04.

Figure 4.2 illustrates in color the linear correlation coefficient[4] of any two variables listed in the vector $\mathbf{x}(t)$.

$$\mathbf{x}(t) = \left[\underbrace{\mathbf{y}(t)}_{BOX_1}, \ \underbrace{\mathbf{y}(t-1:t-3)}_{BOX_2}, \ \underbrace{\mathbf{u}(t:t-5)}_{BOX_3} \right]$$

with

$$\mathbf{u} = [u_1, \ u_2]^T, \ \ \mathbf{y} = [y_1, \ y_2]^T \tag{4.17}$$

BOX_1, BOX_2, and BOX_3 correspond to the three red rectangles located from the upper left corner to the lower right corner in Figure 4.2. Here, black indicates that two variables are linearly dependent, while white indicates that they are independent. Due to the independency in $\mathbf{u}$, there does not exist correlation among the regressors of the inputs $\mathbf{u}(t:t-n_k-n_b+1)$ in BOX_3. However, significant correlation exists among the output variables $\mathbf{y}(t-1:t-n_a)$ in BOX_1 and BOX_2.

[4]The correlation coefficient of two variables x and y is defined as $\rho_{xy} = \frac{R_{xy}}{\sigma_x \sigma_y}$, where R_{xy} denotes the covariance between x and y, and σ_x and σ_y denote their standard deviations.

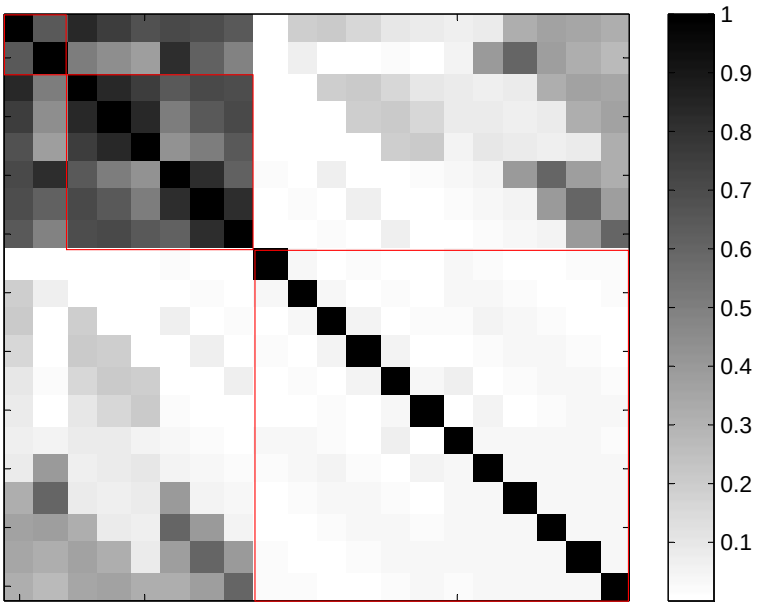

Figure 4.2: Normalized linear correlation coefficient among the regressors of the inputs and outputs in Example 1

In this example, the maximum order for dynamic parameters n_a and n_b in (4.10) are set as $(n_a)_{max} = 3$ and $(n_b)_{max} = 3$, while the maximum delay n_k in (4.9) is set as $(n_k)_{max} = 7$, which determines their corresponding GA parameters to be $B_{n_a} = 2$, $B_{n_b} = 2$, and $B_{n_k} = 3$, respectively. With a properly selected set of GA parameters, the convergence behavior of the proposed method during one simulation is illustrated in the lower plot of Figure 4.3. In addition to its fast convergence in the evolutionary process of selecting the proper input variables, it has also been illustrated in the upper and middle plot of Figure 4.3 that the solution derived in (4.18) can lead to desirable accuracy in identifying the nonlinear dynamic model with a multiple model system. Note that Figure 4.3(a)-4.3(b) and Figure 4.7 all include (1) upper plot: actual output values in blue solid line and estimated values in red dotted line, (2) middle plot: residuals between the actual and estimated values, (3)

lower plot: convergence behavior of the fitness function in the evolutionary process.

$$\left.\begin{array}{rcl} g_1 & = & \underbrace{01}_{g_{y_1}^{n_a}}\underbrace{01}_{g_{y_2}^{n_a}}\underbrace{10}_{g_{u_1}^{n_b}}\underbrace{01}_{g_{u_2}^{n_b}}\underbrace{001}_{g_{u_1}^{n_k}}\underbrace{010}_{g_{u_2}^{n_k}} \\ g_2 & = & \underbrace{00}_{g_{y_1}^{n_a}}\underbrace{10}_{g_{y_2}^{n_a}}\underbrace{01}_{g_{u_1}^{n_b}}\underbrace{10}_{g_{u_2}^{n_b}}\underbrace{001}_{g_{u_1}^{n_k}}\underbrace{001}_{g_{u_2}^{n_k}} \end{array}\right\}$$

$$\rightarrow n_a = \begin{bmatrix} 1 & 1 \\ 0 & 2 \end{bmatrix}, \quad n_b = \begin{bmatrix} 2 & 1 \\ 1 & 2 \end{bmatrix}, \quad n_k = \begin{bmatrix} 1 & 2 \\ 1 & 1 \end{bmatrix} \tag{4.18}$$

Figure 4.4show the estimated probability distribution and power spectral density of the model residuals, $\mathbf{r} = [r_1,\ r_2]^T$. It can be observed that residuals, $\mathbf{r}$, are white noise, which indicates the multiple linear model with the identified input variables captured the dynamics in (4.16).

In order to investigate the effects of GA parameters on the convergence performance, the proposed input variable selection algorithm has been simulated with commonly used values for the crossover and mutation rates. In this work, the values of the crossover and mutation rate that are considered are $R_c = [0.75,\ 0.80,\ 0.85]$ and $R_m = [0.1,\ 0.2,\ 0.3]$. Figure 4.5 shows the histogram of the number of runs to converge with different crossover rate, R_c, and mutation rate, R_m. Each plot in the figure was obtained by running 100 simulations with randomly generated initial populations. The mean number of runs to converge listed in Table 4.2 suggests that the optimal crossover and mutation rates for output y_1 and y_2 are $R_c = 0.85,\ \ R_m = 0.1$ and $R_c = 0.75,\ \ R_m = 0.1$, respectively.

Table 4.2: Mean number of runs to converge in Example 1

	y_1			y_2		
	$R_m = 0.1$	$R_m = 0.2$	$R_m = 0.3$	$R_m = 0.1$	$R_m = 0.2$	$R_m = 0.3$
$R_c = 0.75$	59.43	67.22	86.72	37.87	53.63	46.47
$R_c = 0.80$	52.47	67.40	76.02	39.97	55.38	69.03
$R_c = 0.85$	52.44	64.17	73.71	37.98	53.76	57.18

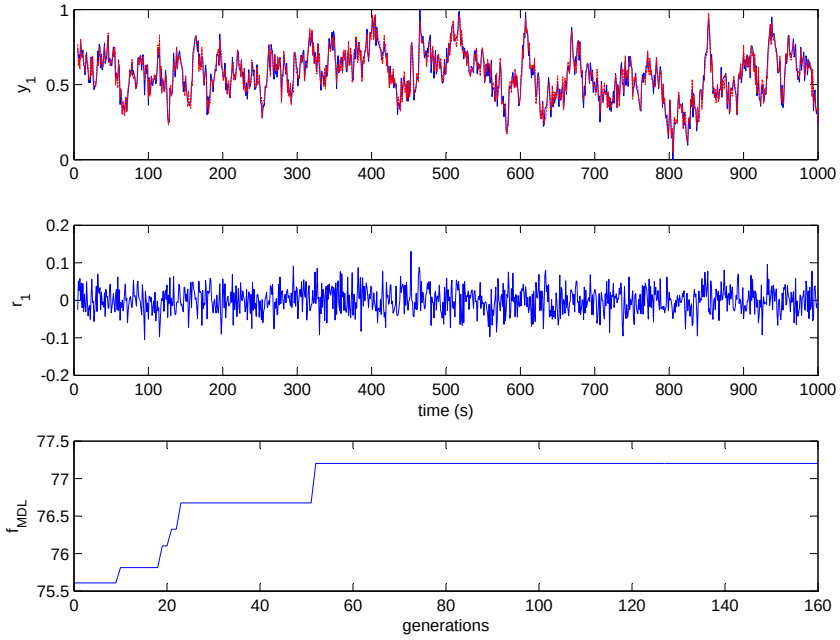

(a) output variable y_1

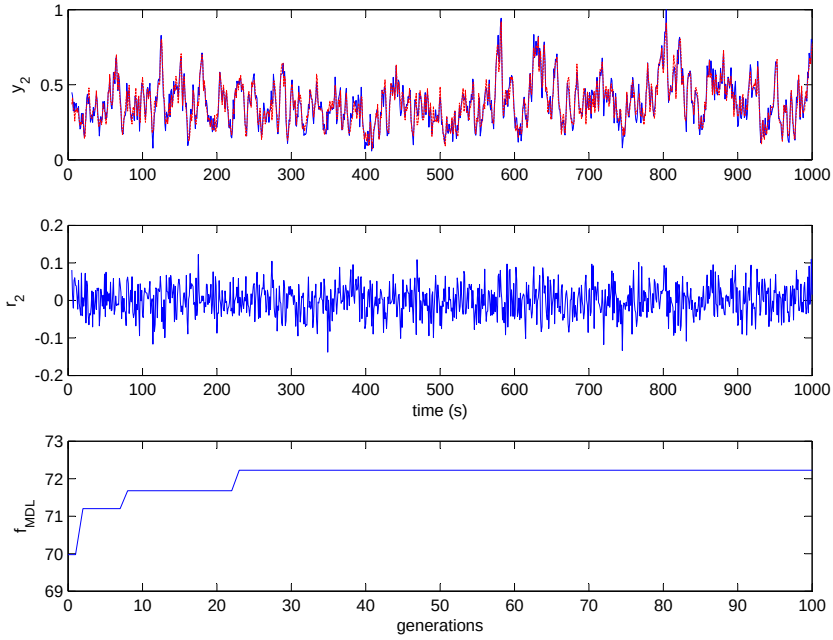

(b) output variable y_2

Figure 4.3: Behaviors of the multiple linear model and evolution of the fitness function for numerical Example 1

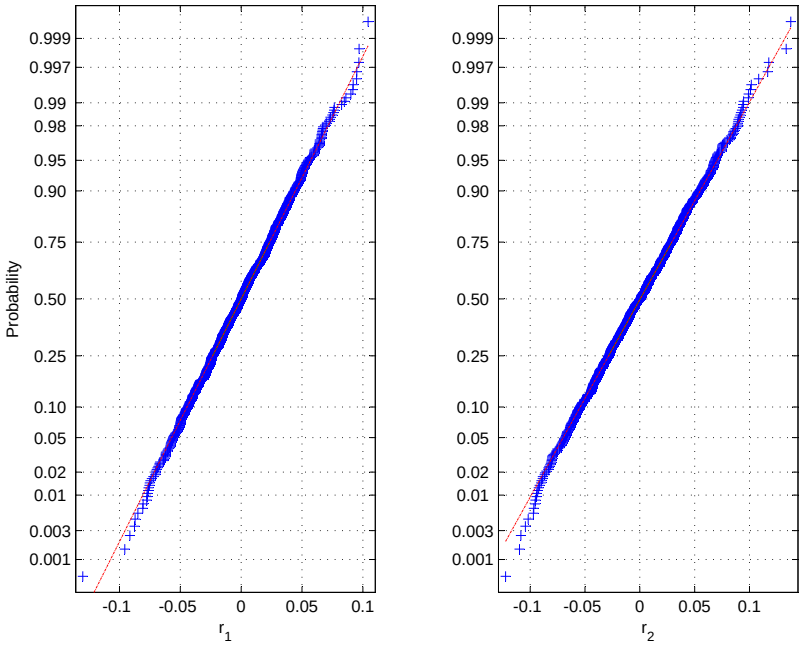

(a) Estimated probability distribution

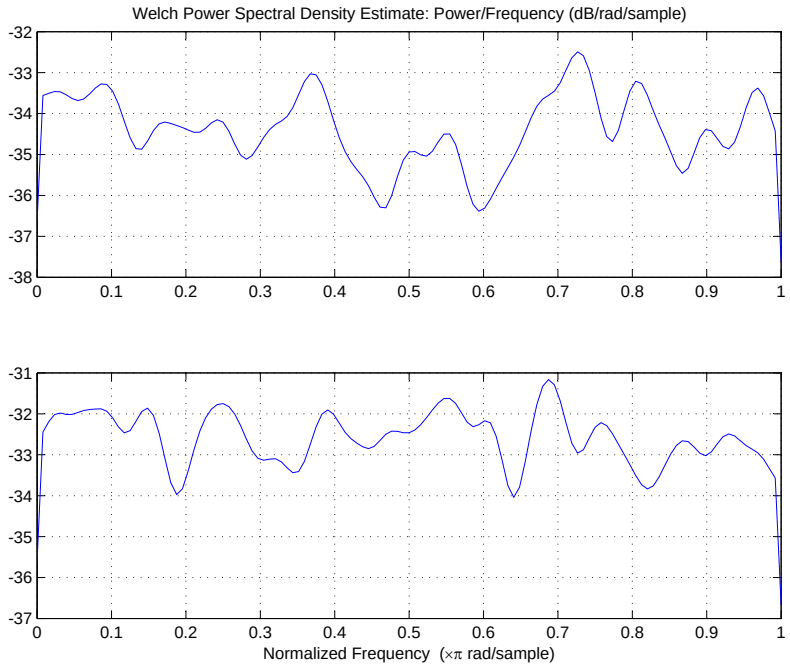

(b) Estimated power spectral density

Figure 4.4: Estimated probability distribution and power spectral density of the model residuals in Example 1

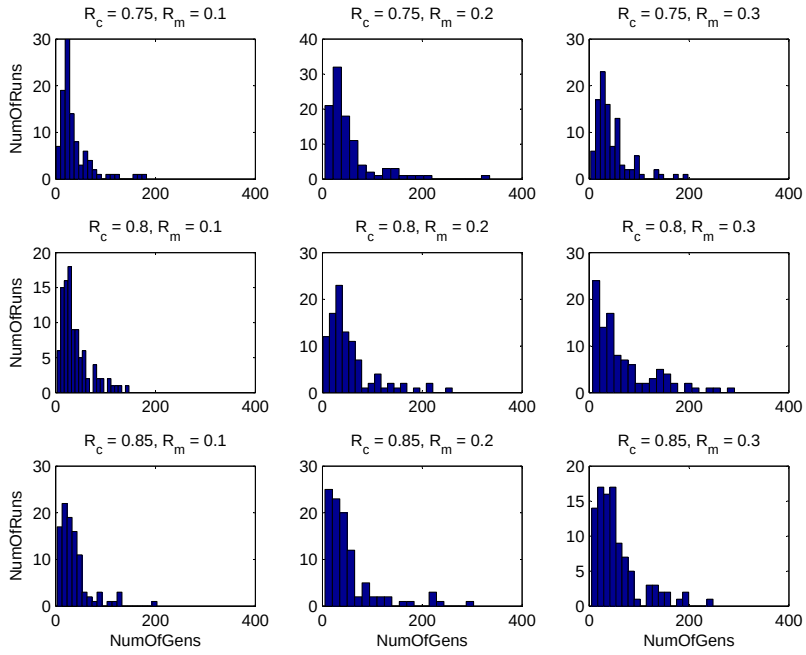

(a) output variable y_1

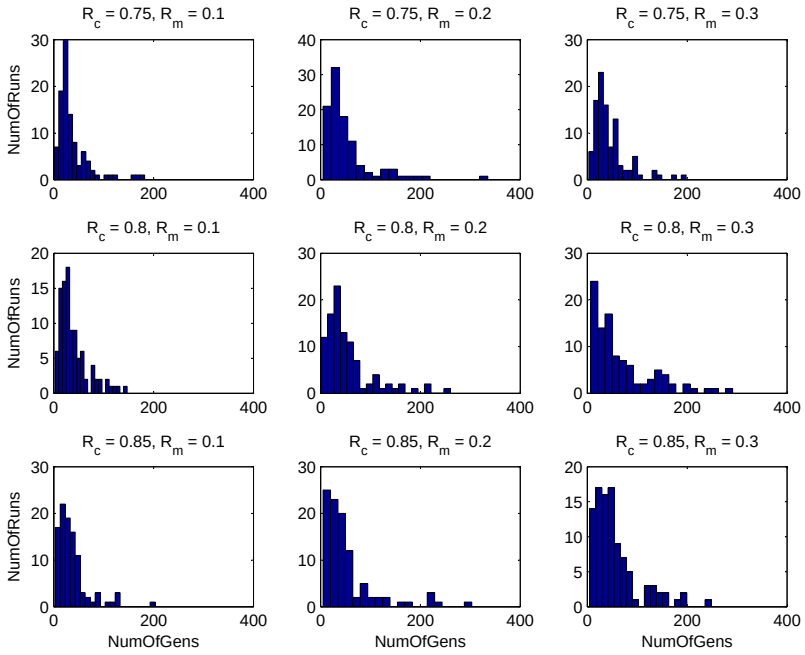

(b) output variable y_2

Figure 4.5: Selection of crossover and mutation rates in Example 1

Example 2 A three-input and one-output nonlinear system

$$\begin{aligned} y(t) &= 0.8y(t-1) + u_1(t-6)u_2(t-4) \\ &\quad +0.5\exp\left(0.4u_1^2(t-6)\right) + e(t) \end{aligned} \tag{4.19}$$

where inputs u_1 and u_2 are independent random variables uniformly distributed in the range of $(-0.5, 0.5)$; noise e is a normally distributed random variable with zero mean and variance 0.0025. To evaluate the performance of the proposed method when there exist abundant highly correlated input variables, a third input $u_3(t) = u_1(t) + u_2(t) + e_u(t)$ where e_u is a normally distributed random variable with zero mean and variance 0.01 is introduced in this example.

Figure 4.6 shows the correlation coefficients of any two variables in the vector $x(t)$.

$$\mathbf{x}(t) = \left[\underbrace{y(t)}_{BOX_1}, \ \underbrace{y(t-1:t-3)}_{BOX_2}, \ \underbrace{\mathbf{u}(t:t-10)}_{BOX_3} \right]$$

with $\mathbf{u} = [u_1,\ u_2,\ u_3]^T$. BOX_1, BOX_2, and BOX_3 correspond to the three red rectangles located from the upper left corner to the lower right corner in Figure 4.6. In addition to the significant correlation among the regressors of the output $y(t-1 : t-n_a)$ in BOX_2, there exists high correlation between the regressors of the redundant input variable u_3 and those of inputs u_1 and u_2 in BOX_3.

In this example, the maximum order for dynamic parameters n_a and n_b in (4.10) are set as $(n_a)_{max} = 3$ and $(n_b)_{max} = 3$, while the maximum delay n_k in (4.9) is set as $(n_k)_{max} = 10$, which determines their corresponding GA parameters to be $B_{n_a} = 2$, $B_{n_b} = 2$, and $B_{n_k} = 3$, respectively. With a properly selected set of GA parameters, the proposed input variable selection approach is able to identify the exact solution

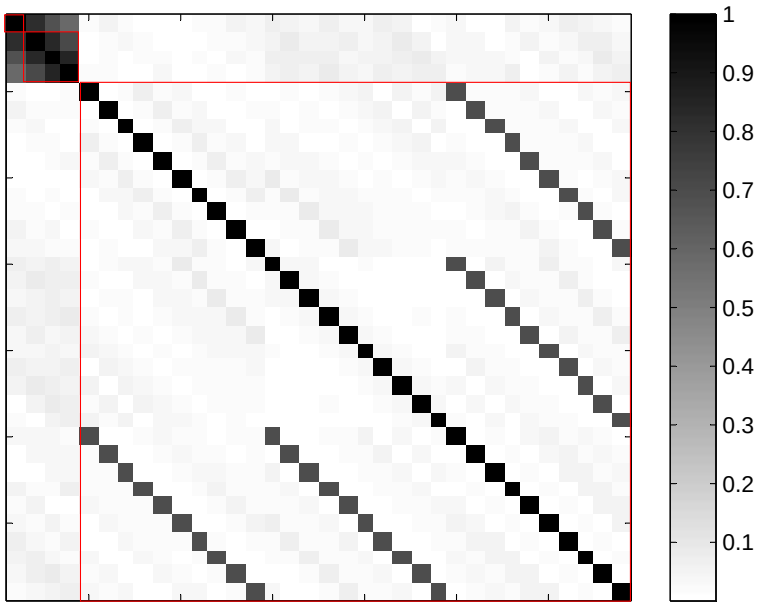

Figure 4.6: Normalized linear correlation coefficient among the regressors of the inputs and outputs in Example 2

as (4.20) and exclude all the redundant variables that are associated with u_3.

$$\begin{aligned} g &= \underbrace{01}_{g_y^{n_a}}\ \underbrace{01}_{g_{u_1}^{n_b}}\ \underbrace{01}_{g_{u_2}^{n_b}}\ \underbrace{00}_{g_{u_3}^{n_b}}\ \underbrace{110}_{g_{u_1}^{n_k}}\ \underbrace{010}_{g_{u_2}^{n_k}}\ \underbrace{000}_{g_{u_3}^{n_k}} \\ \rightarrow n_a = 1,\ n_b &= \begin{bmatrix} 1 & 1 & 0 \end{bmatrix},\ n_k = \begin{bmatrix} 6 & 4 & 0 \end{bmatrix} \end{aligned} \tag{4.20}$$

Figure 4.8 show the estimated probability distribution and power spectral density of the model residuals, r. It can be observed that residuals are white noise, which indicates the multiple linear model with the identified input variables captured the dynamics in (4.19).

The convergence performance of the proposed approach in this example is also investigated for the same set of crossover and mutation rates in Example 1. It can be observed from Figure 4.9 and Table 4.3 that $R_c = 0.75$ and $R_m = 0.3$ leads to the best performance.

It can observed in the mean number of runs to converge in Table 4.2 and Table 4.3

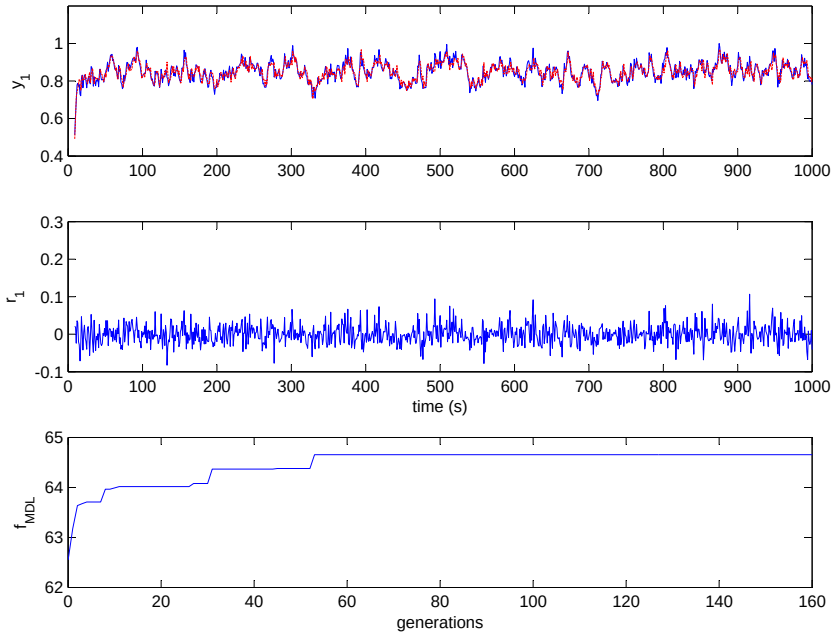

Figure 4.7: Behaviors of the multiple linear model and evolution of the fitness function for numerical Example 2

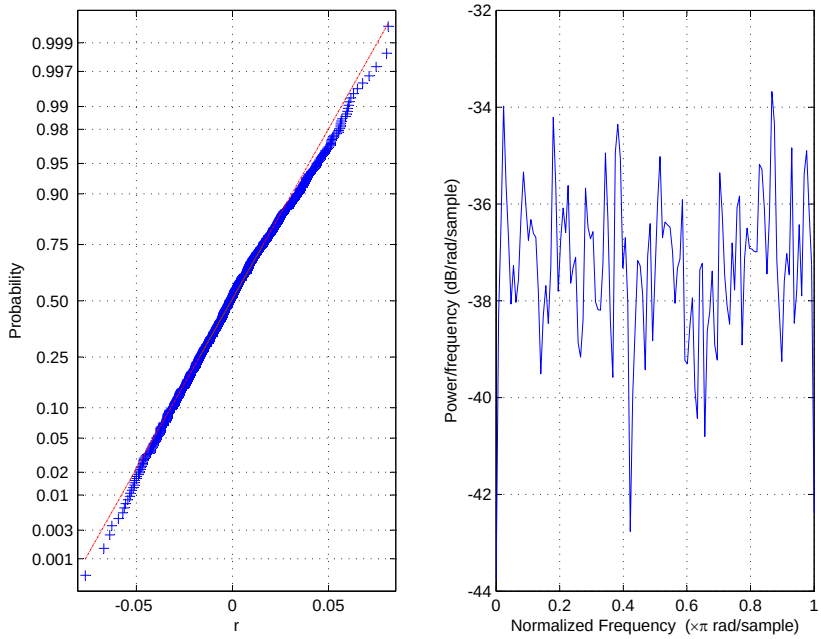

Figure 4.8: Estimated probability distribution and power spectral density of the model residuals in Example 2

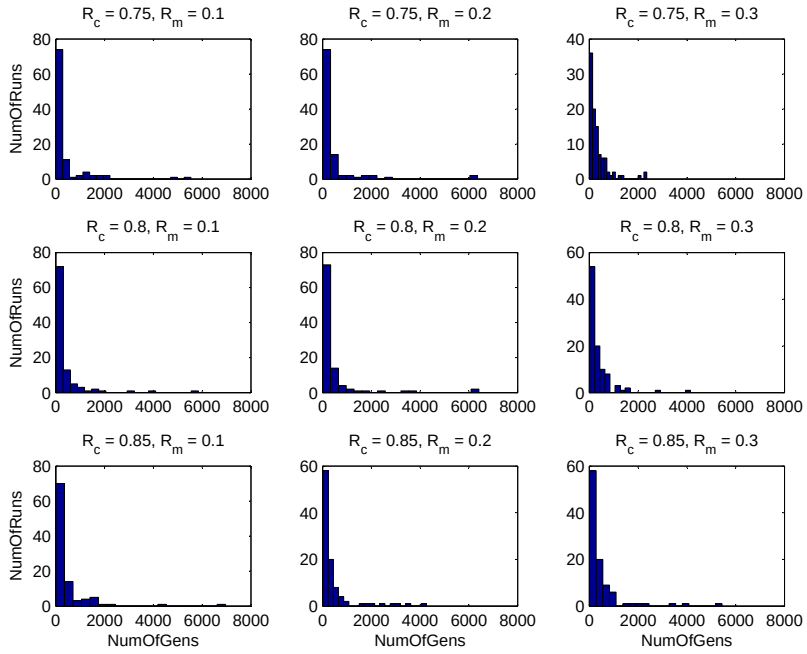

Figure 4.9: Selection of crossover and mutation rates for GA in Example 2

Table 4.3: Mean number of runs to converge in Example 2

	y_1		
	$R_m = 0.1$	$R_m = 0.2$	$R_m = 0.3$
$R_c = 0.75$	413.27	450.99	348.43
$R_c = 0.80$	404.76	475.27	389.93
$R_c = 0.85$	471.71	446.60	483.22

that the proposed approach demonstrated a better convergence performance in Example 1. The existence of the highly nonlinear term $\exp\left(0.4u_1^2\left(t-6\right)\right)$ in (4.19) and the introduction of the highly correlated input variable, u_3, makes the selection of the most significant input variables in Example 2 a more challenging task.

4.3.2 Diesel Engine Air Path System

The input variable selection approach proposed in this paper has also been applied to construct fault detectors for the air path system of a four-cylinder diesel engine as illustrated in Figure 4.10. The target air path consists of the components: [C.1] hot-wire air flow meter, [C.2] turbocharger, [C.2a] compressor, [C.2b] variable noz-

zle turbine (Vnt), [C.3] boost manifold, [C.4] charge air cooler, [C.5] throttle valve (Thr), [C.6] air intake manifold, [C.7] exhaust gas recirculation valve (Egr), [C.8] exhaust gas recirculation cooler, [C.9] exhaust gas manifold (Exh), and [C.10] engine (Eng). The use of the turbocharger and exhaust gas recirculation (EGR) results in coupled dynamics in the intake and exhaust systems. The recirculated cooled exhaust gas affects the temperature, pressure, and oxygen concentration of the air mixture in the intake manifold. In turn, the air mixture entering the engine influences the combustion behaviors, thus affecting the exhaust gas conditions. Similarly, the turbocharger couples the intake and exhaust systems by utilizing the exhaust gas energy to improve the engine volumetric efficiency. The air path is controlled by the position of the electro-pneumatic actuated throttle valve [C.5], X_{Thr} , the exhaust gas recirculation valve [C.7], X_{Egr}, and the variable nozzle turbine [C.2b], X_{Vnt}. The injected fuel quantity, W_{Fuel}, directly commanded by the torque, and the engine speed, N_{Eng}, measured by the engine speed sensor, are considered as measurable disturbances in this work. In order to enable the close-loop air/fuel control, an Exhaust Gas Oxygen (EGO) sensor measuring the oxygen concentration in the exhaust gas, λ, is installed at the exit of the system.

Figure 4.11(a) shows the system inputs that include the control commands and the measurable disturbances, while Figure 4.11(b) shows the system outputs that include the key sensor measurements. Here, (X_{Thr}, X_{Egr}, X_{Vgt}) denote the relative position of the throttle, EGR valve, and VGT vane in reference to their lower mechanical limits. Other variables, except the ambient pressure, p_{Amb}, are normalized using the min-max method in (4.21) with the minimum and maximum of the variables derived from the training data.

$$\bar{z} = \frac{z - \min(z)}{\max(z) - \min(z)} \tag{4.21}$$

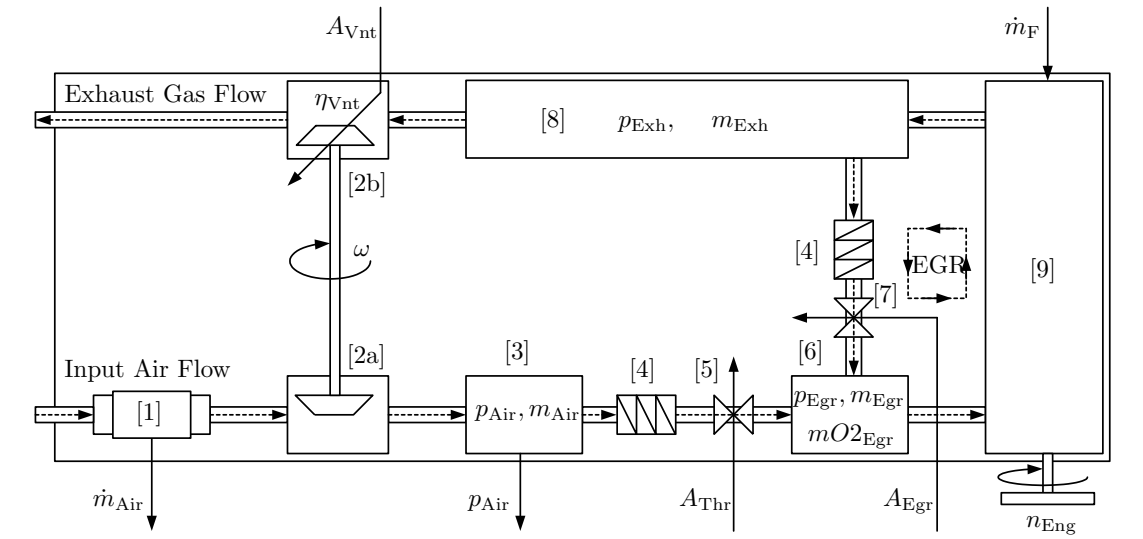

Figure 4.10: Air path of a diesel combustion engine [Aßfalg et al., 2006]

where $\bar{z}$ denote the normalized variable of z, $\min(z)$ and $\max(z)$ are the minimum and maximum values of z. In this work, the intake air mass flow rate, W_{Air}, and the pressure in the boost manifold [C.4], p_{Bst} are selected as the key performance variables for air path system diagnosis, thus $\mathbf{y} = [W_{Air},\ p_{Bst}]^T$. In a diesel engine, the injected fuel quantity, W_{Fuel}, are commanded to deliver the desired torque demands, while λ is employed as the feedback signal to derive the desired intake air quantity. It can be observed in Figure 4.11 that the data are collected under wide-open throttle conditions, $W_{Thr} = 100\%$, with little variations in the ambient pressure, p_{Amb}. In addition, measurements of the turbocharger rational speed, N_{tc}, that were collected at the engine dynamometer in this work are generally not available in a commercial vehicle platform. Therefore, in order construct models for output variables, W_{Air} and p_{Bst}, the input variables are selected $\mathbf{u} = [T_{Bst},\ X_{Egr},\ X_{Vgt},\ N_{Eng}]^T$.

The experimental data were collected at the rate of 50Hz, thus resulting in a sample time of 20ms. In order to avoid error propagation through the feedback of

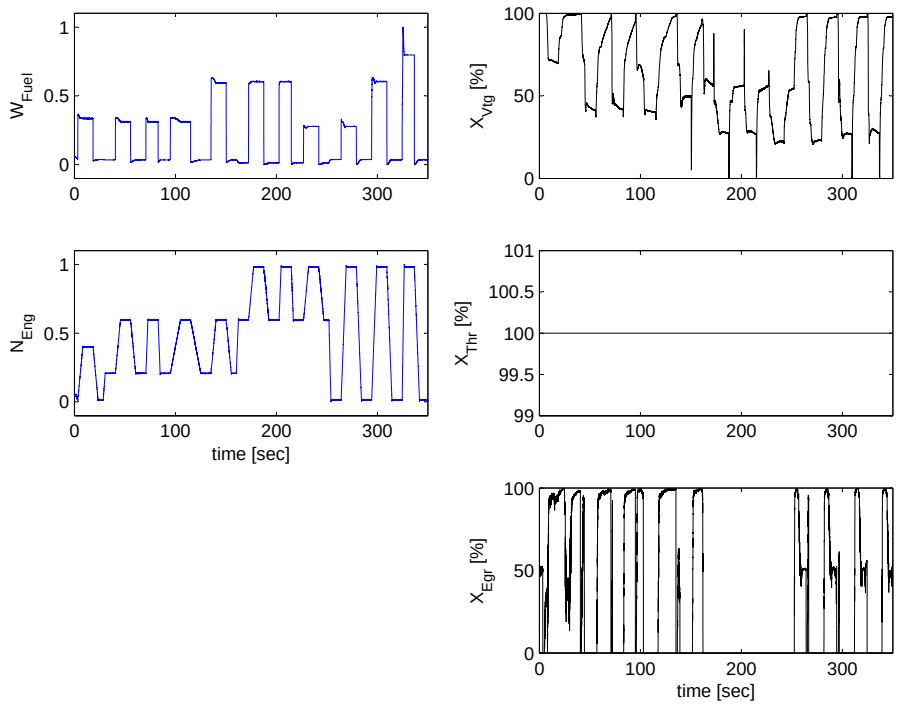

(a) system inputs

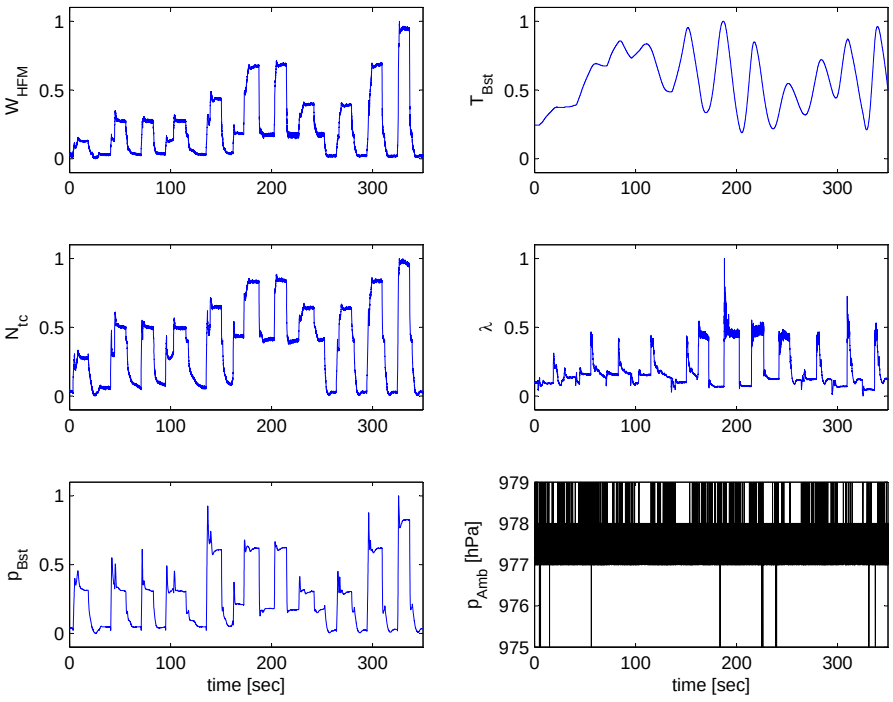

(b) system outputs

Figure 4.11: Diesel engine system inputs (control commands and measurable disturbances) and outputs (sensor measurements)

Table 4.4: Modeling performance evaluation via χ

	Data A	Data B	Data C
Model with full inputs	1.84%	2.07%	1.45%
Model with selected inputs	1.47%	1.99%	1.32%

the output variable itself which could potentially hamper the diagnostic capability, the auto-regressive terms are not included in this work, that is $(n_a)_{\max} = 0$. With the engine speeds ranging from 1500RPM up to 4000RPM, an average combustion cycle lasts about 40ms. Thus, the dynamic parameters are set as $(n_b)_{\max} = 3$, and $(n_k)_{\max} = 3$, thus $B_{n_b} = 2$, and $B_{n_k} = 2$. With a properly selected GA parameters, the proposed method converged to a solution within 60 generations for output $\mathbf{y} = [W_{Air},\ p_{Bst}]^T$.

To illustrate the effectiveness of the proposed method, the performance of two Growing Structure Multiple Model System (GSMMS) Liu et al. [2009a] in the form of (4.11) are compared in Table 4.4. One of the model includes the full set of input variables with $n_{b,j} = (n_b)_{\max}$ and $n_{k,j} = (n_k)_{\max}$ for $j = 1, ..., q\ (q = 4)$, while the other model only includes those input variables that are selected by the proposed approach. Both of the models are identified using one set of training data, and their performances are evaluated via χ, defined in (4.22), using three separate sets of testing data. All the training and test data are collected under normal operations under the same drive cycle.

$$\chi = \frac{1}{p}\sum_{i=1}^{p}\frac{\bar{e}_i}{max(\bar{y}_i)} \times 100\% \tag{4.22}$$

$$\bar{e}_i = \sqrt{\frac{1}{N}\sum_{t=0}^{N}\left(\bar{y}_i(t) - \hat{\bar{y}}_i(t)\right)^2} \tag{4.23}$$

$\bar{y}_i,\ i = 1, \ldots, p$ denotes the output variables normalized as in (4.21).

As shown in Table 4.4, the input selection method with the fitness function defined

in (4.16) is able to reduce the model complexity without compromising its accuracy, which could help avoid the problem of over-parametrization and potentially improve the generalization capability of the identified model.

4.4 Summary

A novel algorithm is proposed in this chapter to solve the input selection problem in nonlinear dynamic system modeling by converting it into one of a set of linear models. Since linearization of the nonlinear function is operating region dependent, the growing self-organizing network is employed to provide an appropriate partition of the operating region, thus enabling the approximation of the nonlinear behavior with a set of linear auto-regressive local models with exogenous inputs.

With parameters B_{n_a}, B_{n_b} and B_{n_k} determined in advance, a set of candidate input variables $\mathcal{S}$ can be derived, from which the proper input variables are selected using the all-possible-regression algorithm. Then, the genetic algorithm is employed to solve the combinational optimization problem introduced by the all-possible-regression algorithm while reducing the computation burdened caused by the huge number of potential solutions. In addition to an efficient encoding scheme, a fitness function based on the minimum description length principle is employed in the genetic algorithm in order to achieve a balance between the model complexity and modeling accuracy.

This input selection method establishes a general approach that can be applied to various nonlinear system identification algorithms. It has been demonstrated in the simulation examples and the modeling of a diesel engine airflow system that this method is able to select the proper input variables for nonlinear dynamic models even in the presence of high correlation among candidate input variables.

CHAPTER V

Modeling and Diagnosis of Leakage and Sensor Faults in a Diesel Engine Air Path System

5.1 Introduction

Introduced by CARB (California Air Resource Board), the On-Board Diagnostic (OBD) system was first made mandatory for gasoline vehicles sold in California around the mid 1990s. Since then, such OBD requirements have been adopted for various automotive applications, in other regions of the USA as well as the European Union. In recent years, the growing demands for emissions and fuel efficiency has driven the development of advanced powertrain with increased system complexity, which in turn imposes higher requirements on the OBD system.

When a fault is detected for the first time, the associated fault code is stored with its status labeled as *pending*. After such a fault is detected during two consecutive driving cycles, the Malfunction Indicator Light (MIL) is triggered and the status of the associated fault code is changed as *confirmed*. The current automotive diagnostic system, as reviewed in [Jones and Li, 2000; Rizzoni et al., 1993; Mohammadpour et al., 2011], performs diagnosis based on a pre-determined fault list that is generated from past experiences using techniques such as fault tree analysis and failure modes / effects analysis. In addition to the limited diagnostic coverage, the current OBD system may not be able to identify the fault due to the similar observable effects

in the target system. For instance, a leakage in the boost manifold or the intake manifold could both lead to decreases in the measured boost pressure and intake pressure as well as an increase in the measured intake air mass flow rate.

The detection of air leakage in the intake manifold of a turbocharged engine, for instance, can be difficult as the turbocharger will inherently be controlled to counteract the fault and maintain the boost pressure at a desired level [Antory, 2007]. As a sensor in the measuring system can also fail, such a problem becomes even more challenging. The failure to locate the air leaks could lead to undesired control action on exhaust gas recirculation, thus resulting in an increase in NO_x emissions. In [Ceccarelli et al., 2009], a nonlinear model-based adaptive observer with fixed and variable gains was investigated to detect leaks in the intake manifold of a diesel engine. A nonlinear observer was also proposed in [Vinsonneau et al., 2002] to estimate in real time the mass air flow rate leaked in the intake manifold of a spark-ignition engine. Such a model derived from the flow equation through a restriction was also used in [Nyberg, 2002, 2003], in which a leak in the intake manifold and one in the induction volume located between the intercooler and throttle, were distinguished using structured hypothesis test. A parameter identification approach via an extended Kalman filter was developed in [Nyberg and Nielsen, 1997; Nyberg and Perkovic, 1998] based on a nonlinear state-space model of a diesel engine air path system in order to detect possible intake manifold leakage.

The detection of air leakage can be even more challenging when taking into account potential sensor failures that could result in similar phenomenon in the measured variables. For instance, a failure in the intake mass air flow sensor and an air leakage in the intake manifold both lead to a deviation in its measurements from the normal values. The potential sensor failures considered in this work for air leakage detection

involve the hot-film mass flow sensor installed at the engine intake and the manifold absolute pressure sensors. Early work was proposed in [Rizzoni and Min, 1991] to construct model-based filters for detecting a manifold absolute pressure sensor failure. Widely adopted in the engine management system, detection of additive or multiplicative failures in the mass air flow and manifold absolute pressure sensor has also investigated in [Namburu et al., 2007; Weinhold et al., 2005; Nyberg, 2002; Vinsonneau et al., 2002; Gunnarsson, 2001; Nilsson, 2007].

In this work, an approach is developed to diagnose faults in the air path of a diesel engine equipped with a Variable Nozzle Turbine (VNT) and Exhaust Gas Recirculation (EGR). Developed based on the analytical redundancies among the variables measured by the existing sensors, the approach constructs three anomaly detectors in terms of mass flow rate in order to detect and isolate the target faults. The faults investigated in this work include both sensor failures in the air path system and air leakage in the manifolds.

The remainder of this chapter is organized as follows. In Section 5.2, a model that describes the normal system behaviors in the diesel engine air path is presented. In addition, sub-models to capture the dynamics in sensors as well as the effects of air leaks are introduced. The nominal model, parameterized with dynamometer measurements from a diesel engine, is augmented with the sub-models to simulate the behaviors of the target system failures. In Section 5.3, the fault detection and isolation residuals, $W_{LeakBst}$, $W_{LeakInt}$, and ΔW_{Cyl} are constructed based on the measurements from a hot-film mass air flow sensor, W_{HFM}, and the estimated mass air flow through the throttle, W_{Thr}, and that into the cylinders, W_{Cyl}. Without the need for a thorough understanding of the dependencies between the estimated variables and the identified input variables, the Growing Structure Multiple Model System

(GSMMS) system identification algorithm is employed. The diagnostic performance of the proposed residual variables are then illustrated.

5.2 Diesel Engine Air Path

5.2.1 Description

The target air path, as illustrated in Figure 5.1, consists of the components: [C.1] hot-wire air flow meter, [C.2] turbocharger, [C.2a] compressor, [C.2b] variable nozzle turbine (Vnt), [C.3] boost manifold, [C.4] charge air cooler, [C.5] throttle valve (Thr), [C.6] air intake manifold, [C.7] exhaust gas recirculation valve (Egr), [C.8] exhaust gas recirculation cooler, [C.9] exhaust gas manifold (Exh), and [C.10] engine (Eng). The variables that used to describe the system are listed in Table 5.1. The use of the turbocharger and exhaust gas recirculation (EGR) results in coupled dynamics in the intake and exhaust systems. The recirculated cooled exhaust gas affects the temperature, pressure, and oxygen concentration of the air mixture in the intake manifold. In turn, the air mixture entering the engine influences the combustion behaviors, thus affecting the exhaust gas conditions. Similarly, the turbocharger couples the intake and exhaust systems by utilizing the exhaust gas energy to improve the engine volumetric efficiency.

The air path is controlled by the effective area A_{Thr} of the electro-pneumatic actuated throttle valve [C.5], the exhaust gas recirculation valve A_{Egr} [C.7], and the variable nozzle turbine A_{Vnt} [C.2b]. The injected fuel quantity, W_{Fuel}, and the engine speed, n_{Eng}, are considered as measured disturbances in this work. Thus, the input signals of the air path system, sampled at a discrete time k, are defined as

$$\mathbf{u}_k = \begin{bmatrix} A_{Vnt,k} & A_{Thr,k} & A_{Egr,k} & n_{Eng,k} & W_{F,k} \end{bmatrix}^T \tag{5.1}$$

In order to capture the system dynamics, the state $\mathbf{z}$ is defined for the diesel engine

Table 5.1: Nomenclature for diesel engine air path system

Symbol	Description
A_{Vnt}	Effective cross-section area of variable nozzle turbine
A_{Thr}	Effective cross-section area of throttle
A_{Egr}	Effective cross-section area of exhaust gas recirculated valve
n_{Eng}	Engine rotational speed
n_{Turb}	Turbocharger rotational speed
p_{Bst}	Boost pressure
p_{Int}	Intake manifold pressure
p_{Exh}	Exhaust manifold pressure
m_{Bst}	Charge mass trapped in boost manifold
$m_{Air,Int}$	Air mass trapped in intake manifold
$m_{Egr,Int}$	Recirculated exhaust gas trapped in intake manifold
$mO2_{Int}$	Mass of oxygen trapped in intake manifold
m_{Exh}	Charge mass trapped in exhaust manifold
$rO2_{Thr}$	Mass ratio of oxygen in air through throttle
$rO2_{Int}$	Mass ratio of charge in intake manifold
$rO2_{Egr}$	Mass ratio of oxygen in recirculated exhaust gas
W_{Air}	Mass flow rate of inducted air
W_{HFM}	Mass flow rate of inducted air measured by hot-film mass air flow sensor
W_{Egr}	Mass flow rate of recirculated exhaust gas
W_{Comp}	Mass flow rate of air through compressor
W_{Turb}	Mass flow rate of charge through turbine
W_{Thr}	Mass flow rate of air through throttle
W_{Cyl}	Mass flow rate of charge inducted into the cylinders
W_{Exh}	Mass flow rate of charge leaving the cylinders
W_{Fuel}	Mass flow rate of injected fuel
$W_{Leak,Bst}$	Mass flow rate of leaked charge in boost manifold
$W_{Leak,Int}$	Mass flow rate of leaded charge in intake manifold
$T_{Comp,dn}$	Charge temperature at compressor downstream
$T_{CAC,up}$	Charge temperature at charge air cooler upstream
$T_{CAC,dn}$	Charge temperature at charge air cooler downstream
T_{EGR}	Exhaust gas temperature recirculated into intake manifold
T_{Exh}	Charge temperature in exhaust manifold
V_{Bst}	Effective volume of boost manifold
V_{Int}	Effective volume of intake manifold
V_{Exh}	Effective volume of exhaust manifold
Q_{LHV}	Low heating value of fuel
R_{Air}	Universal gas constant of air
R_{Int}	Universal gas constant of charge in intake manifold
R_{Exh}	Universal gas constant of charge in exhaust manifold
$c_{p,Air}$	Specific heat capacity at constant pressure of air
$c_{p,Int}$	Specific heat capacity at constant pressure of charge in intake manifold
$c_{p,Exh}$	Specific heat capacity at constant pressure of charge in exhaust manifold
$c_{v,Air}$	Specific heat capacity at constant volume of air

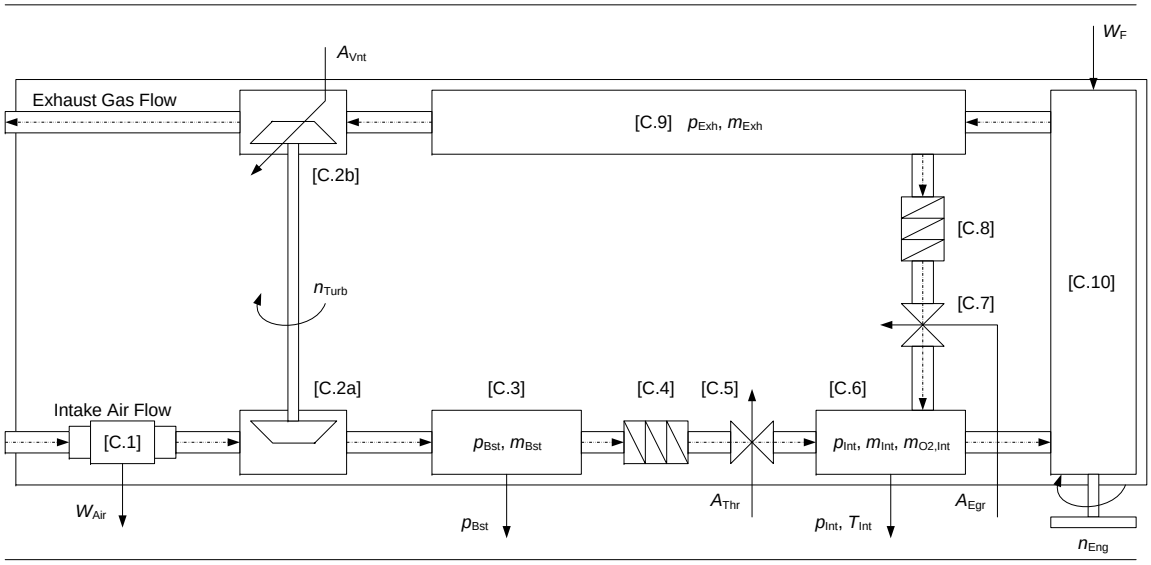

Figure 5.1: Air path of a diesel combustion engine [Aßfalg et al., 2006]

air path system as

$$\mathbf{z} = \begin{bmatrix} \mathbf{p} & \mathbf{m} & n_{Turb} \end{bmatrix} \tag{5.2}$$

where n_{Turb} denotes the turbocharger speed, and $\mathbf{p}$ and $\mathbf{m}$ denote the pressures and charge masses in manifolds [C.3], [C.6], and [C.9] as

$$\begin{aligned} \mathbf{p} &= \begin{bmatrix} p_{Bst} & p_{Int} & p_{Exh} \end{bmatrix}^T \\ \mathbf{m} &= \begin{bmatrix} m_{Bst} & m_{Air,Int} & m_{Egr,Int} & mO2_{Int} & m_{Exh} \end{bmatrix}^T \end{aligned}$$

In the target system, the following output signals are measured at discrete time k.

$$\mathbf{y}_k = \begin{bmatrix} p_{Bst,k} & p_{Int,k} & W_{Air,k} \end{bmatrix}^T \tag{5.3}$$

5.2.2 System Modeling

The model used in the diagnosis algorithm is based on the principles described in [Heywood, 1992; Nyberg and Perkovic, 1998]. Following the law of mass and enthalpy conservation, the pressure p_{Bst} and mass m_{Bst} in the boost manifold can be modeled

as

$$\dot{p}_{Bst} = \frac{R_{Air}}{V_{Bst}c_{v,Air}}\left(c_{p,Air}W_{Comp}T_{Comp,dn} - c_{p,Air}W_{Thr}T_{CAC,up}\right) \tag{5.4}$$

$$\dot{m}_{Bst} = W_{Comp} - W_{Thr} \tag{5.5}$$

where W_{Comp} and W_{Thr} denote the mass air flow rate through the compressor and throttle, $T_{Comp,dn}$ and $T_{CAC,up}$ denote the compressor downstream and charge air cooler upstream temperature. R_{Air}, $c_{p,Air}$, and $c_{v,Air}$ denote the gas constant, the specific heat capacity at constant pressure, and the specific heat capacity at constant volume for air, respectively. The mass air flow rate through the throttle, W_{Thr}, can be modeled below as an orifice.

$$W_{Thr} = A_{Thr}\frac{p_{Bst}}{\sqrt{R_{Air}T_{Bst}}}\Phi_{\kappa_{Air},Thr}\left(\frac{p_{Int}}{p_{Bst}}\right) \tag{5.6}$$

where $\Phi_{\kappa,[C.x]}$ captures the restriction of flow to subsonic speeds across the orifice component [C.x] with the heat capacity ratio $\kappa = \frac{c_p}{c_v}$. In a specific component, Φ_κ can be expressed as

$$\Phi_\kappa\left(\frac{p_{up}}{p_{dn}}\right) = \begin{cases} \sqrt{\frac{\kappa}{\kappa-1}\left(\left(\frac{p_{dn}}{p_{up}}\right)^{\frac{2}{\kappa}} - \left(\frac{p_{dn}}{p_{up}}\right)^{\frac{\kappa+1}{\kappa}}\right)} & \left(\frac{p_{dn}}{p_{up}}\right) > \left(\frac{2}{\kappa+1}\right)^{\frac{\kappa}{\kappa-1}} \\ \sqrt{\frac{\kappa}{\kappa-1}}\left(\frac{2}{\kappa+1}\right)^{\frac{1}{\kappa-1}} & \left(\frac{p_{dn}}{p_{up}}\right) \leq \left(\frac{2}{\kappa+1}\right)^{\frac{\kappa}{\kappa-1}} \end{cases} \tag{5.7}$$

where p_{up} and p_{dn} denote the upstream and downstream pressures.

The dynamics for the intake manifold [C.6] can be modeled with the state $\mathbf{z}_{Int} = \begin{bmatrix} p_{Int} & m_{Air,Int} & m_{Egr,Int} & m_{O2,Int} \end{bmatrix}^T$ as

$$\begin{aligned} \dot{p}_{Int} = \frac{R_{Int}}{V_{Int}c_{v,Int}}\big(&c_{p,Air}W_{Thr}T_{CAC,dn} \\ &+c_{p,Exh}W_{Egr}T_{Egr} - c_{p,Int}W_{Cyl}T_{Int}\big) \end{aligned} \tag{5.8}$$

$$\dot{m}_{Air,Int} = W_{Thr} - \frac{m_{Air,Int}}{m_{Air,Int}+m_{Egr,Int}}W_{Cyl} \tag{5.9}$$

$$\dot{m}_{Egr,Int} = W_{Egr} - \frac{m_{Egr,Int}}{m_{Air,Int}+m_{Egr,Int}}W_{Cyl} \tag{5.10}$$

and

$$\dot{m}_{O2,Int} = W_{Egr} rO2_{Egr} + W_{Thr} rO2_{Thr} - W_{Cyl} rO2_{Int} \tag{5.11}$$

W_{Egr} and W_{Cyl} denote the mass flow rate of the exhaust gas recirculated into the intake manifold and that of the cylinder charger entering the cylinders. The EGR flow rate, W_{Egr}, is also modeled as

$$W_{Egr} = A_{Egr} \frac{p_{Exh}}{\sqrt{R_{Exh} T_{Exh}}} \Phi_{\kappa_{Exh}, Egr} \left(\frac{p_{Int}}{p_{Exh}} \right) \tag{5.12}$$

and the associated temperature can be modeled as

$$T_{EGR} = \left(\frac{p_{Int}}{p_{Exh}} \right)^{1 - \frac{1}{\kappa_{Exh}}} T_{Exh} \tag{5.13}$$

The intake manifold temperature, T_{Int}, can be derived from the ideal gas law as

$$T_{Int} = \frac{p_{Int} V_{Int}}{(m_{Air,Int} + m_{Egr,Int}) R_{Int}} \tag{5.14}$$

$rO2_{(\cdot)}$ denote the mass fraction of oxygen in the associated flow. Thus, $rO2_{Thr} = rO2_{Air} = 21\%$, $rO2_{Int}$ can be defined as

$$rO2_{Int} = \frac{mO2_{Int}}{m_{Air,Int} + m_{Egr,Int}}, \tag{5.15}$$

and $rO2_{Egr}$ depends on the exhaust gas composition. Due to the different composition of fresh charge and recirculated exhaust gas, thermodynamic properties of the charge in the intake manifold can be derived as follows.

$$\begin{aligned} R_{Int} &= \frac{m_{Air,Int} R_{Air} + m_{Egr,Int} R_{Exh}}{m_{Air,Int} + m_{Egr,Int}} \\ c_{v,Int} &= \frac{m_{Air,Int} c_{v,Air} + m_{Egr,Int} c_{v,Exh}}{m_{Air,Int} + m_{Egr,Int}} \\ c_{p,Int} &= c_{v,Int} + R_{Int} \end{aligned} \tag{5.16}$$

In order to establish the coupling between intake and exhaust system, a simple engine model is used in this work. The mass flow rate of the charge entering the

cylinders, W_{Cyl}, and the exhaust gas leaving the cylinders, W_{Exh}, are modeled as

$$W_{Cyl} = f_{vol}\frac{n_{Eng}}{60}\frac{V_{Eng}}{2}\frac{p_{Int}}{R_{Int}T_{Int}} \tag{5.17}$$

$$W_{Exh} = W_{Cyl} + W_{Fuel} \tag{5.18}$$

where f_{vol} denotes the volumetric efficiency and identified to be dependent of engine speed n_{Eng} in RPM. The exhaust gas temperature

$$T_{Exh} = T_{Int} + \frac{f_{comb}W_{Fuel}Q_{LHV}}{c_{p,Exh}(W_{Cyl} + W_F)} \tag{5.19}$$

where f_{comb} captures the combustion efficiency of the engine and identified to be dependent of cylinder charge composition, λ_c, and engine speed, n_{Eng}. Based on the estimated T_{Exh}, the pressure in the exhaust manifold [C.9] can be modeled as

$$p_{Exh} = \frac{m_{Exh}R_{Exh}T_{Exh}}{V_{Exh}} \tag{5.20}$$

and the dynamics of the exhaust manifold can be captured as

$$\dot{m}_{Exh} = W_{Exh} - W_{Turb} - W_{Egr} \tag{5.21}$$

Controlled by the turbine vane position, A_{Vnt}, the flow rate of the exhaust gas through the turbine, W_{Turb}, can be modeled as orifice with effective cross-section area of A_{Vnt}.

$$W_{Turb} = A_{Vnt}\frac{p_{Exh}}{\sqrt{R_{Exh}T_{Exh}}}\Phi_{\kappa_{Exh},Turb} \tag{5.22}$$

where A_{Vnt} is dependent of the turbine vane position, θ_{Vnt}, and the pressure ratio across the turbine, $\frac{p_{Exh}}{p_{Amb}}$. Here, p_{Amb} denotes the ambient pressure.

Experimental data were collected to parameterize the baseline model for simulations. Due to limited available data, the model was only calibrated for operations during which the throttle angle, θ_{Thr}, was left wide open, and the EGR valve, θ_{Egr}, was kept closed. Therefore, the main actuator for the air path system is the vane

position, θ_{Vnt}, of the variable nozzle turbine. In addition, the fuel injection quantity, W_{Fuel}, as the main actuator for torque control, and the engine speed, n_{Eng}, considered as external disturbances, are illustrated in Figure 5.2. In the remainder of this chapter, (A_{Thr}, A_{Egr}, A_{Vgt}) denote the relative effective cross-section area of the throttle, EGR valve, and VGT vane in reference to their lower mechanical limits. Other variables, except the ambient pressure are normalized using the min-max method in (4.21) with the minimum and maximum of the variables derived from the training data.

$$\bar{z} = \frac{z - \min(z)}{\max(z) - \min(z)} \tag{5.23}$$

where $\bar{z}$ denote the normalized variable of z, $\min(z)$ and $\max(z)$ are the minimum and maximum values of z.

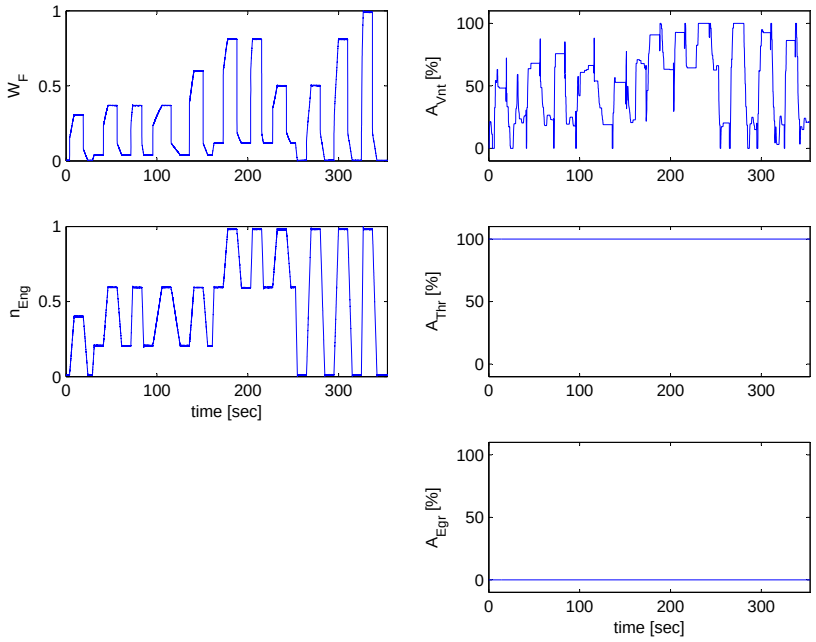

Figure 5.2: Diesel engine air path system simulation inputs

In addition to the measured system outputs, $\mathbf{y} = [\ p_{Bst},\ \ p_{Int},\ \ W_{Air},\ \ \lambda\ ]$, the simulation model also provides insights into the exhaust manifold pressure, p_{Exh}, the

turbocharger speed, n_{Turb}, and the charge temperatures in the manifolds. It can be observed that the target system with its key measured and simulated outputs illustrated in Figure 5.3 is highly dynamic.

5.2.3 Modeling of Faults

5.2.3.1 Leakage

The leakage is modeled in this work to be located in the induction volume or the intake manifold. The leak size is assumed to be constant, and the flow through the leakage is modeled as the flow through a restriction. Such a model has been validated in [Nyberg and Perkovic, 1998] with desirable results.

If a leak occurs in the boost manifold, its dynamics can be captured as

$$\begin{aligned} \dot{p}_{Bst} &= \frac{R_{Air}}{V_{Bst}c_{v,Air}}\left(c_{p,Air}W_{Comp}T_{Comp,dn}\right. \\ &\quad \left. -c_{p,Air}(W_{Thr}+W_{Leak,Bst})T_{CAC,up}\right) \end{aligned} \tag{5.24}$$

$$\dot{m}_{Bst} = W_{Comp} - W_{Thr} - W_{Leak,Bst} \tag{5.25}$$

where

$$W_{Leak,Bst} = A_{Leak,Bst}\frac{p_{Bst}}{\sqrt{R_{Air}T_{Bst}}}\Phi_{\kappa_{Air},Leak_{Bst}}\left(\frac{p_{Amb}}{p_{Int}}\right) \tag{5.26}$$

If a leak occurs in the intake manifold, its dynamics can be captured as

$$\begin{aligned} \dot{p}_{Int} &= \frac{R_{Int}}{V_{Int}c_{v,Int}}\left(c_{p,Air}W_{Thr}T_{CAC,dn}\right. \\ &\quad \left. +c_{p,Exh}W_{Egr}T_{Egr} - c_{p,Int}(W_{Cyl}+W_{Leak,Int}T_{Int})\right) \end{aligned} \tag{5.27}$$

$$\dot{m}_{Air,Int} = W_{Thr} - \frac{m_{Air,Int}}{m_{Air,Int}+m_{Egr,Int}}(W_{Cyl}+W_{Leak,Int}) \tag{5.28}$$

$$\dot{m}_{EGR,Int} = W_{Egr} - \frac{m_{Egr,Int}}{m_{Air,Int}+m_{Egr,Int}}(W_{Cyl}+W_{Leak,Int}) \tag{5.29}$$

$$\dot{m}_{O2,Int} = W_{Egr}rO2_{Egr} + W_{Thr}rO2_{Thr} - (W_{Cyl}+W_{Leak,Int})rO2_{Int} \tag{5.30}$$

where

$$W_{Leak,Int} = A_{Leak,Int}\frac{p_{Int}}{\sqrt{R_{Int}T_{Int}}}\Phi_{\kappa_{Air},Leak_{Int}}\left(\frac{p_{Amb}}{p_{Int}}\right) \tag{5.31}$$

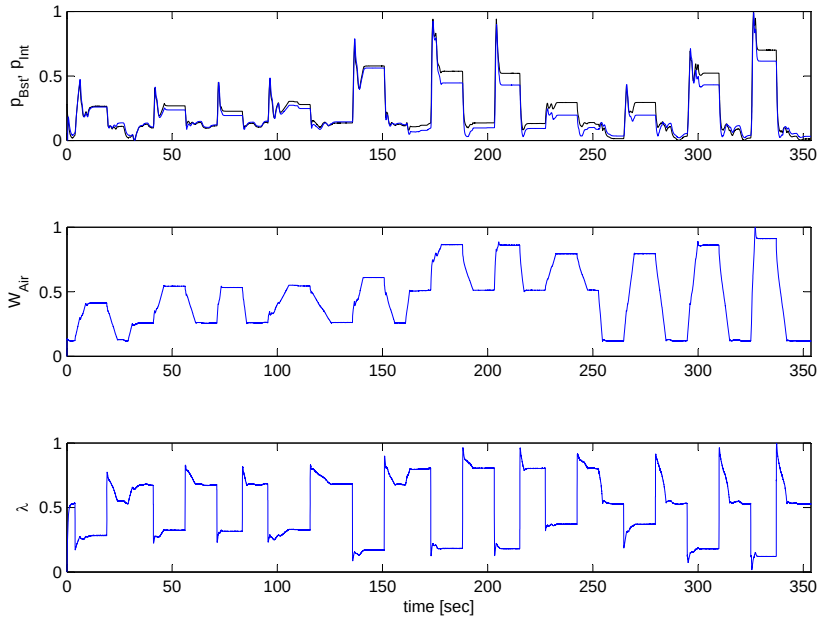

(a) Measured Outputs

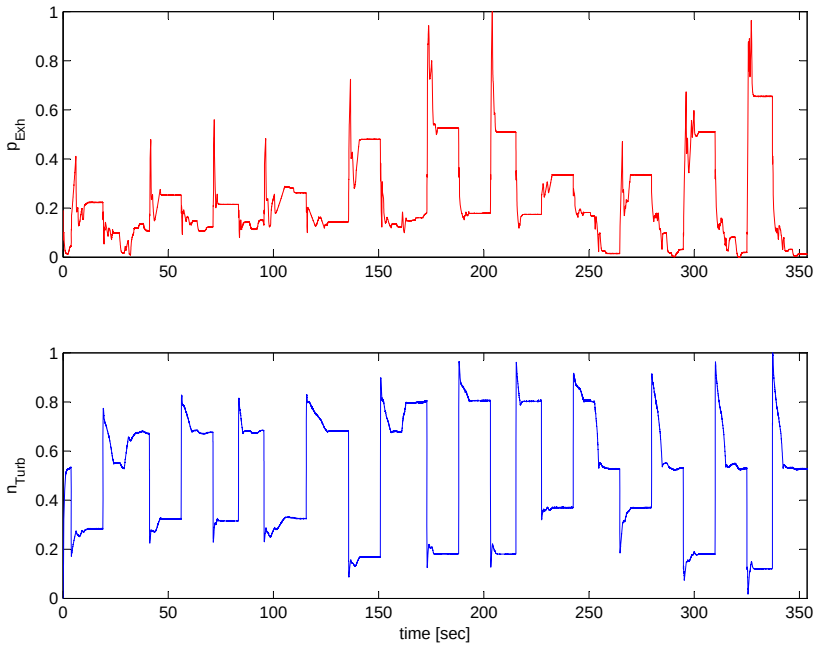

(b) Estimated Outputs

Figure 5.3: Diesel engine air path system simulation outputs under fault-free conditions

In this work, the leakage size in the boost manifold, $A_{Leak,Bst}$, and that in the intake manifold, $A_{Leak,Int}$, are assumed to be the same. Figure 5.4 compares the system behavior under fault-free conditions ($F0$) with those under boost manifold leakage ($F4$) and intake manifold leakage ($F5$). It can be observed that these two failure modes result in similar behaviors in the measured system outputs $\mathbf{y} = \begin{bmatrix} p_{Bst}, & p_{Int}, & W_{Air,HFM} \end{bmatrix}^T$, which indicates the need for a dedicated fault diagnostic algorithm. The leakage in the boost and intake manifold both lead to decreases in the boost pressure, p_{Bst}, and intake manifold pressure, p_{Int}, as well as an increase in the intake mass air flow sensor measurements. For the estimated variables, both faults have similar effects on the exhaust manifold pressure, p_{Exh}, and result in a decrease in the turbocharger speed, n_{Turb}.

5.2.3.2 Pressure Sensor Bias

The dynamics of a pressure sensor is modeled as first-order system.

$$p_s + \tau_p^s \dot{p}_s = k_p^s p \tag{5.32}$$

where k_p^s and τ_p^s denote the gain and time constant of the pressure sensor. When a sensor bias fault occurs, $k_p^s \neq 1$ is an unknown constant. The pressure sensor measurements are then filtered with a varying filter time constant.

$$p_{s,f} + \tau_{LPF} \dot{p}_{s,f} = p_s \tag{5.33}$$

where $\tau_{LPF} = \frac{180}{n_{Eng}}$ denotes its time constant.

5.2.3.3 Temperature Sensor Bias

The dynamics of a temperature sensor is modeled as a first-order system.

$$T_s + \tau_T^s \dot{T}_s = k_T^s T \tag{5.34}$$

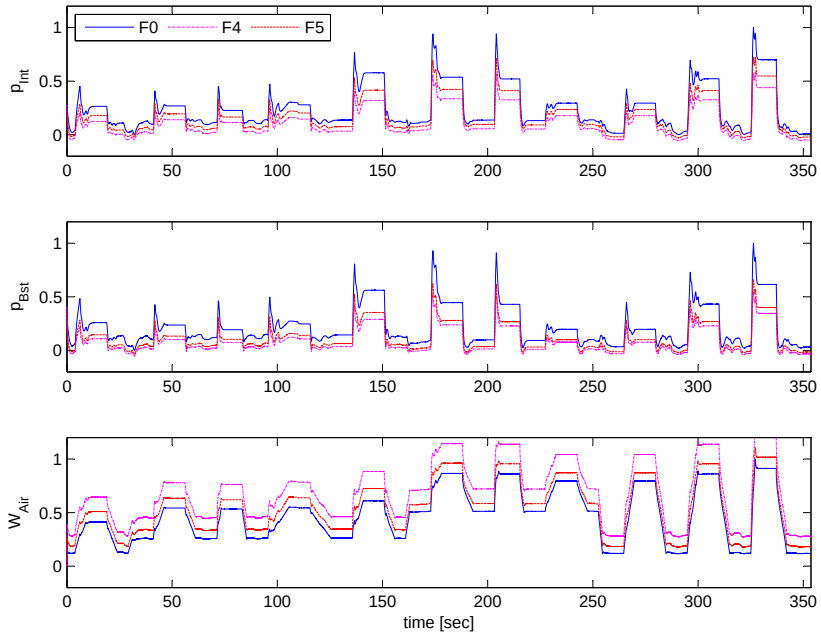

(a) Measured Outputs

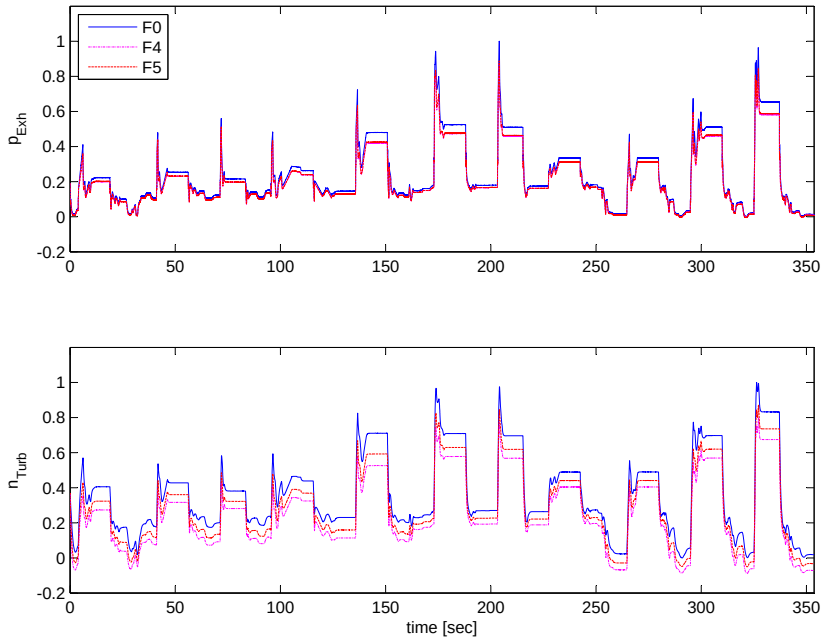

(b) Estimated Outputs

Figure 5.4: Diesel engine air path system simulation outputs under ($F0$) fault-free conditions, ($F4$) leakage in the boost manifold, and ($F5$) leakage in the intake manifold

where k_T^s and τ_T^s denote the gain and time constant of the temperature sensor. When a sensor bias fault occurs, $k_T^s \neq 1$ is an unknown constant.

5.2.3.4 Mass Air Flow Sensor Bias

The intake air mass information is necessary for the engine control unit to enable air/fuel control and thus deliver the desired amount of fuel. With the advantages of quick response and low air flow restriction, the hot-film mass air flow sensor has been widely used in automotive industry. The use of a hot-film mass air flow sensor at the engine intake improves the reliability of the air mass estimation and the engine system diagnostic capability.

As the electric resistance of the embedded wire varies with temperature, the current required to maintain the wire temperature is thus directly proportional to the mass of air flowing through the sensor. In this work, the dynamics of the mass air flow sensor is simplified as a first-order system.

$$W_{HFM} + \tau_{HFM}\dot{W}_{HFM} = k_{HFM}W_{Air} \tag{5.35}$$

where k_{HFM} and τ_{HFM} denote the gain and time constant of the temperature sensor. When a sensor bias fault occurs, $k_{HFM} \neq 1$ is an unknown constant.

5.3 System Diagnosis

5.3.1 Fault Detector Design

As described above, the charge flow rate through the throttle, W_{Thr}, and that into cylinders, W_{Cyl}, can be modeled as

$$\begin{aligned} \hat{W}_{Thr} &= f_{Thr}\left(p_{Bst},\ \theta_{Thr},\ p_{Int} \right) \\ \hat{W}_{Cyl} &= f_{Cyl}\left(p_{Int},\ n_{Eng} \right) \end{aligned} \tag{5.36}$$

Without the need for extremely fast detection of faults, only static relations are considered in this work [Nyberg, 2002]. In a fault-free air path system, the relations among W_{Thr}, W_{Cyl}, and the measured mass air flow rate, W_{HFM}, under steady-state engine operation conditions can be described as

$$W_{HFM} = W_{Thr},\ and\, W_{Thr} + W_{Egr} = W_{Cyl} \tag{5.37}$$

When a leakage occurs in the boost or intake manifold, such relations can be augmented as

$$\begin{aligned} W_{HFM} &= W_{Thr} + W_{Leak,Bst} \\ W_{Thr} &= W_{Cyl} \end{aligned} \tag{5.38}$$

and

$$\begin{aligned} W_{HFM} &= W_{Thr} \\ W_{Thr} + W_{Egr} &= W_{Cyl} + W_{Leak,Int} \end{aligned} \tag{5.39}$$

$W_{Leak,Bst}$ and $W_{Leak,Int}$ denote the leaked charge mass flow rate in the boost and intake manifold. Based on these physical models, $W_{Leak,Bst}$, $W_{Leak,Int}$ and W_{Cyl} in (5.38) and (5.39) can be derived from the intake air mass flow sensor measurements W_{HFM}, and the estimated charge flow rate $\hat{W}_{Thr}$ and $\hat{W}_{Cyl}$.

$$\begin{aligned} W_{Leak,Bst} &= W_{HFM} - \hat{W}_{Thr} \\ W_{Leak,Int} &= \hat{W}_{Thr} + \hat{W}_{Egr} - \hat{W}_{Cyl} \\ \Delta W_{Cyl} &= W_{HFM} - \hat{W}_{Cyl} \end{aligned} \tag{5.40}$$

When the EGR valve is close (i.e. $A_{Egr} = 0\%$ as illustrated in Figure 5.2, the

above fault detectors can be simplified as

$$\begin{aligned} W_{Leak,Bst} &= W_{HFM} - \hat{W}_{Thr} \\ W_{Leak,Int} &= \hat{W}_{Thr} - \hat{W}_{Cyl} \\ \Delta W_{Cyl} &= W_{HFM} - \hat{W}_{Cyl} \end{aligned} \tag{5.41}$$

5.3.2 Fault Detection Construction

The Growing Structure Multiple Model System (GSMMS) system identification algorithm proposed in [Liu et al., 2009a], combines the advantages of a Growing Self-Organizing Network (GSON) with efficient local model parameter estimation into an integrated framework for modeling and identification of general nonlinear dynamic systems. Based on the "divide and conquer" philosophy, the GSMMS approach captures the nonlinear system dynamics with a set of connected multiple models, each of which is relatively simple in nature and can be analyzed in an analytically tractable manner.

Consider a nonlinear dynamic system with p outputs and q inputs described by

$$\begin{aligned} \mathbf{y}(k+1) &= \mathbf{F}\left(\mathbf{y}(k), \ldots, \mathbf{y}(k-n_a+1),\right. \\ &\qquad \left.\mathbf{u}(k-n_d), \ldots, \mathbf{u}(k-n_d-n_b+1)\right) + \mathbf{w}(k) \end{aligned} \tag{5.42}$$

where $\mathbf{u}(k) = [u_1(k), \ldots, u_q(k)]^T$ are the system inputs, $\mathbf{y}(k) = [y_1(k), \ldots, y_p(k)]^T$ are the system outputs, $\mathbf{w}(k) = [w_1(k), \ldots, w_p(k)]^T$ are the system disturbances. Here, $n_a \in \mathbb{R}^{p\times p}$ and $n_b \in \mathbb{R}^{p\times q}$ are the system orders, and $n_d \in \mathbb{R}^{p\times q}$ is the time lag from the moment that excitation is applied until when its effects can be observed from the outputs.

Assume the reconstruction space S can be described by the vector

$$\begin{aligned}\mathbf{s}(k) &= \big[\mathbf{y}^T(k), \ldots, \mathbf{y}^T(k-n_a+1) \\ &\quad \mathbf{u}^T(k-n_d), \ldots, \mathbf{u}^T(k-n_d-n_b+1)\big]^T \end{aligned} \tag{5.43}$$

As described in Section 4.2, the dynamics of such a nonlinear system can be approximated by combining the local linear models from the appropriately partitioned sub-regions.

$$\hat{y}(k+1) = \sum_{m=1}^{M} \nu_m(\mathbf{s}(k))\hat{\mathbf{F}}_m(\mathbf{s}(k)) \tag{5.44}$$

In the sub-region V_m, $\hat{\mathbf{F}}_m(\cdot)$ denotes the local model, and $\nu_m(\cdot)$ denotes the weighting functions that determine the validity of local function $\hat{\mathbf{F}}$ for the operation vector $\mathbf{s}$. Here, the Kronecker delta function is employed for simplicity.

$$\nu_m(\mathbf{s}(k) = \begin{cases} 1, & \text{if } \mathbf{s}(k) \in V_m \\ 0, & o.w. \end{cases} \tag{5.45}$$

Various model structures can be utilized to describe the local dynamics [Liu et al., 2009b]. In this work, the linear local model with parameters $\theta_m = [\mathbf{a}_m, \mathbf{b}_m]$ is used.

$$\hat{\mathbf{F}}_m(\mathbf{s}(k)) = \mathbf{a}_m + \mathbf{b}_m\mathbf{s}(k) \tag{5.46}$$

The growing mechanism of a SON enables the GSMMS algorithm to start with a small number of regions and then grow until a certain stopping criterion is satisfied. As described in Section 4.2, the topology of the self-organizing map can be described by a set of weight vectors $\xi_1, \ldots, \xi_M$. After the partition of the operating space is defined by the network, the best matching unit $c(k)$ can then be determined as

$$c(k) = \arg\min_m \|\mathbf{s}(k) - \xi_m\| \tag{5.47}$$

For local model identification, the parameters $\theta_m, m = 1, \ldots, M$ are determined by minimizing the sum of the weighted squared output errors in each sub-region.

$$J_m(\theta_m) = \frac{1}{k_m} \sum_{i=1}^{k_m} \omega_m(\mathbf{s}(k)) \|y(i) - \hat{y}_m(i)\|^2 \tag{5.48}$$

where k_m is number of samples in the m^{th} sub-region, and $\omega_m(\mathbf{s}(i))$ is the weight factor for the i^{th} observation when updating the model parameters of sub-region V_m. The weight factor $\omega_m(\mathbf{s}(k))$ is selected as

$$\omega_m(\mathbf{s}(k)) = \exp\left(\frac{-dis(m, c(k))^2}{2\sigma^2}\right), \quad m = 1, \ldots, M \tag{5.49}$$

where σ^2 denotes the effective range of the weighting function, and $dis(m, c(k))$ is defined as the shortest path distance between the representative node m and the best matching unit $c(k)$ on the self-organizing network. In this work, $dis(m, c(k))$ is calculated using the Breath-first algorithm from the adjacency matrix [Sedgewick, 1995].

Assume that all the data are available before the system identification, and thus the model parameters $\hat{\theta}_m, m = 1, \ldots, M$ can be estimated using the weighted linear least square algorithm.

$$(X_m^T W_m X_m)\hat{\theta}_m = X_m^T W_m y_m \tag{5.50}$$

where W_m is a diagonal matrix with $W_{m,ii} = \omega(\mathbf{s}(i)), \forall \mathbf{s}(i) \in V_m$ as defined in (5.49). X_m and $y_m(i)$ are constructed with the reconstruction vector $\mathbf{s}(i)$ and associated $y(i)$ in the sub-region m.

5.3.3 Fault Detection

Figure 5.5 illustrates a local fault detection and isolation scheme based on a multiple model structure. With sufficient data from the monitored system, the key relations between the inputs $\mathbf{u}$ and the measured outputs $\mathbf{y}_s$ are identified using

the GSMMS system identification algorithm. With the knowledge of the underlying physics, properly designed residuals, $\mathbf{r}$, can be generated using the measured outputs, $\mathbf{y}_s$, and the estimated outputs from the GSMMS model, $\hat{\mathbf{y}}_s$, identified using fault-free data. The GSMMS model provides additional information about the operation regime of the monitored system and the associated behaviors of the system outputs, $\mathbf{y}_{s,m}$, and the generated residuals, $\mathbf{r}_m$. The system controller determines the actuator signals, $\mathbf{u}$, based on the measured system outputs, $\mathbf{y}_s$, and the identified system fault, $\mathbf{I}_f$.

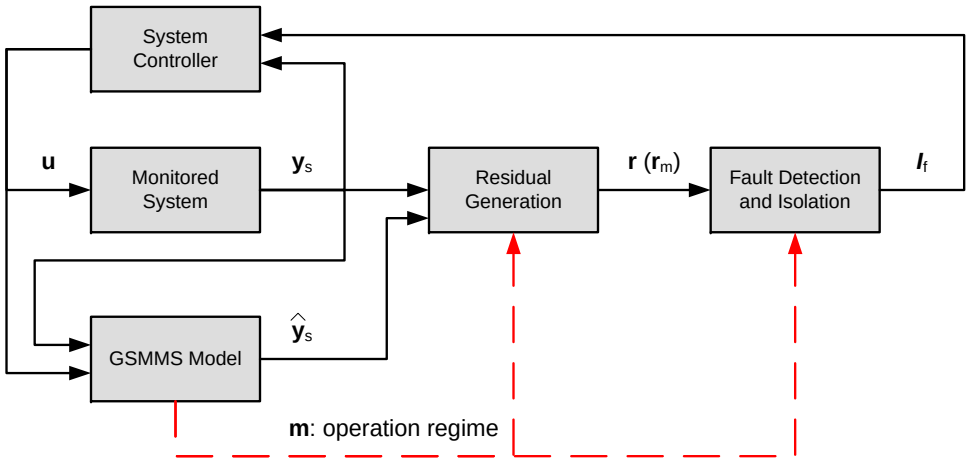

Figure 5.5: Local diagnostic scheme based on multiple model structure

Under normal operation conditions, the residuals in each region of the GSMMS model should in principle follow a Gaussian distribution. Therefore, at a certain time step, one of the local models is selected to best describe the current system dynamics and the residual variable follow a Gaussian distribution in the corresponding region. However, due to the filling dynamics in the manifolds, the residuals as defined in (5.41) should have non-zero values during transient operations. In addition, the switching among the local models in a GSMMS model due to the dynamic operations also introduces non-Gaussian global behaviors.

As discussed in Section 5.3.1, the relations $f_{Thr}(\cdot)$ and $f_{Cyl}(\cdot)$ in (5.36) are identi-

fied based on fault-free data from the diesel engine air path system using the GSMMS system identification algorithm. As shown in Figure 5.6, the identified model captures the air path system dynamics in charge mass flow rate and manifold pressures. Based on the assumption that the models identified using the GSMMS algorithm are able to capture the dynamics in the associated variables, the residuals generated from the fault detectors $W_{Leak,Bst}$, $W_{Leak,Int}$, and ΔW_{Cyl} should follow gaussian distribution with zero mean value under normal conditions. A fault can thus be detected if the residuals generated from any of the three fault detectors depict different behaviors. The residual variables $\hat{W}_{Leak,Int}$, $\hat{W}_{Leak,Bst}$, and $\Delta\hat{W}_{Cyl}$ in Figure 5.6 follow the quasi-gaussian distribution with mean value of zero and variance of σ, $\mathbf{r} \sim \mathfrak{N}(0, \sigma^2)$.

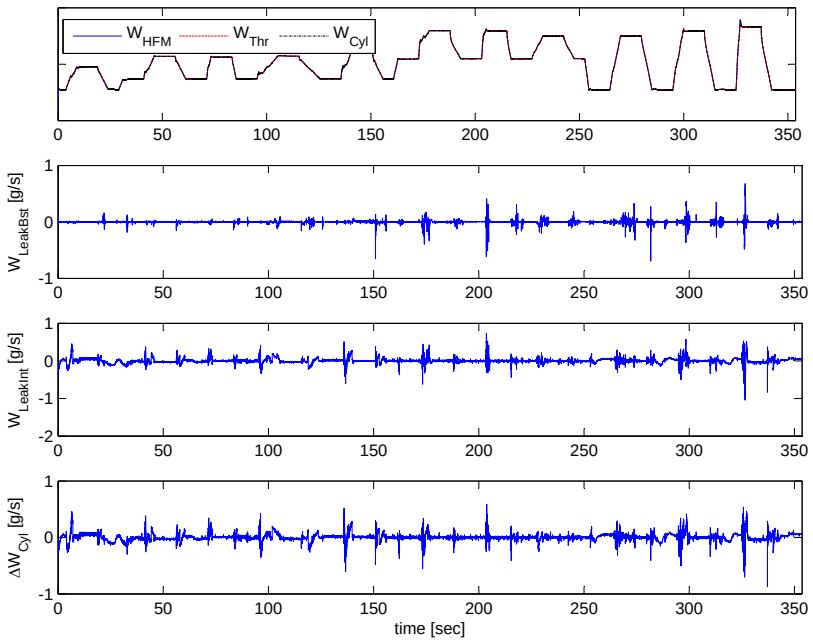

Figure 5.6: Model behaviors under normal engine operations

Using the simulation model developed in Section 5.2, various faults as listed in Table 5.2 are simulated. The behaviors of the fault detectors, constructed based on

the variables of $\hat{W}_{Leak,Int}$, $\hat{W}_{Leak,Bst}$, and $\Delta\hat{W}_{Cyl}$, under various faults are illustrated in Figure 5.7-5.11.

5.3.4 Fault Isolation

In order to avoid interpreting the effects caused by the engine transients on the residual variables as faults, the residuals as defined in (5.41) are evaluated globally at a sufficiently long period of time. As summarized in Table 5.2, the residuals, $W_{Leak,Bst}$, $W_{Leak,Int}$, and ΔW_{Cyl}, that illustrate a global pattern with zero mean value are marked with ✓, while those that illustrate a either static or dynamic global pattern with non-zero mean value are marked with ×. Based on the different patterns associated with the three residual variables, all the target faults can be detected.

Table 5.2: Diagnostic Summary

	System Condition	$W_{Leak,Bst}$	$W_{Leak,Int}$	ΔW_{Cyl}
$F0$	Normal	✓	✓	✓
$F1$	Intake air mass flow sensor bias	×	✓	×
$F2$	Boost pressure sensor bias	×	×	✓
$F3$	Intake manifold pressure sensor bias	×	×	×
$F4$	Boost manifold leakage	×	✓	×
$F5$	Intake manifold leakage	×	×	×

It can be noted that the intake air mass flow sensor bias ($F1$) and the boost manifold leakage ($F4$) demonstrate the same pattern of $\begin{pmatrix} W_{Leak,Bst}, & W_{Leak,Int}, & \Delta W_{Cyl} \end{pmatrix} = \begin{pmatrix} \times, & ✓, & \times \end{pmatrix}$. However, as illustrated in Figure 5.7(b) and 5.10(a), the behaviors of the residuals of $W_{LeakBst}$ and dW_{Cyl} are significantly different. Under the fault of intake mass air flow sensor bias, the residuals of $W_{LeakBst}$ and dW_{Cyl} show a static pattern. When a leakage in the boost manifold occurs, these two residuals, on the other hand, illustrate highly dynamic behaviors. This phenomenon can be explained by the fact there is actually no change in the dynamics of the target system when the intake air mass flow sensor fails, while dynamics of a leakage is introduced into

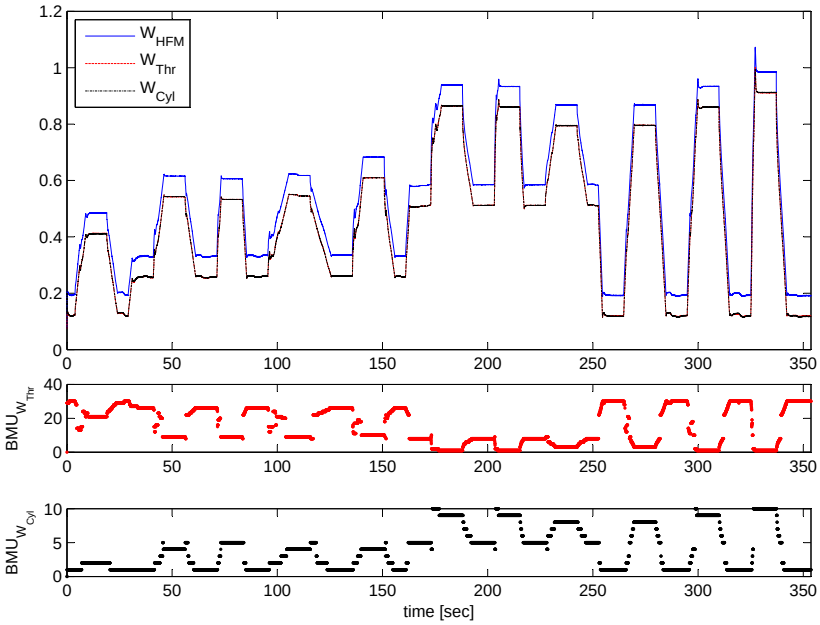

(a) Mass Air Flow Estimation

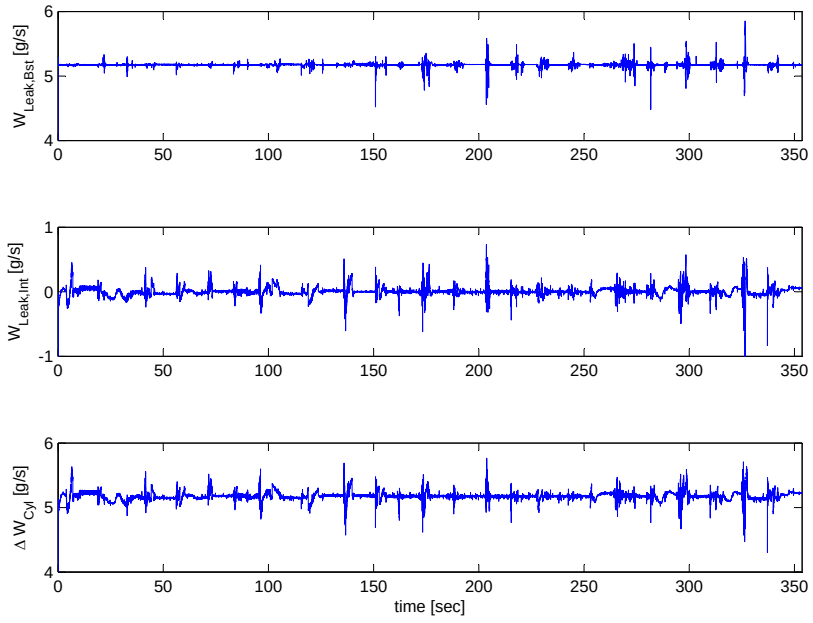

(b) Fault Detectors

Figure 5.7: Diesel engine air path system fault diagnosis under ($F1$) intake hot-film mass air flow sensor bias

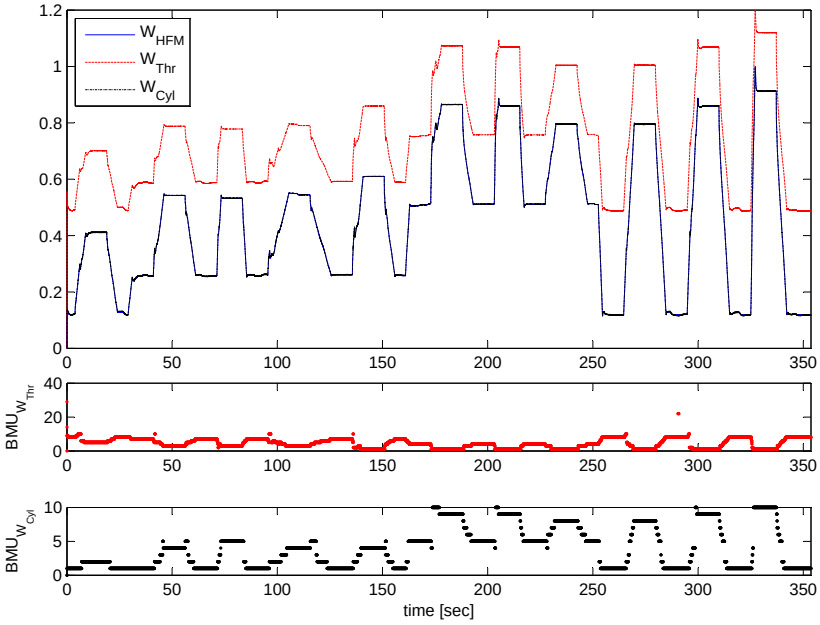

(a) Mass Air Flow Estimation

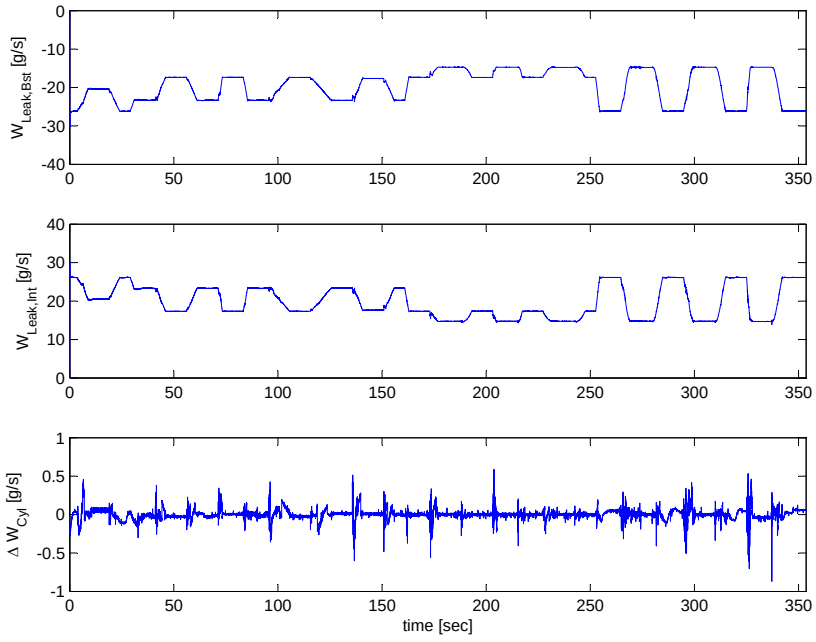

(b) Fault Detectors

Figure 5.8: Diesel engine air path system fault diagnosis under ($F2$) boost manifold pressure sensor bias

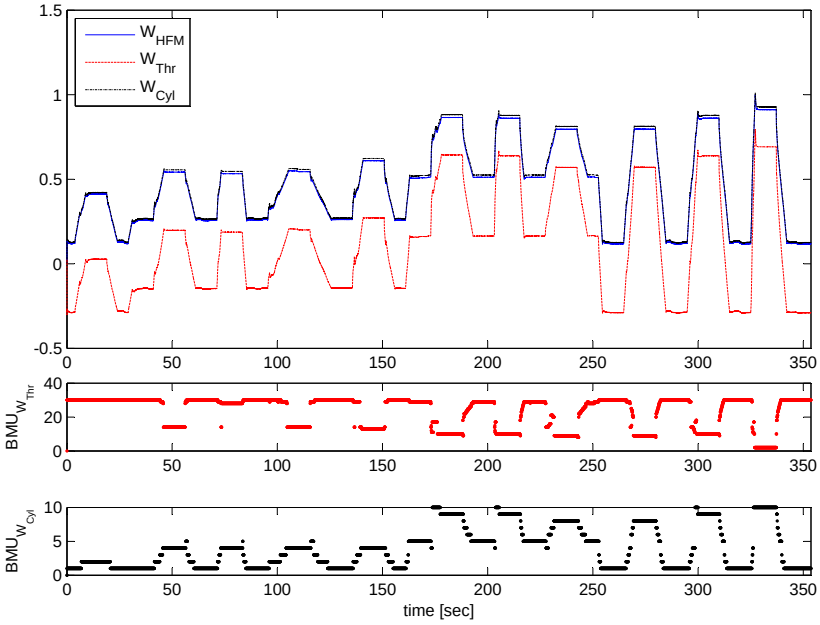

(a) Mass Air Flow Estimation

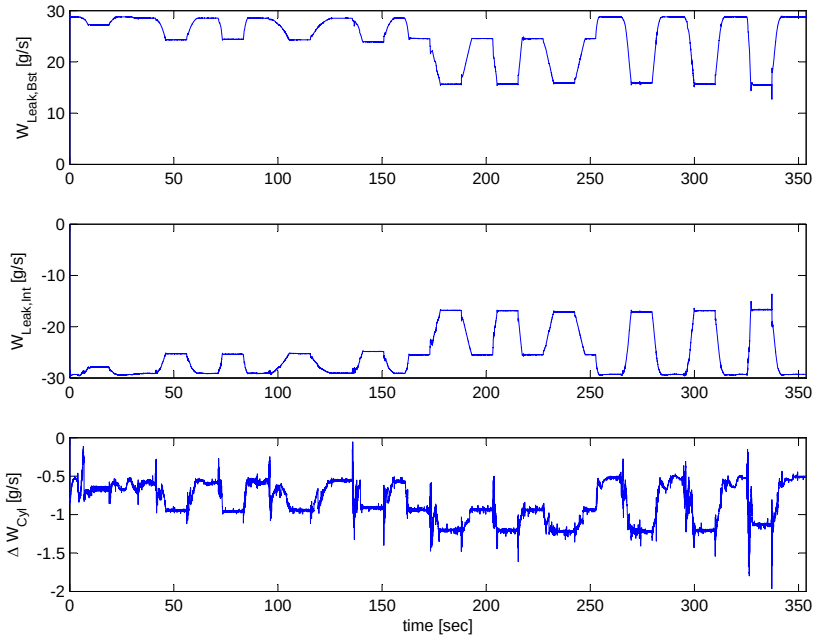

(b) Fault Detectors

Figure 5.9: Diesel engine air path system fault diagnosis under ($F3$) intake manifold pressure sensor bias

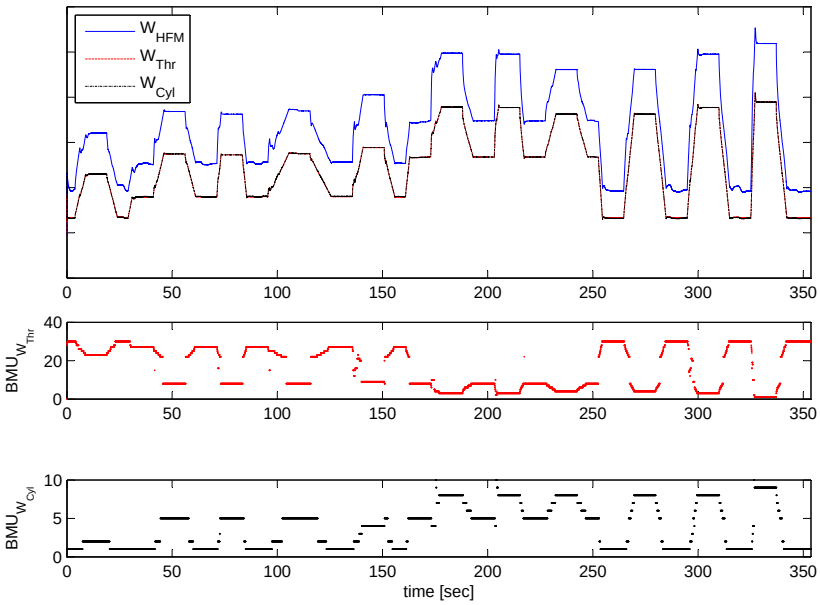

(a) Mass Air Flow Estimation

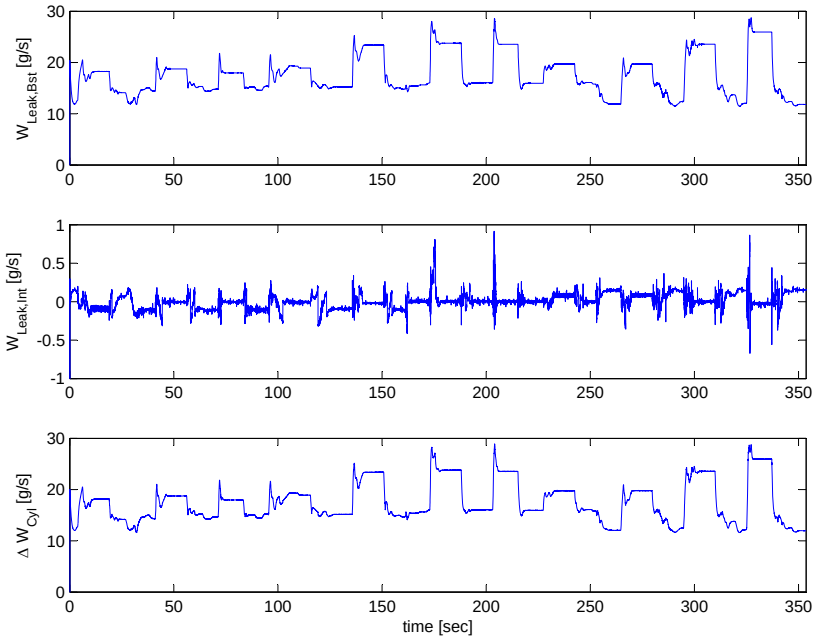

(b) Fault Detectors

Figure 5.10: Diesel engine air path system fault diagnosis under ($F4$) leakage in the boost manifold

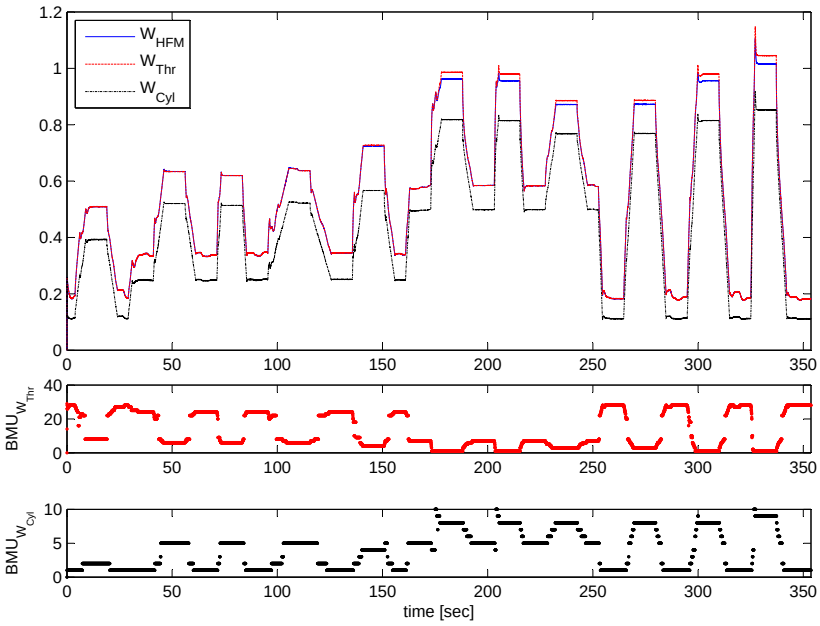

(a) Mass Air Flow Estimation

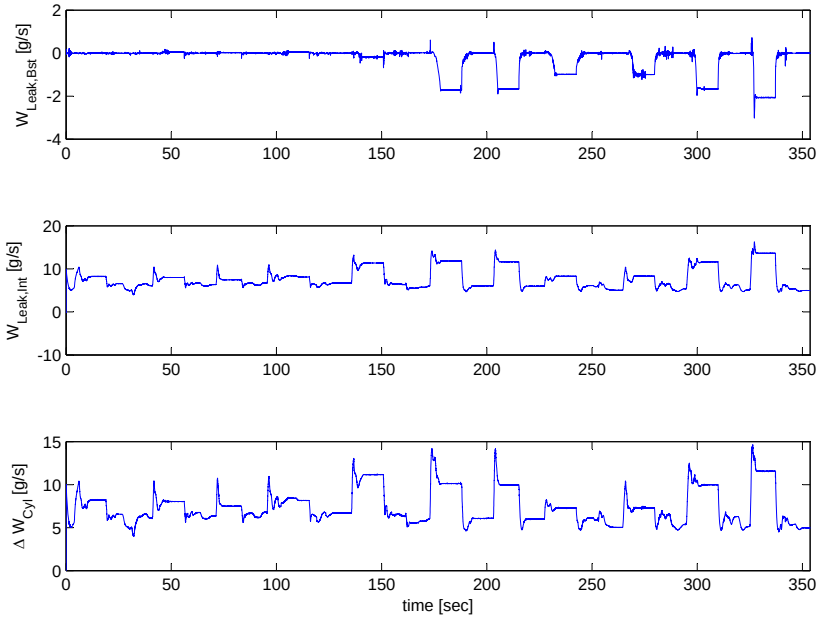

(b) Fault Detectors

Figure 5.11: Diesel engine air path system fault diagnosis under ($F5$) leakage in the intake manifold

$W_{LeakBst}$ and dW_{Cyl} due to their dependencies on p_{Bst} and p_{Int}. Based on the estimated cumulative probability distribution of all the three residuals in Figure 5.12, fault $F1$ and $F4$ can be also isolated.

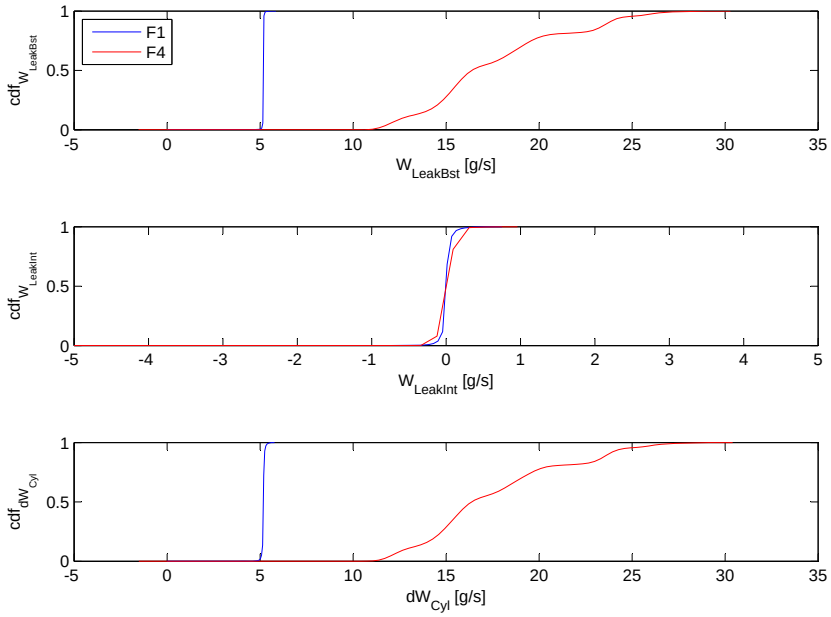

Figure 5.12: Cumulative probability distribution of the generated residuals under ($F1$) intake mass air flow sensor bias, and ($F4$) leakage in the boost manifold

It can be also noted that the boost pressure sensor bias ($F2$) and the intake manifold leakage ($F5$) demonstrate the same pattern of $\begin{pmatrix} W_{Leak,Bst}, & W_{Leak,Int}, & \Delta W_{Cyl} \end{pmatrix} = \begin{pmatrix} \times, & \times, & \times \end{pmatrix}$. When the residual variable $W_{Leak,Bst}$ is analyzed in specific operation regime as indicated by the pressure ratio across the throttle, $\frac{p_{Bst}}{p_{Int}}$ in Figure 5.13, it can concluded that the abnormal behavior in $W_{Leak,Bst}$ is caused by the unexpected operation condition. Since the fault detector has not been trained in these operation regimes, it interprets the unobserved system behavior as faults. With the additional information given the GSMMS, the fault detector can distinguish the impacts of potential faults and unexpected operation conditions on the target residual variables.

As illustrated in Figure 5.13, within the well-trained operation regime, the residual variable $W_{Leak,Bst}$ indicates normal operation, i.e. $W_{Leak,Bst} = \checkmark$. As a result, the boost pressure sensor bias ($F2$) and the intake manifold leakage ($F5$) can be isolated.

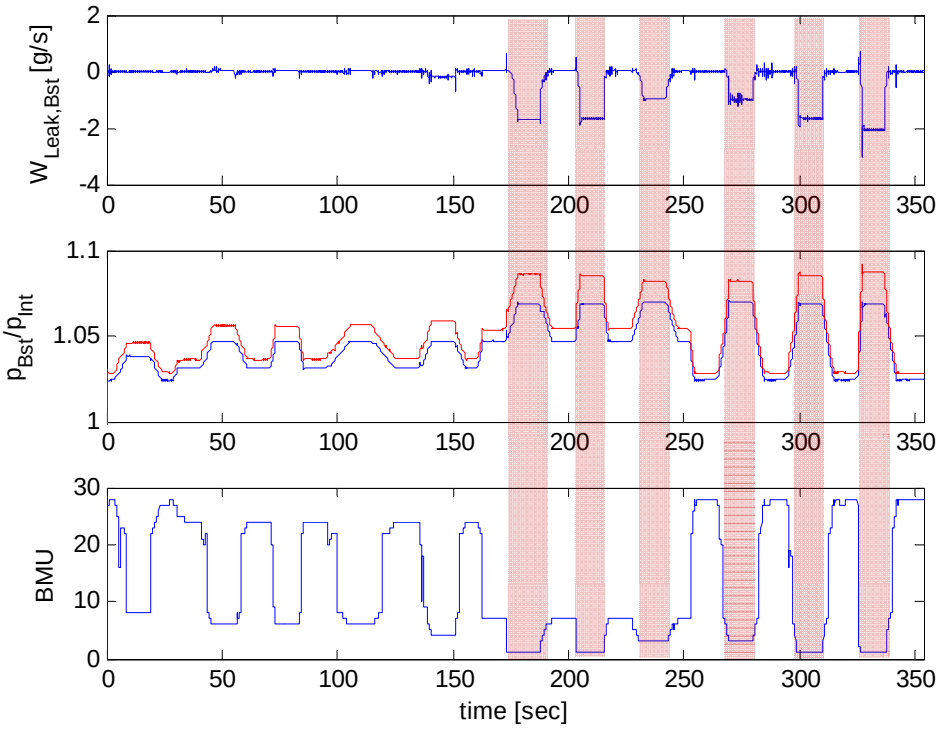

Figure 5.13: Residual variable $W_{Leak,Bst}$ within different operation regimes

5.4 Summary

In this chapter, an engine model is introduced to capture the dynamics in the diesel air path system via the variables of intake mass air flow rate and pressures in the various manifolds. Validated against experimental data, such a model not only serves as the virtual engine to simulate the potential faults of sensors and components in the target system, but also provides insight into the behavior of the target system. Based on the knowledge of the target system as well as the engine management system, fault detectors were designed in order to best isolate the potential faults. The system input

selection approach developed in Chapter IV was then employed to identify the order of system dynamics. The growing structure multiple model system identification algorithm captures the target nonlinear dynamics using multiple linear models in an appropriate number of sub-regions identified by the growing self-organizing network. Based on the generated residuals, all the faults can be detected once they statistically deviate from zero. Evaluated based on the different patterns illustrated by the three residual variables, most of the faults can also be isolated except the intake mass air flow sensor bias and leakage in the boost manifold. Due to the dynamic changes introduced by the boost manifold leakage, these two faults can be further isolated by investigating the behaviors of the generated residuals. In this work, the cumulative probably distribution was employed for such investigation.

CHAPTER VI

Contribution and Future Work

6.1 Contribution of the Thesis

This thesis has presented the research attempts in developing practical approaches for system and sensor fault diagnosis with applications to the automotive system. The work first looked into the problem of sensor degradation detection and isolation in a single-input-single-output system as presented in Chapter III, and extended such efforts to a multiple-input-multiple-output system as presented in Chapter V. In order to deal with a complex system such as the diesel engine air path system, an approach is developed in Chapter IV to identify the most related input variables for the target system performance variable. In particular, the research focused on:

System Dynamics Identification and Analysis The method presented in Chapter III is able to identify the dynamics in a single-input-single-output dynamic system. Based on the assumption that the dynamics of the sensor is much faster than that of the monitored system, the proposed approach identifies the dynamics and the associated gain factors of the sensor and the monitored system. As a result, the method can detect and quantify sensor performance degradation in the compound system without the use of redundant sensing equipment. It is able to distinguish sensor and plant degradation in an environment where either the plant, or the sensor

monitoring that plant could undergo degradation in their dynamic properties. In addition, the method accomplishes identification of sensor and plant dynamics using inputs observed during normal system operations, rather than using special inputs. Consequently, such a method is capable of assessing the sensor health condition as the system operates. Furthermore, this method is able to improve the accuracy of collected information despite the presence of sensor degradation by directly compensating for the adverse effects of the degradation in its measurements.

System Input Selection for Nonlinear System Identification In order to deal with the increasing complexity in a multiple-input-multiple-output dynamic system, a method is proposed in Chapter IV to identify the most correlated input variables and the associated dynamic dependence with the output variable in a nonlinear system. Without requiring a thorough understanding of the target system, the proposed method establish a general approach that can be applied to various nonlinear system identification algorithms. The growing self-organizing network provides an appropriate partition of the target operation regime, thus enabling the approximate of the nonlinear behaviors with a set of linear models. As the number of system inputs including measured variables and control signals increases, the complexity of the input variable and model structure selection problem in a nonlinear system increases dramatically. The introduction of the genetic algorithm provides an efficient way to search for the best solution as defined by the minimum description length principle. The proposed approach has shown its effectiveness with commonly cited numerical examples and diesel engine air path dynamics modeling.

Diesel Engine Air Path System Diagnosis The method presented in Chapter V is developed to detect and isolate potential sensor faults and air leaks in a diesel engine

air path system, a highly dynamic and nonlinear multiple-input-multiple-output system. Established using the growing structure multiple model system identification algorithm, the fault detectors captures the dynamics between the key performance variable, the intake air mass air flow rate, and the identified most correlated input variables including the boost and intake manifold pressures. Given the additional operation region information, the fault detectors can distinguish between the effects of a fault and unexpected operating condition on generated residuals by looking into the local models.

6.2 Future Work

The work in this thesis mainly focused on nonlinear system modeling and system dynamics identification as well as their application to the detection and isolation of faults in the monitored system and sensors. To enable the application of such methods in real-world applications such as the diesel engine air path system, some of the possible future work directions are listed in the following sections.

Improvement of Input Selection Approach The input selection approach for nonlinear system dynamics modeling developed in Chapter IV employs the genetic algorithm in a piecewise linear model structure in which the local regions are identified using the self-organizing network. The genes are encoded with the model order, $n_a \in \mathbb{R}^{p\times p}$, $n_b \in \mathbb{R}^{p\times q}$, and $n_k \in \mathbb{R}^{p\times q}$ with an understanding of the maximum order of system dynamics. In this work, the maximum order of system dynamics is derived from prior knowledge of the target system. Future work to eliminate such pre-determined parameters can further help reduce the amount prior knowledge required. In addition, the current approach compares the accuracy performance of the multiple linear models based on one common topology. As discussed in [Liu

et al., 2008], the degree of topology preservation also has an impact on the modeling accuracy. Therefore, future work could be conducted to optimize both the model structure as well as the topology for best accuracy.

Exploitation of Fault Detector for Best Coverage In addition, after a fault is detected, it is important to have a scalable fault identification and localization scheme that can also track new faults in the field. In Chapter V, five potential sensor and component failures were investigated with the use of two fault detectors constructed based on the mass flow rate through the throttle, W_{Thr}, and that into the cylinders, W_{Cyl}. Derived from the measurements obtained via the hot-film mass air flow sensor and the estimated values from these two fault detectors, three residual variables of $W_{Leak,Bst}$, $W_{Leak,Int}$, and dW_{Cyl} were generated. These three residuals have shown capability in detecting and isolating all the target failures. In order to fully exploit the potential of these two fault detectors, future work can be conducted to further investigate the possibility of detecting other faults such as a stuck valve for exhaust gas recirculation.

Online Adaptation of Fault Detectors For on-board diagnosis, it is important to adapt the fault detectors to the component wear in the monitored system. In addition, a fault detector that is trained offline needs to adapt for unexpected operation conditions and distinguish such effects from a potential fault. In order to enable online adaptation, a sequential training approach with the following cost function can be investigated in future to adapt the relations in the fault detectors with real-time measurements from the system. Due to the limited off-line training data especially during transients, not only the parameters in the local region but also the partition of the local regime may need to be updated. Therefore, future work needs to be

conducted to determine the enabling conditions for such adaptation and investigate its impacts on on-board system diagnosis.

$$J_m(\theta_m) = \frac{1}{k_m} \sum_{i=1}^{k_m} \omega_m(\mathbf{s}(k)) \lambda^{k_m - i} \|y(i) - \hat{y}_m(i)\|^2 \tag{6.1}$$

where λ is the forgetting factor that adjust the speed of adaptation.

Bibliography

Akaike, H. (1974). A new look at the statistical model identification. *IEEE Transactions on Automatic Control*, AC-19(6):716–23.

Alag, S., Agogino, A., and Morjaria, M. (2001). A methodology for intelligent sensor measurement, validation, fusion, and fault detection for equipment monitoring and diagnostics. *(AI EDAM) Artificial Intelligence for Engineering Design, Analysis and Manufacturing*, 15(4):307–20.

Alahakoon, D., Halgamuge, S. K., and Srinivasan, B. (2000). Dynamic self-organizing maps with controlled growth for knowledge discovery. *IEEE Transactions on Neural Networks*, 11(3):601–614.

Alcorta Garcia, E. and Frank, P. (1999). A novel design of structured observer-based residuals for fdi. In *Proceedings of the 1999 American Control Conference (Cat. No. 99CH36251)*, volume vol.2, pages 1341–5, San Diego, CA, USA. IEEE.

Antory, D. (2007). Application of a data-driven monitoring technique to diagnose air leaks in an automotive diesel engine: A case study. *Mechanical Systems and Signal Processing*, 21(2):795–808.

Aradhye, H. (2002). Sensor fault detection, isolation, and accommodation using neural networks, fuzzy logic and bayesian belief networks. Master's thesis, University of New Mexico.

Aßfalg, J., Allgöwer, F., and Fritz, M. (2006). Constrained derivative-free augmented state estimation for a diesel engine air path. In *Proceedings of the 14th IFAC Symposium on System Identification*, volume 14, Australia.

Babuska, R. (1998). *Fuzzy modeling for control*. Kluwer Academic Publishers, Boston Dordrecht London.

Barreto, G. and Araujo, A. (2004). Identification and control of dynamical systems using the self-organizing map. *IEEE Transactions on Neural Networks*, 15(5):1244–59.

Battiti, R. (1994). Using mutual information for selecting features in supervised neural net learning. *IEEE Transactions on Neural Networks*, 5(4):537–50.

Bauer, D., Deistler, M., and Scherrer, W. (2001). On the impact of weighting matrices in subspace algorithms. In *System Identification (SYSID 2000). Proceedings volume from the 12th IFAC Symposium on System Identification*, volume vol.1, pages 97–102, Santa Barbara, CA, USA. Elsevier Science.

Bauer, D. and Ljung, L. (2002). Some facts about the choice of the weighting matrices in larimore type of subspace algorithms. *Automatica*, 38(5):763–73.

Benitez-Perez, H., Garcia-Nocetti, F., and Thompson, H. (2005). Fault classification som and pca for inertial sensor drift. In *2005 IEEE International Workshop on Intelligent Signal Processing (IEEE Cat. No. 05EX1039)*, pages 177–82, Faro, Portugal. IEEE.

Bernieri, A., Betta, G., Pietrosanto, A., and Sansone, C. (1995). A neural network approach to instrument fault detection and isolation. *IEEE Transactions on Instrumentation and Measurement*, 44(3):747–50.

Betta, G., D'Apuzzo, M., and Pietrosanta, A. (1995). A knowledge-based approach to instrument fault detection and isolation. *IEEE Transactions on Instrumentation and Measurement*, 44(6):1009–16.

Betta, G., Dell'Isola, M., Liguori, C., and Pietrosanta, A. (1997). Expert systems for the detection and isolation of faults on low-accuracy sensor systems. In *IEEE Workshop ET&VS-IM/97*, Niagara Falls, Ontario, Canada.

Betta, G., Liguori, C., and Pietrosanto, A. (1996). The use of genetic algorithms for advanced instrument fault detection and isolation schemes. In *Quality Measurements: The Indispensable Bridge between Theory and Reality (No Measurements? No Science!) Joint Conference - 1996: IEEE Instrumentation and Measurement Technology Conference and IMEKO Technical Committee 7. Conference Proceedings (Cat. No.96CH35936)*, volume vol.2, pages 1129–34, Brussels, Belgium. IEEE.

Betta, G., Liguori, C., and Pietrosanto, A. (1998). An advanced neural-network-based instrument fault detection and isolation scheme. *IEEE Transactions on Instrumentation and Measurement*, 47(2):507–12.

Betta, G. and Pietrosanto, A. (2000). Instrument fault detection and isolation: state of the art and new research trends. *IEEE Transactions on Instrumentation and Measurement*, 49(1):100–7.

Billings, S. and Voon, W. (1987). Piecewise linear identification of non-linear systems. *International Journal of Control*, 46(1):215–35.

Bittanti, S., Gatti, E., Ripamonti, G., and Savaresi, S. (1997). High-accuracy fit of the poles of spectroscopy amplifiers designed for mixed analog-digital filtering. *IEEE Transactions on Nuclear Science*, 44(2):125–133.

Bittanti, S., Gatti, F., Ripamonti, G., and Savaresi, S. (2000). Poles identification of an analog filter for nuclear spectroscopy via subspace-based techniques. *IEEE Transactions on Control Systems Technology*, 8(1):127–37.

Broen, R. B. (1974). Nonlinear voter-estimator for redundant systems. In *IEEE Conf on Decis and Control, 1974, incl Symp on Adapt Processes, 13th, Proc, Nov 20-22 1974, Nov 20-22 1974*, pages 743–748, Phoenix, AZ, USA. IEEE (74CHO900-1 CS), New York, NY.

Brownell, T. (1992). Neural networks for sensor management and diagnostics. In *Proceedings of the IEEE 1992 National Aerospace and Electronics Conference, NAECON 1992 (Cat. No.92CH3158-3)*, pages 923–9, Dayton, OH, USA. IEEE.

Campa, G., Fravolini, M., Napolitano, M., and Seanor, B. (2002). Neural networks-based sensor validation for the flight control system of a b777 research model. In *Proceedings of the 2002 American Control Conference (IEEE Cat. No.CH37301)*, volume vol.1, pages 412–17, Anchorage, AK, USA. American Automatic Control Council.

Capriglione, D., Liguori, C., Pianese, C., and Pietrosanto, A. (2002). On-line sensor fault detection, isolation, and accommodation in automotive engines. In *IMTC/2002. Proceedings of the 19th IEEE Instrumentation and Measurement Technology Conference (IEEE Cat. No.00CH37276)*, volume vol.2, pages 1711–16, Anchorage, AK, USA. IEEE.

Ceccarelli, R., Moulin, P., and Canudas-de Wit, C. (2009). Robust strategy for intake leakage detection in diesel engines. In *2009 IEEE International Conference on Control Applications (CCA)*, pages 340–5, Piscataway, NJ, USA. IEEE.

Chandrasekaran, B. and Punch, W. (1988). Hierarchical classification: its usefulness for diagnosis and sensor validation. *IEEE Journal on Selected Areas in Communications*, 6(5):884–91.

Chen, G. and McAvoy, T. J. (1998). Predictive on-line monitoring of continuous processes. *Journal of Process Control*, 8(5-6):409–420.

Chen, J., Patton, R., and Liu, G. (1994). Detecting incipient sensor faults in flight control systems. In *Proceedings of the Third IEEE Conference on Control Applications (Cat. No.94CH3420-7)*, volume vol.2, pages 871–6, Glasgow, UK. IEEE.

Cho, J.-H., Lee, J.-M., Choi, S. W., Lee, D., and Lee, I.-B. (2004). Sensor fault identification based on kernel principal component analysis. In *Proceedings of the 2004 IEEE International Conference on Control Applications (IEEE Cat. No.04CH37596)*, volume Vol.2, pages 1223–8, Taipei, Taiwan. IEEE.

Chow, E. and Willsky, A. (1984). Analytical redundancy and the design of robust failure detection systems. *IEEE Transactions on Automatic Control*, AC-29(7):603–14.

Clark, R. (1978a). Instrument fault detection. *IEEE Transactions on Aerospace and Electronic Systems*, AES-14(3):456–65.

Clark, R. (1978b). A simplified instrument failure detection scheme. *IEEE Transactions on Aerospace and Electronic Systems*, AES-14(4):558–53.

Clark, R., Fosth, D., and Walton, V. (1975). Detecting instrument malfunctions in control systems. *IEEE Transactions on Aerospace and Electronic Systems*, AES-11(4):465–73.

Conatser, R., Wagner, J., Ganta, S., and Walker, I. (2004). Diagnosis of automotive electronic throttle control systems. *Control Engineering Practice*, 12(1):23–30.

Crossman, J., Guo, H., Murphey, Y., and Cardillo, J. (2003). Automotive signal fault diagnostics - part i: signal fault analysis, signal segmentation, feature extraction and quasi-optimal feature selection. *IEEE Transactions on Vehicular Technology*, 52(4):1063–75.

Crowe, C. (1996). Data reconciliation - progress and challenges. *Journal of Process Control*, 6(2-3):89–98.

Cubedo, M. and Oller, J. (2002). Hypothesis testing: a model selection approach. *Journal of Statistical Planning and Inference*, 108(1-2):3–21.

Dasgupta, D. and Gonzalez, F. (2002). An immunity-based technique to characterize intrusions in computer networks. *IEEE Transactions on Evolutionary Computation*, 6(3):281–91.

De Ridder, F., Pintelon, R., Schoukens, J., and Gillikin, D. P. (2005). Modified aic and mdl model selection criteria for short data records. *IEEE Transactions on Instrumentation and Measurement*, 54(1):144–150.

Deckert, J., Desai, M., Deyst, J., and Willsky, A. (1977). F-8 dfbw sensor failure identification using analytic redundancy. *IEEE Transactions on Automatic Control*, AC-22(5):795–803.

Desai, M. and Ray, A. (1984). A fault detection and isolation methodology-theory and application. In *Proceedings of the 1984 American Control Conference (IEEE Cat. No. 84CH2024-8)*, pages 262–70, San Diego, CA, USA. IEEE.

Djurdjanovic, D., Ni, J., and Lee, J. (2002). Time-frequency based sensor fusion in the assessment and monitoring of machine performance degradation. In *American Society of Mechanical Engineers, Dynamic Systems and Control Division (Publication) DSC*, volume 71, pages 15–22, New Orleans, LA, United States. American Society of Mechanical Engineers, New York, NY 10016-5990, United States.

Dong, D. and McAvoy, T. (1996). Nonlinear principal component analysis-based on principal curves and neural networks. *Computers & Chemical Engineering*, 20(1):65–78.

Donoho, D. L. (1995). De-noising by soft-thresholding. *IEEE Transactions on Information Theory*, 41(3):613–627.

Donoho, D. L. and Johnstone, I. M. (1994). Ideal spatial adaptation by wavelet shrinkage. *Biometrika*, 81:425–455.

Donoho, D. L., Johnstone, I. M., Kerkyacharian, G., and Picard, D. (1995). Wavelet shrinkage: asymptotia. *Journal of the Royal Statistical Society, Series B*, 57(2):301–369.

Dorr, R., Kratz, F., Ragot, J., Loisy, F., and Germain, J. (1997). Detection, isolation, and identification of sensor faults in nuclear power plants. *IEEE Transactions on Control Systems Technology*, 5(1):42–60.

Dunia, R., Qin, S. J., Edgar, T. F., and McAvoy, T. J. (1996). Identification of faulty sensors using principal component analysis. *AIChE Journal*, 42(10):2797–2812.

Etezadi-Amoli, J. and McDonald, R. (1983). A second generation nonlinear factor analysis. *Psychometrika*, 8:315–27.

Frank, P. (1987). Fault diagnosis in dynamic systems via state estimation - a survey. *System Fault Diagnostics, Reliability, and Related Knowledge-Based Approaches*, 1:35–98.

Frank, P. (1990). Fault diagnosis in dynamic systems using analytical and knowledge-based redundancy-a survey and some new results. *Automatica*, 26(3):459–74.

Frank, P. and Keller, L. (1980). Sensitivity discriminating observer design for instrument failure detection. *IEEE Transactions on Aerospace and Electronic Systems*, AES-16(4):460–7.

Fritzke, B. (1994). Growing cell structures - a self-organizing network for unsupervised and supervised learning. *Neural Networks*, 7(9):1441–1460.

Fritzke, B. (1995). A growing neural gas network learns topologies. In *Advances in Neural Information Processing Systems 7*, pages 625–32, Denver, CO, USA. MIT Press.

Gaweda, A., Zurada, J., and Setiono, R. (2001). Input selection in data-driven fuzzy modeling. In *10th IEEE International Conference on Fuzzy Systems. (Cat. No.01CH37297)*, volume vol.2, pages 1251–4, Melbourne, Vic., Australia. IEEE.

Ge, M., Chiu, M.-S., and Wang, Q.-G. (2000). Extended self-organizing map for nonlinear system identification. *Industrial and Engineering Chemistry Research*, 39(10):3778–3788.

Gertler, J. (1998). *Fault-detection and diagnosis in engineering systems*. Marcel Dekker, New York.

Gertler, J., Costin, M., Fang, X., Kowalczuk, Z., Kunwer, M., and Monajemy, R. (1995). Model based diagnosis for automotive engines-algorithm development and

testing on a production vehicle. *IEEE Transactions on Control Systems Technology*, 3(1):61–9.

Gertler, J., Fang, X., and Luo, Q. (1990). Detection and diagnosis of plant failures: the orthogonal parity equation approach. *Control and Dynamic Systems*, 37:159–216.

Gertler, J., Li, W., Huang, Y., and McAvoy, T. (1999). Isolation enhanced principal component analysis. *AIChE Journal*, 45(2):323–334.

Gertler, J. and McAvoy, T. (1997). Principal component analysis and parity relations - a strong duality. In *Preprints of IFAC Safe Process Symposium*, Hull, UK.

Gertler, J. and Monajemy, R. (1995). Generating directional residuals with dynamic parity relations. *Automatica*, 31(4):627–35.

Gertler, J. and Singer, D. (1990). A new structural framework for parity equation-based failure detection and isolation. *Automatica*, 26(2):381–8.

Glockler, O., Upadhyaya, B., Morgenstern, V., and Olvera, J. (1989). Generalized consistency checking of multivariable redundant measurements and common-mode failure detection. In *7th Power Plant Dynamics, Control and Testing Symposium Proceedings*, pages 82–01, Knoxville, TN, USA. Univ. Tennessee.

Gnanadesikan, R. (1997). *Methods for statistical data analysis of multivariate observations*. Willey, New York.

Goldberg, D. E. (1989). *Genetic Algorithm in Search, Optimization and Machine Learning*. Reading, Massachusetts: Addison-Wesley.

Gunnarsson, M. (2001). *Parameter Estimation for Fault Diagnosis of an Automotive Enigne using Extended Kalman Filter*. PhD thesis, Linkping University, Sweden.

Gunst, R. F. (1980). *Regression Analysis and Its Application: A Data-oriented Approach*. New York: Dekker, USA.

Guo, T.-H. and Musgrave, J. (1995). Neural network based sensor validation for reusable rocket engines. In *Proceedings of the 1995 American Control Conference (IEEE Cat. No.95CH35736)*, volume vol.2, pages 1367–72, Seattle, WA, USA. American Autom Control Council.

Guo, T.-H. and Nurre, J. (1991). Sensor failure detection and recovery by neural networks. In *IJCNN-91-Seattle: International Joint Conference on Neural Networks (Cat. No.91CH3049-4)*, pages 221–6, Seattle, WA, USA. IEEE.

Halder, P., Chaudhuri, S., and Mukhopadhyay, S. (2004). On line sensor fault detection, isolation and accommodation in tactical aerospace vehicle. In *TENCON 2004. 2004 IEEE Region 10 Conference (IEEE Cat. No. 04CH37582)*, volume Vol. 4, pages 684–6, Chiang Mai, Thailand. IEEE.

Harmer, P., Williams, P., Gunsch, G., and Lamont, G. (2002). An artificial immune system architecture for computer security applications. *IEEE Transactions on Evolutionary Computation*, 6(3):252–80.

Hastie, T. and Stuetzle, W. (1989). Principal curves. *Journal of the American Statistical Association*, 84:502–16.

Heywood, J. (1992). *Internal Combustion Engine Fundamentals*. McGraw-Hill.

Hines, J. W., Uhrig, R. E., and Wrest, D. J. (1998). Use of autoassociative neural networks for signal validation. *Journal of Intelligent and Robotic Systems: Theory & Applications*, 21(2):143–154.

Holbert, K. and Upadhyaya, B. (1990). An integrated signal validation system for nuclear power plants. *Nuclear Technology*, 92(3):411–27.

Hotelling, H. (1933). Analysis of a complex of statistical variables into principal components. *Journal of Educational Psychology*, 24:417–41.

Hsiao, T. and Tomizuka, M. (2005). Sensor fault detection in vehicle lateral control systems via switching kalman filtering. In *Proceedings of the 2005 American Control Conference (IEEE Cat. No. 05CH37668)*, volume vol. 7, pages 5009–14, Portland, OR, USA. IEEE.

Huang, Y., Gertler, J., and McAvoy, T. (2000). Sensor and actuator fault isolation by structured partial pca with nonlinear extensions. *Journal of Process Control*, 10(5):459–69.

Huber, W., Lieberoth-Leden, B., Maisch, W., and Reppich, A. (1991). Electronic throttle control. *Automotive Engineering (Warrendale, Pennsylvania)*, 99(6):15–18.

Ibarguengoytia, P., Sucar, L., and Vadera, S. (2001). Real time intelligent sensor validation. *IEEE Transactions on Power Systems*, 16(4):770–5.

Ibarguengoytia, P., Vadera, S., and Sucar, L. (2006). A probabilistic model for information and sensor validation. *Computer Journal*, 49(1):113–26.

Isermann, R. (1984). Process fault detection based on modeling and estimation methods-a survey. *Automatica*, 20(4):387–404.

Isermann, R. (1997). Supervision, fault-detection and fault-diagnosis methods-an introduction. *Control Engineering Practice*, 5(5):639–52.

Isermann, R. (2005). Model-based fault-detection and diagnosis - status and applications. *Annual Reviews in Control*, 29(1):71–85.

Johansson, A. and Norlander, T. (2003). Parametric uncertainty in sensor fault detection for turbofan jet engine. In *42nd IEEE International Conference on Decision and Control (IEEE Cat. No.03CH37475)*, volume Vol.2, pages 1950–5, Maui, HI, USA. IEEE.

Jones, N. and Li, Y.-H. (2000). Review of condition monitoring and fault diagnosis for diesel engines. *TriboTest*, 6(3):267–292.

Kaistha, N. and Upadhyaya, B. (2001). Incipient fault detection and isolation of field devices in nuclear power systems using principal component analysis. *Nuclear Technology*, 136(2):221–30.

Kerschen, G., De Boe, P., Golinval, J., and Worden, K. (2005). Sensor validation using principal component analysis. *Smart Materials and Structures*, 14(1):36–42.

Kim, Y., Wood, W., and Agogino, A. (1992). Signal validation for expert system development. In *Second International Forum on Expert Systems and Computer Simulation in Energy Engineering*.

Kobayashi, T. and Simon, D. (2005). Hybrid neural-network genetic-algorithm technique for aircraft engine performance diagnostics. *Journal of Propulsion and Power*, 21(4):751–8.

Kohonen, T. (1995). *Self-organizing maps*. Springer Verlag, Berlin; New York.

Kramer, M. A. (1991). Nonlinear principal component analysis using autoassociative neural networks. *AIChE Journal*, 37(2):233–243.

Kresta, J. V., MacGregor, J. F., and Marlin, T. E. (1991). Multivariate statistical monitoring of process operating performance. *Canadian Journal of Chemical Engineering*, 69(1):35–47.

Krishnamoorthy, G. (2010). *A Framework for Utilizing Data from Multiple Sensors in Intelligent Mechanical Systems*. PhD thesis, University of Texas, Austin.

Lee, S. (1994). Sensor value validation based on systematic exploration of the sensor redundancy for fault diagnosis kbs. *IEEE Transactions on Systems, Man and Cybernetics*, 24(4):594–605.

Li, H., Zhang, Y., Hou, A., and Havel, J. (2006). Artificial neural networks based on principal component analysis input selection for quantification in overlapped capillary electrophoresis peaks. *Chemometrics and Intelligent Laboratory Systems*, 82(1-2):165–75.

Li, W. and Shah, S. (2002). Structured residual vector-based approach to sensor fault detection and isolation. *Journal of Process Control*, 12(3):429–43.

Lin, Y., Cunningham, G.A., I., and Coggeshall, S. (1996). Input variable identification-fuzzy curves and fuzzy surfaces. *Fuzzy Sets and Systems*, 82(1):65–71.

Liu, J., Djurdjanovic, D., Marko, K., and Ni, J. (2009a). Growing structure multiple model system for anomaly detection and fault diagnosis. *Transaction of ASME Journal of Dynamic Systems, Measurements and Control*, 131(5):051001–1 – 051001–13.

Liu, J., Djurdjanovic, D., and Ni, J. (2008). Topology preservation and cooperative learning in identification of mulitple model systems. *IEEE Transaction on Neural Networks*, 19(12):2065–2072.

Liu, J., Djurdjanovic, D., and Ni, J. (2009b). A novel method for anomaly detection, localization and fault isolation for dynamic control systems. *Mechanical Systems and Signal Processing*, 23(8):2488–2499.

Ljung, L. (1999). *System identification: theory for the user*. Prentice-Hall.

Lou, X.-C., Willsky, A., and Verghese, G. (1986). Optimally robust redundancy relations for failure detection in uncertain systems. *Automatica*, 22(3):333–44.

Lunze, J. and Schroder, J. (2004). Sensor and actuator fault diagnosis of systems with discrete inputs and outputs. *IEEE Transactions on Systems, Man and Cybernetics, Part B (Cybernetics)*, 34(2):1096–107.

Luo, R., Misra, M., and Himmelblau, D. M. (1999). Sensor fault detection via multiscale analysis and dynamic pca. *Industrial and Engineering Chemistry Research*, 38(4):1489–1495.

Luo, R., Misra, M., Qin, S. J., Barton, R., and Himmelblau, D. M. (1998). Sensor fault detection via multiscale analysis and nonparametric statistical inference. *Industrial & Engineering Chemistry Research*, 37(3):1024–1032.

MacGregor, J. F., Jaeckle, C., Kiparissides, C., and Koutoudi, M. (1994). Process monitoring and diagnosis by multiblock pls methods. *AIChE Journal*, 40(5):826–838.

Mao, K. (2004). Orthogonal forward selection and backward elimination algorithms for feature subset selection. *IEEE Transactions on Systems, Man, and Cybernetics, Part B: Cybernetics*, 34(1):629–634.

Mao, K. and Billings, S. (1999). Variable selection in non-linear systems modelling. *Mechanical Systems and Signal Processing*, 13(2):351–366.

Mathioudakis, K. and Romessis, C. (2004). Probabilistic neural networks for validation of on-board jet engine data. *Proceedings of the Institution of Mechanical Engineers, Part G (Journal of Aerospace Engineering)*, 218(G1):59–72.

Mehra, R. and Peschon, J. (1971). An innovations approach to fault detection and diagnosis in dynamic systems. *Automatica*, 7(5):637–40.

Mehranbod, N., Soroush, M., and Panjapornpon, C. (2005). A method of sensor fault detection and identification. *Journal of Process Control*, 15(3):321–339.

Mehranbod, N., Soroush, M., Piovoso, M., and Ogunnaike, B. A. (2003). Probabilistic model for sensor fault detection and identification. *AIChE Journal*, 49(7):1787–1802.

Mengshoel, O., Darwiche, A., and Uckun, S. (2008). Sensor validation using bayesian networks. In *the 9th International Symposium on Artificial Intelligence, Robotics and Automation in Space*, Los Angelos, CA.

Mesbahi, E. (2001). An intelligent sensor validation and fault diagnostic technique for diesel engines. *Transactions of the ASME. Journal of Dynamic Systems, Measurement and Control*, 123(1):141–4.

Mohammadpour, J., Franchek, M., and Grigoriadis, K. (2011). A survey on diagnostics methods for automotive engines. In *In Proceedings of 2011 American Control Conference*, San Francisco, CA.

Murphey, Y., Crossman, J., Chen, Z., and Cardillo, J. (2003). Automotive fault diagnosis - part ii: a distributed agent diagnostic system. *IEEE Transactions on Vehicular Technology*, 52(4):1076–98.

Namburu, S. M., Chigusa, S., Prokhorov, D., Qiao, L., Choi, K., and Pattipati, K. (2007). Application of an effective data-driven approach to real-time fault diagnosis in automotive engines. In *IEEE Aerospace Conference Proceedings*, pages IEEE; AIAA–, Big Sky, MT, United states. Inst. of Elec. and Elec. Eng. Computer Society.

Napolitano, M., Silvestri, G., Windon, D.A., I., Casanova, J., and Innocenti, M. (1998). Sensor validation using hardware-based on-line learning neural networks. *IEEE Transactions on Aerospace and Electronic Systems*, 34(2):456–68.

Neapolitan, R. (1990). *Probabilistic reasoning in expert systems, theory and algorithms*. Willey, New York.

Negiz, A. and Cinar, A. (1992). On the detection of multiple sensor abnormalities in multivariate processes. In *Proceedings of the 1992 American Control Conference (IEEE Cat. No.92CH3072-6)*, pages 2364–8, Evanston, IL, USA. American Autom. Control Council.

Negiz, A. and Cinar, A. (1997). Monitoring sensor performance in multivariable continuous processes. In *Proceedings of the 1997 American Control Conference (Cat. No.97CH36041)*, volume vol.1, pages 314–18, Evanston, IL, USA. American Autom. Control Council.

Neter, J., Kutner, M. H., and Nachtstheim, C. J. (1996). *Applied linear statistical models*. McGraw-Hill, New York, USA, 4th edition.

Nicholson, A. and Brady, J. (1994). Dynamic belief networks for discrete monitoring. *IEEE Transactions on Systems, Man and Cybernetics*, 24(11):1593–610.

Nilsson, F. (2007). *Diagnosis of a Truck Engine using Nonlinear Filtering Techniques*. PhD thesis, Linkping University, Sweden.

Norton, M. (2005). *A quick course in statistical process control*. Prentice-Hall.

Nyberg, M. (1999). *Model based fault diagnosis: method, theory, and automotive engine applications*. PhD thesis, Linkping University.

Nyberg, M. (2002). Model-based diagnosis of an automotive engine using several types of fault models. *IEEE Transaction on Control System Technology*, 10(5):679–689.

Nyberg, M. (2003). Using hypothesis testing theory to evaluate principles for leakage diagnosis of automotive engines. *Control Engineering Practice*, 11(11):1263–72.

Nyberg, M. and Nielsen, L. (1997). Model based diagnosis for the air intake system of the si engine. In *SAE Technical Paper 970209*. SAE International.

Nyberg, M. and Perkovic, A. (1998). Model based diagnosis of leaks in the air-intake system of an si engine. In *SAE Technical Paper 980514*. SAE International.

Nyberg, M. and Stutte, T. (2004). Model based diagnosis of the air path of an automotive diesel engine. *Control Engineering Practice*, 12(5):513–525.

Ohsumi, A. and Kawano, T. (2002). Identification of continuous-time time-varying stochastic systems via distribution-based approach. In *Proceedings of the 33rd ISCIE International Symposium on Stochastic Systems Theory and its Applications*, pages 69–74, Tochigi, Japan. Inst. Syst., Control & Inf. Eng.

Park, S. and Lee, C. (1993). Fusion-based sensor fault detection. In *Proceedings. IEEE International Symposium on Intelligent Control (Cat. No.93CH3278-9)*, pages 156–61, Chicago, IL, USA. IEEE.

Patton, R. and Chen, J. (1997). Observer-based fault detection and isolation: robustness and applications. *Control Engineering Practice*, 5(5):671–82.

Patton, R., Frank, P., and Clark, R. (1989). *Fault diagnosis in dynamic systems - theory and application*. Prentice-Hall, London, U.K.

Pearl, J. (1998). *Probabilistic reasoning in intelligent systems: networks of plausible inference*. Morgan Kauffmann, California.

Pearson, K. (1901). Lines and planes of closest fit. *Philosophical Magazine*, 2:559–572.

Perla, R., Mukhopadhyay, S., and Samanta, A. (2004). Sensor fault detection and isolation using artificial neural networks. In *TENCON 2004. 2004 IEEE Region 10 Conference (IEEE Cat. No. 04CH37582)*, volume Vol. 4, pages 676–9, Chiang Mai, Thailand. IEEE.

Pike, P. and Pennycook, K. (1992). Commissioning of bems - a code of practice. Technical report, BSRIA.

Pintelon, R. and Schoukens, J. (2001). *System identification: a frequency domain approach*. IEEE Press, New York.

Potter, J. and Suman, M. (1977). Thresholdless redundancy management with arrays of skewed instruments. In *Integrity in electronic flight control systems*, volume AGARD-AG-224, pages 15–1, Northrop Corp., Electronics Div., Norwood, MA, USA. AGARD, Neuilly sur Seine, France.

Principe, J., Wang, L., and Motter, M. (1998). Local dynamic modeling with self-organizing maps and applications to nonlinear system identification and control. *Proceedings of the IEEE*, 86(11):2240–58.

Qin, G., Ge, A., and Dai, Y. (1998). Local model on-line sensor fault detection method in the automotive environment. In *Proceedings of the IEEE International*

Conference on Intelligent Processing Systems, ICIPS, volume 2, pages 1495–1498, Beijing, China. IEEE, Piscataway, NJ, USA.

Qin, S. and Li, W. (2001). Detection and identification of faulty sensors in dynamic processes. *AIChE Journal*, 47(7):1581–1593.

Qin, S. J. and Li, W. (2004). Detection, identification, and reconstruction of faulty sensors with maximized sensitivity. *AlChE Journal*, 45:1963–76.

Qin, S. J., Yue, H., and Dunia, R. (1997). Self-validating inferential sensors with application to air emission monitoring. *Industrial & Engineering Chemistry Research*, 36(5):1675–1685.

Rao, B. (1996). *Handbook of condition monitoring*. Elsevier Advanced Technology.

Rissanen, J. (1978). Modeling by shortest data description. *Automatica*, 14(5):465–71.

Rizzoni, G. and Min, P. (1991). Detection of sensor failures in automotive engines. *IEEE Transactions on Vehicular Technology*, 40(2):487–500.

Rizzoni, G., Soliman, A., and Passino, K. (1993). A survey of automotive diagnostic equipment and procedures. In *SAE Technical Paper 930769*. SAE International.

Rojas-Guzman, C. and Kramer, M. (1993). Comparison of belief networks and rule-based expert systems for fault diagnosis of chemical processes. *Engineering Applications of Artificial Intelligence*, 6(3):191–202.

Romesis, C. and Mathioudakis, K. (2003). Setting up of a probabilistic neural network for sensor fault detection including operation with component faults. *Transactions of the ASME. Journal of Engineering for Gas Turbines and Power*, 125(3):634–41.

Scarl, E., Jamieson, J., and Delaune, C. (1987). Diagnosis and sensor validation through knowledge of structure and function. *IEEE Transactions on Systems, Man and Cybernetics*, SMC-17(3):360–8.

Scattolini, R., Siviero, C., Mazzucco, M., Ricci, S., Poggio, L., and Rossi, C. (1997). Modeling and identification of an electromechanical internal combustion engine throttle body. *Control Engineering Practice*, 5(9):1253–1259.

Scheding, S., Nebot, E., and Durrant-Whyte, H. (1998). The detection of faults in navigation systems: a frequency domain approach. In *Proceedings. 1998 IEEE International Conference on Robotics and Automation (Cat. No.98CH36146)*, volume vol.3, pages 2217–22, Leuven, Belgium. IEEE.

Scholkopf, B., Smola, A., and Muller, K.-R. (1998). Nonlinear component analysis as a kernel eigenvalue problem. *Neural Computation*, 10(5):1299–319.

Sedgewick, R. (1995). *Algorithms in C++: Part 5, Graph Algorithms*. Addison-Wesley, London.

Simani, S., Fantuzzi, C., and Beghelli, S. (2000). Diagnosis techniques for sensor faults of industrial processes. *IEEE Transactions on Control Systems Technology*, 8(5):848–55.

Spina, P. (2000). Reliability in the determination of gas turbine operating state. In *Proceedings of the 39th IEEE Conference on Decision and Control (Cat. No.00CH37187)*, volume vol.3, pages 2639–44, Sydney, NSW, Australia. IEEE.

Strang, G. (1998). *Introduction to Linear Algebra*. Wellesley-Cambridge Press.

Sugeno, M. and Yasukawa, T. (1993). A fuzzy-logic-based approach to qualitative modeling. *IEEE Transactions on Fuzzy Systems*, 1(1):7–31.

Tong, H. and Crowe, C. (1995). Detection of gross errors in data reconciliation by principal component analysis. *AIChE Journal*, 41(7):1712–1722.

Turkcan, E. and Ciftcioglu, O. (1991). Sensor failure detection in dynamical systems by kalman filtering methodology [nuclear plant sensors]. In *Dynamics and Control in Nuclear Power Stations*, pages 133–9, London, UK. Thomas Telford.

Uluyol, O., Buczak, A., and Nwadiogbu, E. (2001). Neural-networks-based sensor validation and recovery methodology for advanced aircraft engines. In *Proc. SPIE - Int. Soc. Opt. Eng. (USA)*, volume 4389, pages 102–9, Orlando, FL, USA. SPIE-Int. Soc. Opt. Eng.

Upadhyaya, B. and Kerlin, T. (1978). Estimation of response time characteristics of platinum resistance thermometers [in pwr] by the noise analysis technique. *ISA Transactions*, 17(4):21–38.

Van Overschee, P. and De Moor, B. (1994). N4sid: subspace algorithms for the identification of combined deterministic-stochastic systems. *Automatica*, 30(1):75–93.

Van Overschee, P. and De Moor, B. (1996). *Subspace identification for linear systems: Theory, Implementation, Applications*. Kluwer Academic Publishers.

van Schrick, D. (1994). A comparison of ifd schemes: a decision aid for designers. In *Proceedings of the Third IEEE Conference on Control Applications (Cat. No.94CH3420-7)*, volume vol.2, pages 889–94, Glasgow, UK. IEEE.

Venkatasubramanian, V., Rengaswamy, R., and Kavuri, S. (2003a). A review of process fault detection and diagnosis. ii. qualitative models and search strategies. *Computers & Chemical Engineering*, 27(3):313–26.

Venkatasubramanian, V., Rengaswamy, R., Kavuri, S. N., and Yin, K. (2003b). A review of process fault detection and diagnosis part iii: Process history based methods. *Computers and Chemical Engineering*, 27(3):327–346.

Venkatasubramanian, V., Rengaswamy, R., Yin, K., and Kavuri, S. (2003c). A review of process fault detection and diagnosis. i. quantitative model-based methods. *Computers & Chemical Engineering*, 27(3):293–311.

Verhaegen, M. and Deprettere, E. (1991). A fast, recursive mimo state space model identification algorithm. In *Proceedings of the 30th IEEE Conference on Decision and Control (Cat. No.91CH3076-7)*, pages 1349–54, Brighton, UK. IEEE.

Verhaegen, M. and Dewilde, P. (1992). Subspace model identification, part 1: The output-error state-space model identification class of algorithms. *International Journal of Control*, 56(5):1187–1210.

Viberg, M. (1995). Subspace-based methods for the identification of linear time-invariant systems. *Automatica*, 31(12):1835–51.

Vinsonneau, J., Shields, D., King, P., and Burnham, K. (2002). Improved si engine modelling techniques with application to fault detection. In *Proceedings of the 2002 IEEE International Conference on Control Applications (Cat. No.02CH37330)*, volume vol.2, pages 719–24, Glasgow, UK. IEEE.

Wang, S. and Xiao, F. (2004). Ahu sensor fault diagnosis using principal component analysis method. *Energy and Buildings*, 36(2):147–60.

Watanabe, K. and Himmelblau, D. (1982). Instrument fault detection in systems with uncertainties. *International Journal of Systems Science*, 13(2):137–58.

Watanabe, K., Komori, A., and Kiyama, T. (1994). Diagnosis of instrument fault. In *Conference Proceedings. 10th Anniversary. IMTC/94. Advanced Technologies in I & M. 1994 IEEE Instrumentation and Measurement Technolgy Conference (Cat. No.94CH3424-9)*, volume vol.1, pages 386–9, Hamamatsu, Japan. IEEE.

Weaver, E. and Richardson, G. (Spring 2006). Threshold setting and the cycling of a decision threshold. *System Dynamics Review*, 22(1):1–26.

Weinhold, N., Ding, S., Jeinsch, T., and Schultalbers, M. (2005). Embedded model-based fault diagnosis for on-board diagnosis of engine control systems. In *2005 IEEE International Conference on Control Applications (CCA) (IEEE Cat. No.05CH37713)*, pages 1206–11, Piscataway, NJ, USA. IEEE.

Whitley, D., Ford, M., and Livingstone, D. (2000). Unsupervised forward selection: a method for eliminating redundant variables. *Journal of Chemical Information and Computer Sciences*, 40(5):1160–8.

Willsky, A. (1976). A survey of design methods for failure detection in dynamic systems. *Automatica*, 12(6):601–11.

Wise, B. and Ricker, N. (1991). Recent advances in multivariate statistical process control: improving robustness and sensitivity. In *IFAC-ADCHEM Symposium*.

Wise, B., Ricker, N., and Veltkamp, D. (1989). Upset and sensor failure detection in multivariable processes. In *AIChE Annual Meeting*.

Xu, L., Oja, E., and Suen, C. (1992). Modified hebbian learning for curve and surface fitting. *Neural Networks*, 5(3):441–57.

Yang, S., Yuan, J., and Ni, J. (1996). Improvement of thermal error modeling and

compensation on machine tools by cmac neural network. *International Journal of Machine Tools & Manufacture*, 36(4):527–537.

Yen, G. G. and Feng, W. (2000). Winner take all experts network for sensor validation. In *IEEE Conference on Control Applications - Proceedings*, volume 1, pages 92–97, Anchorage, USA. Institute of Electrical and Electronics Engineers Inc., Piscataway, NJ, USA.

Ying, C.-M. and Joseph, B. (2000). Sensor fault detection using noise analysis. *Industrial and Engineering Chemistry Research*, 39(2):396–407.

Zhang, Y. X. (2007). Artificial neural networks based on principal component analysis input selection for clinical pattern recognition analysis. *Talanta*, 73(1):68–75.

Zheng, G. and Billings, S. (1996). Radial basis function network configuration using mutual information and the orthogonal least squares algorithm. *Neural Networks*, 9(9):1619–37.